Enhancing MIMO Array Imaging Quality

Ying Zhang

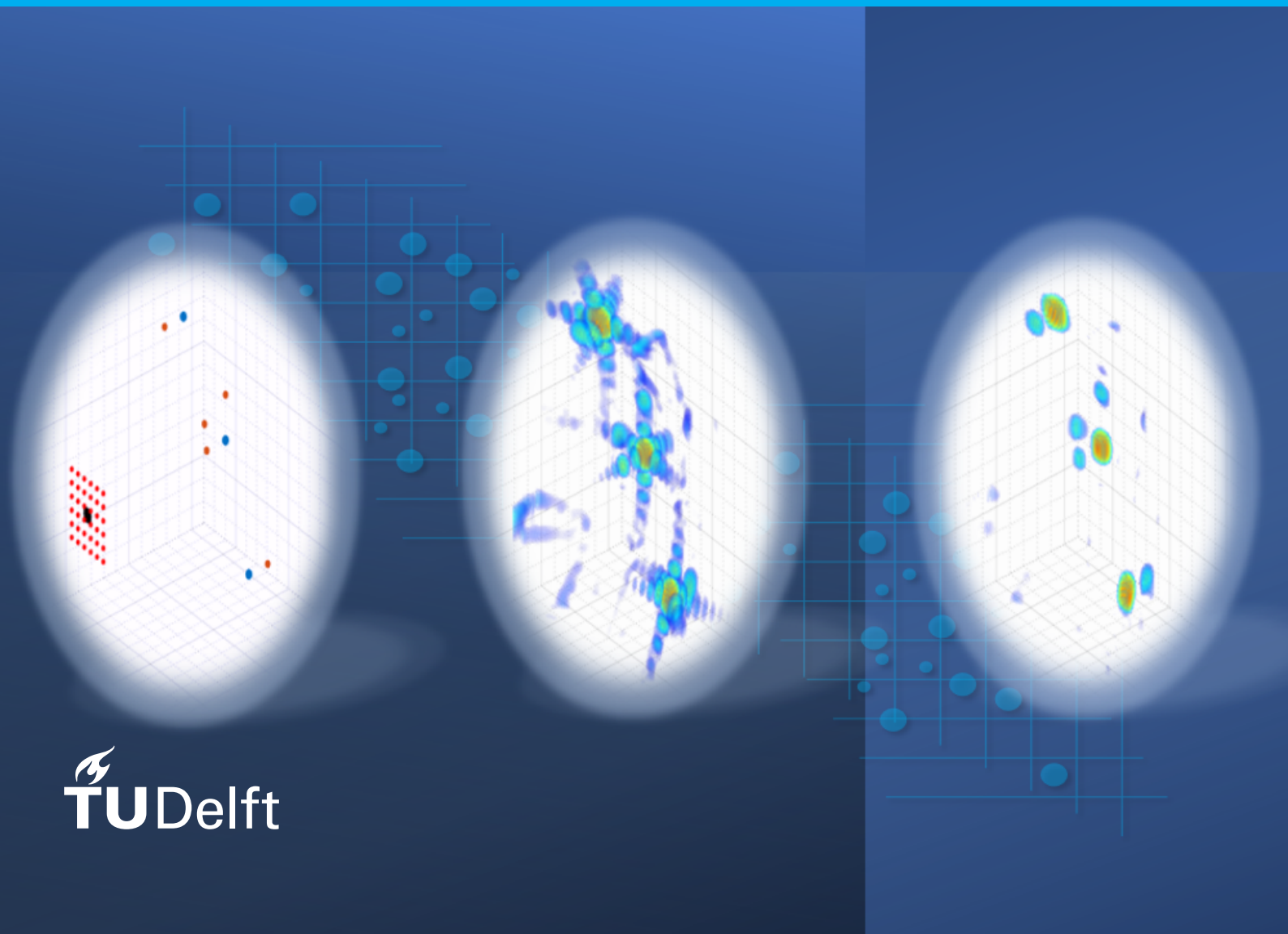

TU Delft

Enhancing MIMO Array Imaging Quality

by

Ying Zhang

to obtain the degree of Master of Science
at the Delft University of Technology,
to be defended publicly on Tuesday November 30, 2021 at 15:00 PM.

Student number:	5122031	
Project duration:	February 1, 2021 – November 30, 2021	
Thesis committee:	Prof. DSc. Alexander Yarovoy,	TU Delft, supervisor
	Dr. Jianping Wang,	TU Delft, daily supervisor
	Dr. Rob Remis,	TU Delft

An electronic version of this thesis is available at `https://repository.tudelft.nl/`

TU Delft

Abstract

For radar imaging, resolution and dynamic range are two critical metrics to measure image quality. MIMO array exploits the spatial diversity of transmitters and receivers to achieve high cross-range resolution with fewer antennas than array-based imaging.

Generally, to make full use of the sparsity, at least the transmit array or the receive array does not satisfy the Nyquist sampling criterion. Therefore, the grating lobes may occur, which would produce ghost targets and submerge the weak targets. For far-field imaging, the grating lobes can be eliminated with various array design methods. In contrast, it cannot be completely eliminated for near-field imaging applications. Besides, the high sidelobes would also mask the weak targets and reduce the image's dynamic range. The traditional weighting method can effectively suppress the sidelobes, but the mainlobe resolution would be reduced.

In this thesis, we propose a method based on the spatially variant apodization method to enhance the image quality of near-field 1-D and 2-D MIMO array imaging. According to the generalized matched filtering imaging method, we can individually analyze the wavenumber spectrum in the cross-range and range directions of the transmit array and the receive array. Then the method can be easily implemented in the space domain to suppress the sidelobes and grating lobes without sacrificing the cross-range and range resolution. Moreover, three acceleration approaches are proposed to reduce the computation burden.

Both numerical simulation and experimental validation indicate that the proposed method can effectively suppress the sidelobes and grating lobes without spreading the mainlobe. Moreover, the acceleration methods can suppress the sidelobe and grating lobe level meanwhile decrease the processing time remarkably under some conditions.

Contents

List of Figures

List of Tables

1 Introduction

This chapter begins with introducing the background and the motivation and then lists the main methods for sidelobe suppression of short-range MIMO array imaging. Next to this, the research problem, the objectives, the challenges, and contributions are given. Lastly, the outline of the thesis is drawn.

1.1 Background and Motivation

Radar is short for **ra**dio **d**etection and **r**anging, well-known for the secret development and use for military purposes in World War II. However, the research of radar started before WW II. Early in 1914, the idea of radar was introduced by Nikola Tesla [1]. In 1922, Guglielmo Marconi gave a speech on the principle of radar about the possibility of object detection at the American Institute of Radar Engineers Conference [2]. The radar system works by sending a signal and receiving the echo reflected from the object, which contains the information of location, angle, speed, etc. After years of development, the radar system is widely used for detection, tracking, surveillance, imaging, etc.

As an important technology, radar imaging can be used all weather and all day compared with optical imaging. Furthermore, it has excellent penetrating ability and accuracy. The commonly used radar systems for imaging include synthetic aperture radar (SAR), inverse synthetic aperture radar (ISAR) and MIMO radar. For an imaging system, the spatial resolution in the cross-range and range directions, as well as the imaging dynamic range, are the primary measures of the performance [3].

High-resolution radar imaging provides a powerful tool to separate adjacent small targets. The range resolution is the minimum distance to distinguish or resolve two targets in the same range direction and is determined by the bandwidth B of the transmit signal

$$\delta_r = \frac{c}{2B} \tag{1.1}$$

where c is the speed of light. Obviously, the large signal bandwidth B results in high range resolution. The cross-range resolution is approximated by

$$\delta_{cr} = R\frac{\lambda}{L} \tag{1.2}$$

where R is the distance between the aperture and the target, λ is the wavelength, and L is the aperture length. So a larger aperture array results in higher cross-range resolution, which means the better capability of radar to distinguish between two targets along the cross-range direction.

In fact, the size of the physical aperture is limited by the size of the equipment and the operating environment. To achieve high cross-range resolution, SAR translates and receives the signal with an antenna or a small array at successive positions along a line to realize an effective large aperture. At each position, both the amplitude and the phase information are stored. And the combination of the successive echo signals can generate a virtual aperture that is much longer than the physical aperture [4]. However, SAR is based on a moving platform and takes longer time for data acquisition. For (near) real-time imaging, SAR is time inefficient. Therefore, another consideration to achieve large aperture is to use MIMO radar.

MIMO radar exploits spatial diversity of transmit and receive antennas to synthesize a large aperture. A MIMO radar with M transmit antennas and N receive antennas results in a large virtual array with $M \times N$ elements [5]. Compared with the traditional linear array system, fewer antennas are used to get the same size aperture. Therefore, MIMO radar can achieve high cross-range resolution by cost-effectively increasing the virtual antennas. Thus, it is an excellent choice to use MIMO radar for high-resolution imaging.

MIMO radar has been widely used in short-range imaging applications, such as security imaging, nondestructive testing, concealed weapon detection, and through-the-wall imaging [6]–[9]. However, the possible high grating lobes and sidelobes of its effective sparse array would significantly degrade the quality of the images. Generally, traditional linear array radar requires the element spacing smaller than a half wavelength to prevent the grating lobes. However, there is no limit of the element spacing for the MIMO array to make full use of the sparsity. Thus, the grating lobes may occur, which will produce unwanted ghost targets. Furthermore, high sidelobes would submerge the weak targets. All these artifacts will degrade the image quality. Therefore, many methods are proposed to suppress the sidelobes and grating lobes.

1.2 Literature Review

The traditional method to suppress the sidelobe and grating lobe level is to apply a non-rectangular weighting function on the aperture or the data in the frequency domain. However, any weighting function is a compromise between the low sidelobe level and the narrow mainlobe resolution.

One idea is based on the pre-setup of the signal or the array. Zhuge [10] applied ultra-wideband technology with the fractional bandwidth greater than 100% to get high resolution and reduce the sidelobes and grating lobes. Unfortunately, it has a high requirement of bandwidth that is not suitable for the more general situation. Tu et al. [11] and Ge et al. [12] utilized the array design method by exploiting the difference of the images with two sub-array to suppress the sidelobes and gratin globes. Furthermore, Tu. combines with the cross-correlation weighting to get a better suppression effect. However, this method is based on the unique array topology, and the suppression effect is determined by how different the two images are. Tian et al. [13] proposed a design method of MIMO array by increasing the antennas to compensate for the mainlobe spreading due to applying the window function on the aperture. However, this method is not suitable in real life for a well-designed radar.

Another idea is based on the processing of the data or the image. The CLEAN method is applied for sparse MIMO array [14] by iteratively subtracting the point spread function of the strong targets from the original image. However, iteration results in complicated implementation and large computation. Liu et al. [15] proposed a weighting method by finding the optimal weighting coefficient on each channel data based on convex optimization. However, although it provides a better sidelobe suppression effect than the traditional weighting function, it generates a high computation load, and the mainlobe resolution is still reduced. Furthermore, a kind of weighting method is based on the image and back-projection (BP) imaging algorithm. The coherence factor (CF) method [16], [17] is an amplitude weighting method with the weighting coefficient CF to suppress the sidelobe and grating lobe. The coherence factor is the ratio of the coherent power over the incoherent power for a point in the image. For the main lobes, the CF ratio is the unity, while for the sidelobes and the grating lobes, due to the incoherence of data channels, the CF ratio is smaller than 1. Therefore, it can reduce the sidelobes and grating lobes level. Furthermore, to make use of the phase information, the phase coherence factor (PCF) method [18] is proposed by J. Camacho et al. Moreover, the PCF method combined with a dual apodization method [19] is proposed to get better suppression effect both in cross-range and range directions. The PCF is related to the standard deviation of the complex exponential term. For the mainlobe, the standard deviation is zero, and the PCF equals 1. For other regions, the standard deviation increases, and the PCF decreases. However, the PCF has complicated computation. In addition, a sign coherence factor method is proposed by Liu [20] to reduce the computation load. However, it requires a low-pass filter to smooth the transitions of the sign. Though all CF-related methods show a good suppression effect, they are only as of the improvement of the BP algorithm and the peak amplitude of the targets would attenuate.

The non-linear multi-apodization method has been applied for MIMO array imaging in recent years. Zhu et al. [21] proposed a grating lobe suppressing method by utilizing a combination of zero migration and multi-apodization. However, this method has a limited suppressing effect, and sidelobe suppression is not considered. They also proposed another method of combining the aperture weighting method with multi-apodization technology [22]. However, since it is only using a finite number of weighting functions, the suppression effect could be improved by considering more weighting functions but with the price of increasing the processing time.

Therefore, a new method [23] based on spatially variant apodization (SVA) for MIMO array imaging is proposed. It has no requirements of the array topology and is easy to implement.

1.3 Research Problem and Objectives

The SVA method is initially used for SAR imagery. By exploiting the spatial property of the cosine-on-pedestal weighting function, it is easy to implement with three-point convolution. Compared with the linear weighting function method, it can effectively reduce the sidelobe level without sacrificing the mainlobe resolution. Therefore, the SVA method is an excellent choice to improve the image quality.

The SVA method is a non-linear operation that allows each pixel to receive its own weighting coefficient. For SAR imagery, the wavenumber spectrum of each pixel is spatially-invariant, which means that the direction of the sidelobes for any target in the image is the same. Further-

more, the window length for the weighting function is also the same. We can directly perform the SVA method on the SAR imagery to achieve sidelobe suppression. The application of the SVA method for SAR imagery is mature. Stankwitz. et al. [24] gave a detailed discussion of the implementation of the SVA method under the integer multiple of Nyquist sampled data. Smith [25] gave the implementation for the non-integer case. Carlos [26] proposed a more robust method for the non-integer case, and Ni [27] proposed a modified SVA method. However, all these are based on SAR imagery.

Zhu [23] proposed the implementation of the SVA method in the cross-range direction for1-D MIMO array imaging but did not consider the sidelobe suppression in the range direction. Therefore, the main objectives of this thesis project is to propose a method to implement SVA both in the cross-range and range direction for 1-D MIMO array imaging, and propose a method to implement SVA for 2-D MIMO array imaging. Moreover, we try to give the acceleration approaches of the SVA method for MIMO array imaging to speed up the implementation.

1.4 Challenges and Contributions

The analysis of the wavenumber spectrum is complicated for a MIMO array due to the transmission and receiving separation, and the wavenumber spectrum is spatially variant for different targets, compared with SAR imaging. Therefore, the SVA method cannot be directly used due to the variant support width and spatially variant sidelobe direction. However, when applying the SVA method, it is crucial to determine the window length and align the central wavenumber to the zero-wavenumber position for each pixel. Therefore, approximating the wavenumber spectrum of a MIMO array for the SVA implementation is a critical problem.

In the cross-range direction, by utilizing the generalized matched filtering (GMF) imaging method, we can individually analyze the cross-range wavenumber spectrum of the transmit array and the receive array, forming a new imaging plane about the cross-range imaging positions corresponding to the sub-arrays. In this way, the complicated analysis of the wavenumber spectrum for the MIMO array is simplified, and we can make some approximations to obtain the support width. Then by compensating the phase term to align the central wavenumber to the zero-wavenumber position, we can apply the 2-D SVA method in the cross-range direction. Assume the array centers of the transmit and the receive array are not coincident; there are two range directions for one target. In one range direction, by analyzing the wavenumber spectrum, the total wavenumber width consists of the original part and the projection part from another range direction. Similarly, a phase term is compensated in the space domain. Then the two 1-D basic SVA method can be applied independently and in parallel.

In this thesis, we propose an approach of the SVA method applied in the range direction for 1-D MIMO array imaging. Besides, by recovering the phase information, the complete implementation of the SVA method both in the cross-range and range directions is provided. The proposed method can achieve a sidelobe reduction of around 20 dB in both directions and at least 4 dB grating lobe suppression in the cross-range direction without sacrificing the cross-range and range resolution.

Moreover, with a similar analysis, we also propose a method of SVA for 2-D MIMO array imaging. The numerical simulation and the experimental validation show that the SVA method could be effectively performed on 2-D MIMO array imaging to suppress the sidelobes and grating lobes without spreading the mainlobe.

Furthermore, we give three acceleration implementations of the SVA method to reduce the computational time. Under a suitable imaging grid, the three approaches can provide a good suppression effect with much less computational time.

1.5 Thesis Outline

Chapter 1 begins with the introduction of the background, the motivation of this thesis project. Next to it, the literature review about sidelobe and grating lobe suppression of MIMO array imaging is listed. Then the research problem, the main objectives, the challenges, and the novel contributions are provided.

Chapter 2 introduces and compares the basic SVA method and its variants, the GSVA method, the RSVA method and the MSVA method for sidelobe suppression. Furthermore, two other variants, the super-SVA and the 3/4-SVA method for resolution improvement, are also introduced.

Chapter 3 deals with the 1-D MIMO array imaging. The analysis and implementation of the BSVA method both in the cross-range and the range direction are drawn. Furthermore, the acceleration implementation of the SVA method is also provided.

Chapter 4 deals with the 2-D MIMO array imaging. The analysis and implementation of the BSVA method both in the cross-range plane and the range direction are drawn. Furthermore, the acceleration implementation of the SVA method is also discussed. Moreover, an experimental validation is provided to verify the suppression performance.

Finally, the conclusion and the future work of the thesis project are discussed in chapter 5.

2

Nonlinear Apodization Method Review

Apodization technique is a sidelobe control method which is initially proposed in optic processing to suppress the diffraction sidelobe [24]. The sidelobe control of radar imaging is analogous to that for optics. Therefore, in radar processing, we borrow the term 'apodization' to describe sidelobe suppression. Actually, the apodization method utilizes different window functions to realize the different combinations of sidelobe suppression level and main-lobe resolution. It can be divided into the linear apodization method and the non-linear apodization method. The common linear apodization form is the multiplication of a sinc function by some non-rectangular window function. As a result, the sidelobe level can be reduced, but the mainlobe resolution is reduced at the same time. With non-linear apodization, the sidelobe can be suppressed while maintaining the mainlobe resolution by using different weighting functions. On account of this remarkable property, it is often used in synthetic aperture radar imagery. This chapter will introduce several main non-linear apodization methods, especially the general spatially variant apodization(SVA) method and its variants. The structure of this chapter is given as follows. In section 2.1, start with introducing a dual apodization method that chooses two different weighting functions and then expands to the multi-apodization method. In section 2.2, the basic SVA method and its variants for sidelobe suppression will be introduced. The SVA method for resolution improvement will be introduced in section 3.3. A summary of the non-linear apodization method is given in section 3.4.

2.1 Dual and Multi-apodization

Considering a family of $2N_i + 1$ finite generalized symmetric frequency domain cosine-on-pedestal weighting functions

$$A(f) = a + \sum_{i=1}^{N_i} 2w_i \cos\left(2\pi i \frac{f}{f_s}\right) \tag{2.1}$$

where a is the normalization parameter, w_i is the weighting coefficient which defines a particular window of the family, f_s is the sampling frequency and f is the frequency whose support region is $\left[-\frac{f_0}{2}, \frac{f_0}{2}\right]$.

Let us begin by considering a simple case that the sampling frequency equals the Nyquist

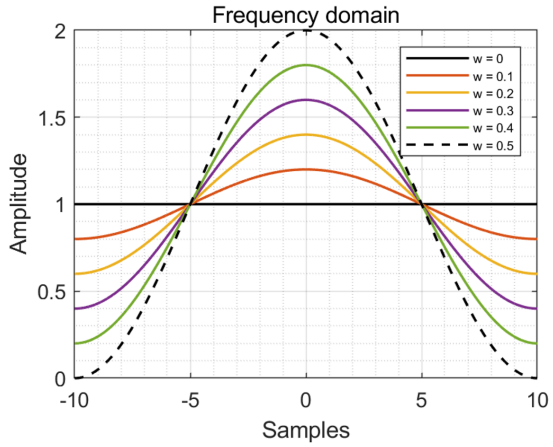

Figure 2.1: Weighting functions with $w_s = 1$ and $N_i = 1$ under different weighting coefficients

sampling rate, namely $f_s = f_0$ and $N_i = 1$. Then the equation (2.1) is expressed as

$$A(f) = 1 + 2w\cos\left(2\pi\frac{f}{f_0}\right) \quad s.t. \quad 0 \leq w \leq 0.5 \tag{2.2}$$

The weighting function $A(f)$ ranges from uniform weighting with $w = 0$ to Hanning weighting with $w = 0.5$. Figure 2.1 gives the weighting functions with different weighting coefficients in frequency domain. The descent speed from the center frequency to the edges is different with different weighting coefficients. By multiplying with the above weighting function in the frequency domain under a fixed weighting coefficient, the sidelobe of a sinc function can be suppressed in the space domain. And this is called amplitude tapering, which is linear apodization.

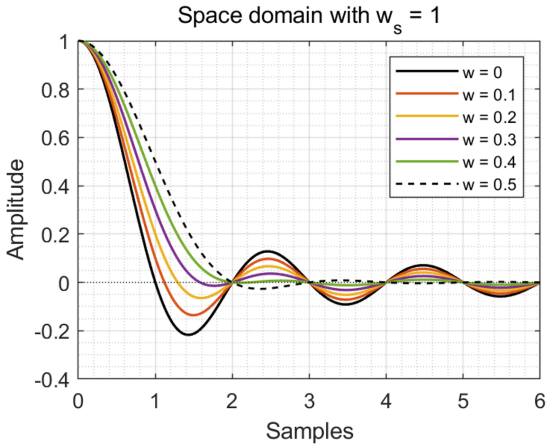

Figure 2.2: Weighted results of a sinc function with diffrent weighting coefficients

The weighted result of a sinc function with different weighting coefficients is shown in Figure 2.2. We can see that the sidelobes have been suppressed while the mainlobe has been broadened. Moreover, the better suppression of the sidelobe means the wider the mainlobe broadened. In this case, if we select the minimum absolute value of two weighted results

at each sample, we can get a new weighted result which has good sidelobe suppression and reasonable resolution. And this is the critical idea of dual apodization (DA).

Logically, triple apodization selects the minimum absolute value at each sample location from the weighted results with three different weighting coefficients, and multiple apodization is with multiple weighting coefficients. Figure 2.3 gives the absolute value of a sinc function after applying DA method with uniform window function $w = 0$ and Hanning window function $w = 0.5$ and triple apodization with $w = 0$, $w = 0.2$ and $w = 0.5$. From the figure, we can see that the TA method's sidelobe suppression performance is better than that of the DA method, and its resolution is also better.

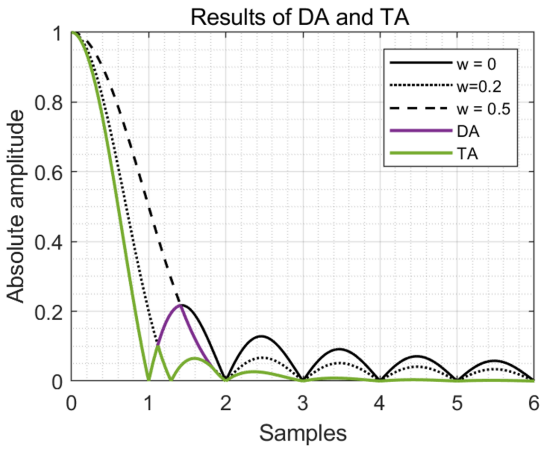

Figure 2.3: Result of applying DA method with $w = 0$ and $w = 0.5$

Furthermore, dual apodization is based on the absolute value at each sample point. Actually, the imaging result is complex-valued. Therefore, we can separately consider the real component (I or in-phase) and the imaginary (Q or quadrature) component. In this case, we can make use of the sign change to get a better sidelobe suppression effect. Suppose the signs of two weighted results are opposite for the real or imaginary component at one sample point. In that case, it means that some other weighting coefficient can make this point achieve its minimum value of zero. Otherwise, if the signs are the same, select the smaller absolute value of the two. Do this operation both in real and imaginary components, then combine them to form the final complex-valued weighted result. This kind of algorithm is called complex dual apodization (CDA). Figure 2.4 compares the results of applying the DA method and the CDA method. Obviously, the CDA method shows a better sidelobe suppression effect.

2.2 Spatially Variant Apodization for sidelobe suppression

From figure 2.2, we can see that with weighting factors in the interval 0 to 0.5, the sidelobes between two nulls are above or below zero, which means that for each sample point, it can achieve its minimum value of zero by finding a proper weighting coefficient in this interval. Therefore, we can perform the multiple-apodization method. In principle, if we apply enough weighting functions with w between 0 and 0.5, we can achieve the minimum value of zero at the sidelobes by taking the min function. However, this procedure is at the expense of a large computational load. Actually, this process can be explained as finding the optimal weighting coefficient w for each sample point. Therefore, the key is to find a method to find

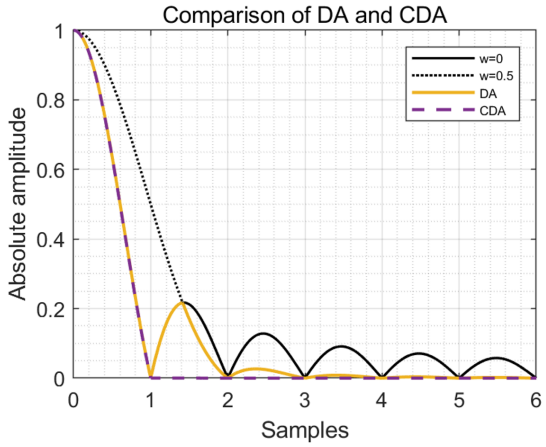

Figure 2.4: Results of applying DA and CDA method with $w = 0$ and $w = 0.5$

the proper weighting coefficient for each sample point adaptively. Fortunately, according to the Fourier transform, the multiplication in the frequency domain is equivalent to the convolution in the time domain. Therefore, the cosine-on-pedestal weighting function can be implemented effectively using a three-point kernel in the space domain. Moreover, the optimal weighted result of each sample point can be calculated by solving a minimization problem subject to some conditions about the weighting factor w. From Figure 2.2, we can see that for different sample points, the optimal weighting coefficient may be different. And this is why we call this method a spatially variant apodization method.

Taking inverse Fourier transform of the weighting function (2.1) with respect to the frequency, it can be expressed in discrete space domain as

$$a[n] = a\delta[n] + \sum_{i=1}^{N_i} w_i \left(\delta\left[n + i\left\lfloor \frac{f_s}{f_0} \right\rfloor\right] + \delta\left[n - i\left\lfloor \frac{f_s}{f_0} \right\rfloor\right] \right) \tag{2.3}$$

where n is the sampling point in the space domain, and $\lfloor\ \rfloor$ means rounding down. Denote the unweighted image as $g(m)$, where m is the index of the pixel, and denote $\left\lfloor \frac{f_s}{f_0} \right\rfloor$ as integer l. When $m = n$, the weighted result can be expressed as

$$\begin{aligned} g'[m] &= g[m] \otimes a[m] \\ &= ag[m] + \sum_{i=1}^{N_i} w_i(m) \left(g[m + i \cdot l] + g[m - i \cdot l] \right) \end{aligned} \tag{2.4}$$

Where $\otimes$ is the convolution operator and $w(m)$ is the weighting coefficient for pixel m dependent on the pixel location. SVA method reduces the sidelobe level by choosing $w(m)$ to minimize the weighted result $g'(m)$. Since the problem is degenerate, some constraints need to be imposed [25].

Considering the frequency f in the weighting function (2.1) having the support over the region $-\frac{f_0}{2} \leq f \leq \frac{f_0}{2}$, then equation (2.1) can be formulated as

$$A(f) = a + \sum_{i=1}^{N_i} 2w_i \cos\left(2\pi i \frac{f}{f_s}\right) \times \mathrm{supp}(f) \tag{2.5}$$

with

$$\text{supp}(f) = \begin{cases} 1, & -f_0/2 \le f \le f_0/2 \\ 0, & \text{others} \end{cases} \tag{2.6}$$

Taking inverse Fourier transform on the above function and express it in the space domain (in continuous form), the impulse response of equation (2.5) is

$$I(x) = a\text{sinc}(x) + \sum_{i=1}^{N_i} w_i \left[\text{sinc}\left(f_0 x + ilw_s\right) + \text{sinc}\left(f_0 x - ilw_s\right)\right] \tag{2.7}$$

with $\text{sinc}(x)$ is defined as

$$\text{sinc}(x) = \frac{\sin(\pi x)}{\pi x} \tag{2.8}$$

and w_s represents the oversampling ratio

$$w_s = \frac{f_0}{f_s} \tag{2.9}$$

Two constraints will be imposed to avoid invalid window function. The first constraint is about unit gain:

$$I(0) = 1 \tag{2.10}$$

The second constraint is the monotonicity of the window function, which can be reduced to require the positive edge of the window and the maximum at the center:

$$\begin{aligned} A(f_0/2) &\ge 0 \\ A(0) &\ge A(f_0/2) \end{aligned} \tag{2.11}$$

2.2.1 Basic Spatially Variant Apodization

1-D basic SVA method

The basic SVA (BSVA) method considers the three-tap window function with $N_i = 1$ and requires the data sampled at an integer multiple of the Nyquist frequency, namely $f_s = l \cdot f_0$, where l is an integer. The constraint of the BSVA method is the simplest by ignoring the influence of l, namely considering $l = 1$ and the constraints (2.10) and (2.11) are simplified as:

$$a = 1 \tag{2.12}$$

$$0 \le w \le 0.5 \tag{2.13}$$

Then the cosine-on-pedestal weighting function is in the form of the equation (2.2). The weighted result of the image is

$$g'_B[m] = g[m] + w(m)\left(g[m+l] + g[m-l]\right) \tag{2.14}$$

The optimal result of the above function can be obtained by minimizing $g'_B[m]$ (2.14) subject to the constraints (2.13):

$$\begin{aligned} \underset{w(m)}{\text{minimize}} \quad & \left|g'_B[m]\right|^2 \\ \text{s.t.} \quad & 0 \le w(m) \le 0.5 \end{aligned} \tag{2.15}$$

The above optimization problem can be solved by setting equal to zero the partial derivative of $|g'_B[m]|^2$ with respect to $w(m)$

$$\frac{\partial |g'_B[m]|^2}{\partial w(m)} = 0 \tag{2.16}$$

Since the image result $g[m]$ is of complex values, there are two approaches to consider.

- **I and Q jointly**
  Considering the complex-value case $g[m] = I[m] + jQ[m]$, the result of the equation (2.16) is

$$w_u(m) = -\left\{\frac{1}{2}\cdot\frac{g[m]}{g[m-l]+g[m+l]}\right\} - \left\{\frac{1}{2}\cdot\frac{g[m]}{g[m-l]+g[m+l]}\right\}^* \tag{2.17}$$

$$= -\mathrm{Re}\left[\frac{g[m]}{g[m-l]+g[m+l]}\right] \tag{2.18}$$

  Since $w(m)$ is constrained in the interval $[0, 1/2]$, let $w(m) = 0$ for $w_u(m) < 0$, $w(m) = 1/2$ for $w_u(m) > 1/2$. The final image $g'_B[m]$ can be expressed as

$$g'_B[m] = \begin{cases} g[m], & w_u(m) < 0 \\ g[m] + w_u(m)\cdot(g[m-l]+g[m+l]), & 0 \le w_u(m) \le 1/2 \\ g[m] + \frac{1}{2}(g[m-l]+g[m+l]), & w_u(m) > 1/2 \end{cases} \tag{2.19}$$

- **I and Q separately**
  Let $g[m]$ is either the real(I) component or the imaginary(Q) component of the complex-valued image, the result of the equation (2.16) is

$$w(m) = \frac{-g[m]}{g[m-l]+g[m+l]} \tag{2.20}$$

  Considering $w_u(m) = 0$ for $w(m) < 0$, $w_u(m) = 1/2$ for $w(m) > 1/2$ again, the final image $g'_B[m]$ can be expressed as

$$g'_B[m] = \begin{cases} g[m], & w_u(m) < 0 \\ 0, & 0 \le w_u(m) \le 1/2 \\ g[m] + \frac{1}{2}(g[m-l]+g[m+l]), & w_u(m) > 1/2 \end{cases} \tag{2.21}$$

  Then the final complex-valued weighted result of the image is the combination of the weighted real component and the imaginary component

$$g'_{out}[m] = g'_R[m] + jg'_I[m] \tag{2.22}$$

  where the subscript R and I represent the real result and imaginary result respectively.

From Figure 2.5, we can see that considering I and Q separately yields better sidelobe suppression. Therefore, in the following content, we will focus on the case of I and Q separately.

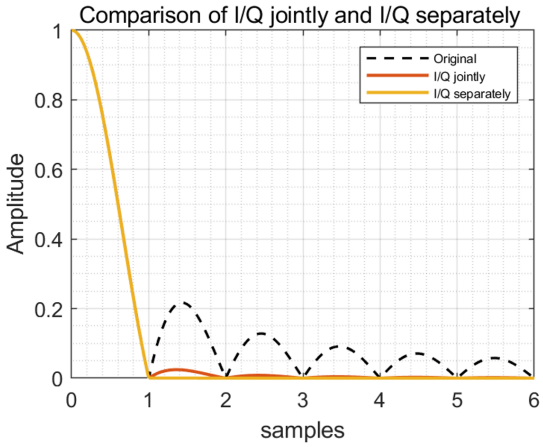

Figure 2.5: Results of BSVA under I/Q separately and I/Q jointly

Multi-dimensional basic SVA Method

- **Multi-dimensional sequentially**
  If the sidelobes along k dimensions need to be suppressed, we can apply the 1-D BSVA method along with each direction one by one. However, this approach has a drawback. After applying the BSVA method on the first dimension, the phase relations of the data change, and applying BSVA in the next dimension is not on a properly Nyquist sampled data. This will result in a worse suppression effect. A better consideration is that after performing the BSVA method on the first dimension, remain the new magnitude but recover the phase information. This is to make sure that the previous operation would not influence the other dimensions to apply BSVA method. The reason is SVA method relies on the relations of phases.

- **Multi-dimensional simultaneously**
  considering k dimensions need to apply the BSVA method. Then the cosine-on-pedestal weighting function is

$$A(f) = \prod_{i=1}^{k} \left[1 + 2w_i \cos\left(2\pi \frac{f}{f_s} \right) \right] \qquad s.t. \quad 0 \le w_i \le 0.5 \tag{2.23}$$

  Taking inverse Fourier transform on the above weighting function and convolved with raw data, the weighted result can be expressed as

$$\begin{aligned} g'[m_1, m_2, ..., m_k] = g[m_1, m_2, ..., m_k] \otimes (\delta[m_1] + w_1(\delta[m_1 - l] + \delta[m_1 + l])) \otimes \\ ... \otimes (\delta[m_k] + w_k(\delta[m_k - l] + \delta[m_k + l])) \end{aligned} \tag{2.24}$$

  The optimal weighted result is still to minimize the problem $|g'[m_1, m_2, ..., m_k]|^2$ subject to the constraints:

$$\begin{aligned} \underset{w_i}{\text{minimize}} \quad & \left| g'[m_1, m_2, ..., m_k] \right|^2 \\ \text{s.t.} \quad & 0 \le (w_1, w_2, ..., w_k) \le 1/2 \end{aligned} \tag{2.25}$$

  There are several ways to solve the above problem.

– Multi-dimensions coupled
considering all the dimensions coupled, then $w_1 = w_2 = ... = w_k$ and denote them as w. Still considering I/Q separately, the steps to perform the BSVA method for considering coupling are as follows.

1) Compute w_0 obtained by setting equation (2.24) equal to zero. We will get two w_0. If the two are real-valued and either one is in the interval $[0, 1/2]$, then $g'[m_1, m_2, ..., m_k] = 0$;
2) Otherwise, compute w_e obtained by setting equal to zero the partial derivative of $|g'[m_1, m_2, ..., m_k]|^2$ with respect to w. Compute $g'[m_1, m_2, ..., m_k]$ with $w = \{0, 1/2, w_e\}$ and select the one with minimum absolute value.

– Multi-dimensions uncoupled
Actually, the constraints form a multi-dimensional polyhedron and $g'[m_1, m_2, ..., m_k]$ is linear for each w_i. Therefore, the maximum value and the minimum value of $g'[m_1, m_2, ..., m_k]$ occur at the vertices of the polyhedron. And since $g'[m_1, m_2, ..., m_k]$ is monotonic for each w_i, it goes through zero if and only if it has a sign-change within the interval. Then the steps of this approach are as follows.

1) Compute $g'[m_1, m_2, ..., m_k]$ for each vertices of the polyhedron composed of all the w_i. If any of the results have the opposite sign with $g[m_1, m_2, ..., m_k]$, then set $g'[m_1, m_2, ..., m_k] = 0$;
2) Otherwise, select the one with minimum absolute value from the results at all vertices.

– Multi-dimensional independently and in parallel
Except considering the dimensions coupled and uncoupled, we can perform BSVA method on each dimensional data independently and in parallel and then take the minimum of these results. The steps of this approach are as follow.

1) Compute $g'[m_1, m_2, ..., m_k]$ for $(w_1, ..., w_i ..., w_k) = (0, ..., 1/2, ...0)$ where i is from 1 to k. If any of the results have the opposite sign with $g[m_1, m_2, ..., m_k]$, then set $g'[m_1, m_2, ..., m_k] = 0$;
2) Otherwise, select the oe with minimum absolute value from all the results.

Next, we will take the 2D implementation of the BSVA method as an example to go into details of the dimensional simultaneous case.

Considering two dimensions to apply BSVA method. The weighting function (2.23) becomes

$$\begin{aligned} A(f) = &\left[1 + 2w_1 \cos\left(2\pi \frac{f}{f_s}\right)\right] \cdot \left[1 + 2w_2 \cos\left(2\pi \frac{f}{f_s}\right)\right] \\ s.t. \quad &0 \le w_1 \le 0.5, \quad 0 \le w_2 \le 0.5 \end{aligned} \tag{2.26}$$

Then after taking inverse Fourier transform on the above function and convolevd with the unweighted data, the equation (2.24) becomes

$$\begin{aligned} g'[m_1, m_2] =& g[m_1, m_2] \otimes (\delta[m_1] + w_1(\delta[m_1 - l] + \delta[m_1 + l])) \\ &\otimes (\delta([m_2] + w_2(\delta[m_2 - l] + \delta[m_2 + l])) \\ =& g[m1, m2] + w_1 w_2 P + w_1 Q_1 + w_2 Q_2 \end{aligned} \tag{2.27}$$

with

$$\begin{aligned} Q_1 &= g[m_1 - l, m_2] + g[m_1 + l, m_2] \\ Q_2 &= g[m_1, m_2 - l] + g[m_1, m_2 + l] \\ P &= g[m_1 - l, m_2 - l] + g[m_1 - l, m_2 + l] + g[m_1 + l, m_2 - l] + g[m_1 + l, m_2 + l] \end{aligned} \tag{2.28}$$

The minimization problem (2.25) becomes

$$\begin{aligned} \underset{w_1, w_2}{\text{minimize}} \quad & \left| g'[m_1, m_2] \right|^2 \\ \text{s.t.} \quad & 0 \le w_1 \le 1/2, \quad \le w_2 \le 1/2 \end{aligned} \tag{2.29}$$

– 2-D coupled
Two dimensions coupled means $w_1 = w_2 = w$. Then the weighted image (2.27) becomes

$$g'[m_1, m_2] = g[m_1, m_2] + w^2 P + wQ \tag{2.30}$$

with

$$Q = Q_1 + Q_2 \tag{2.31}$$

The zeros of $g'[m_1, m_2]$ can be found by setting it equal to zero:

$$\begin{aligned} w_{01} &= \frac{-Q + \sqrt{Q^2 - 4P \cdot g[m_1, m_2]}}{2P} \\ w_{02} &= \frac{-Q - \sqrt{Q^2 - 4P \cdot g[m_1, m_2]}}{2P} \end{aligned} \tag{2.32}$$

If $Q^2 - 4Pg[m_1, m_2] < 0$, then w_{01} and w_{02} are complex values and there is no zeros for $g'[m_1, m_2]$. Then by setting the partial derivative of the problem (2.29) with respect to w equal to zero, we can get its local extremum at $w_e = \frac{-Q}{2P}$.
Then the ultimate weighted result of this case can be expressed as

$$g'[m_1, m_2] = g'_R[m_1, m_2] + j \cdot g'_I[m_1, m_2] \tag{2.33}$$

with

$$g'_R[m_1, m_2] = \begin{cases} 0, & \text{if } Q^2 - 4Pg[m_1, m_2] > 0 \quad \& \quad 0 \le w_{01} \text{ or } w_{02} \le 1/2 \\ \min\left\{ |g'_R[m_1, m_2]| \quad \text{s.t. } w \in \Gamma \right\}, & \text{others.} \end{cases} \tag{2.34}$$

$$g'_I[m_1, m_2] = \begin{cases} 0, & \text{if } Q^2 - 4Pg[m_1, m_2] > 0 \quad \& \quad 0 \le w_{01} \text{ or } w_{02} \le 1/2 \\ \min\left\{ |g'_I[m_1, m_2]| \quad \text{s.t. } w \in \Gamma \right\}, & \text{others.} \end{cases} \tag{2.35}$$

where $\Gamma = \{0, 1/2, w_e\}$.

– 2-D uncoupled
Two dimensions uncoupled means that the weighting coefficients can be different. Then the weighted result is like the function (2.27) and the ultimate result of the minimization problem (2.29) is

$$g'[m_1, m_2] = g'_R[m_1, m_2] + j \cdot g'_I[m_1, m_2] \tag{2.36}$$

with

$$g'_R[m_1,m_2] = \begin{cases} 0, & \text{if } g'_R[m_1,m_2]\cdot g[m_1,m_2] < 0 \quad \text{s.t. } (w_1,w_2)\in\Gamma \\ \min\{|g'_R[m_1,m_2]| \quad \text{s.t. } (w_1,w_2)\in\Gamma\}, & \text{others.} \end{cases} \tag{2.37}$$

$$g'_I[m_1,m_2] = \begin{cases} 0, & \text{if } g'_R[m_1,m_2]\cdot g[m_1,m_2] < 0 \quad \text{s.t. } (w_1,w_2)\in\Gamma \\ \min\{|g'_I[m_1,m_2]| \quad \text{s.t. } (w_1,w_2)\in\Gamma\}, & \text{others.} \end{cases} \tag{2.38}$$

where $\Gamma = \{(0,0),(0,1/2),(1/2,0),(1/2,1/2)\}$.

– 2-D independently and in parellel
In this case, since we treat the two dimensions independently and in parallel, the weighted image can be expressed as

$$\begin{aligned} g'_1[m_1,m_2] &= g[m_1,m_2] + w_1(g[m_1-l,\ m_2] + g[m_1+l,\ m_2]) \\ g'_2[m_1,m_2] &= g[m_1,m_2] + w_2(g[m_1,\ m_2-l] + g[m_1,\ m_2+l]) \end{aligned} \tag{2.39}$$

The two functions can be combined into one:

$$\begin{aligned} g'[m_1,m_2] =& g[m_1,m_2] + w_1(g[m_1-l,m_2] + g[m_1+l,m_2]) \\ &+ w_2(g[m_1,m_2-l] + g[m_1,m_2+l]) \end{aligned} \tag{2.40}$$

We can see that the weighted image function is the same as that of the case I/Q separately and uncoupled. And the result is also similar to that of the uncoupled case, but considering Γ different by ignoring the term $(w_1,w_2) = (1/2,1/2)$. Therefore, the suppression effect of the case I/Q separately and uncoupled is better than the case independently and in parallel.

And from the article [24], we know that considering the suppression performance and the computational efficiency, the best choice for 2-D BSVA method is the case I/Q separately and uncoupled.

The BSVA method requires that it be performed on an integer of multiple Nyquist sampled data. If the data is not sampled at an integer multiple Nyquist frequency, it must be upsampled at an integer rate. However, this process will increase the computation load. Therefore, a more general variant of SVA will be introduced, which can be implemented on any over-sampled data.

2.2.2 General Spatially Variant Apodization

The GSVA method [25] is also considering the three-tap window function with $N_i = 1$, but there is no requirement for the sampling rate. The constraints (2.10) and (2.11) are simplified as

$$a = 1 - 2w\,\mathrm{sinc}\,(l\cdot w_s) \tag{2.41}$$

$$w \geq 0 \tag{2.42}$$

$$w\cdot[\mathrm{sinc}(l\cdot w_s) - \cos(2\pi\cdot w_s)] \leq \frac{1}{2} \tag{2.43}$$

To get a valid upper limit of w in the equation (2.43), there is a hidden limitation of oversampling rate that it should not be over the two times of Nyquist frequency; otherwise, we can not get valid weighting coefficients.

To extend to the more general case of any sampling rate, we can regard the sampling rate as the oversample of the integer multiple of the Nyquist rate. Denote the sampling frequency as f_s, the Nyquist frequency as f_{Ny}. The l' times of Nyquist frequency can be expressed as

$$f_{in} = l' \cdot f_{Ny} \tag{2.44}$$

where l' is an integer. Since we consider the oversampling case, the real sampling freqeuncy f_s should be bigger than f_{in}

$$f_s > f_{in} \tag{2.45}$$

Inserting the equation (2.44) into the above function, we can get

$$l' \leq \left\lfloor \frac{f_s}{f_{Ny}} \right\rfloor \tag{2.46}$$

And since the real sampling freqeuncy f_s should be smaller than the double of f_{in}, we can get

$$f_s < 2 \cdot f_{in} \tag{2.47}$$

Inserting (2.44) into the above function, we can get

$$l' \geq \left\lceil \frac{f_s}{2f_{Ny}} \right\rceil \tag{2.48}$$

The operators $\lfloor\ \rfloor$ and $\lceil\ \rceil$ represent rounding down and rounding up respectively. Then l' could be any integer from $\left\lceil \frac{f_s}{2f_{Ny}} \right\rceil$ to $\left\lfloor \frac{f_s}{f_{Ny}} \right\rfloor$.
Then the equivalent oversampling ratio w_s can be expressed as

$$\begin{aligned} w_s' &= \frac{f_{in}}{f_s} \\ &= \frac{l' \cdot f_{Ny}}{f_s} \end{aligned} \tag{2.49}$$

The equivalent oversampling multiple is

$$k = \frac{1}{w_s'} \tag{2.50}$$

where k is in the interval $(1,2)$.

Then the constraints of GSVA method can be expressed as

$$a = 1 - 2w\mathrm{sinc}\,(w_s) \tag{2.51}$$

$$0 \leq w \leq \frac{\pi w_s'}{2\cos(\pi w_s')[\tan(\pi w_s') - \pi w_s']} \tag{2.52}$$

And the weighted result of the image is

$$\begin{aligned} g_G'[m] &= (1 - 2w(m)\mathrm{sinc}(w_s'))g[m] + w(m)\left(g[m+l'] + g[m-l']\right) \\ &= g[m] + w(m)\left(-2\mathrm{sinc}(w_s')g[m] + g[m+l'] + g[m-l']\right) \end{aligned} \tag{2.53}$$

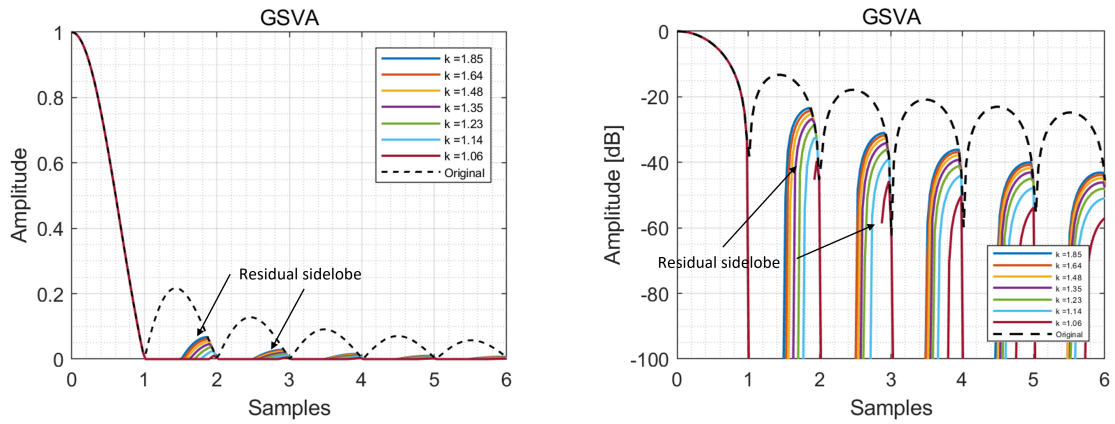

(a) (b)

Figure 2.6: Result of applying the GSVA method on the non-integer Nyquist sampled data with $f_s = 14.8 f_0$. (a) Absolute value, (b) dB.

The GSVA method is performed by minimizing the weighted result (2.53) subject to the constraint (2.52):

$$\begin{aligned} \underset{w(m)}{\text{minimize}} \quad & \left|g'_G[m]\right|^2 \\ \text{s.t.} \quad & 0 \leq w \leq \frac{\pi w'_s}{2\cos(\pi w'_s)[\tan(\pi w'_s) - \pi w'_s]} \end{aligned} \tag{2.54}$$

Calculate the weighted image $g'_G[m]$ for $w = 0$ and $w = w_{max}$ which are the lower and the upper limit in the equation (2.54) respectively and denote them as $g'_{G_1}[m]$ and $g'_{G_2}[m]$. The solution of the above optimization problem can be expressed as

$$g'_G[m] = \begin{cases} 0, & \text{if } g'_{G_1}[m] \cdot g'_{G_2}[m] < 0 \\ \min\{|g'_{G_1}[m]|,\ |g'_{G_2}[m]|\}, & \text{others.} \end{cases} \tag{2.55}$$

What should be noted is that When f_s is over three times of f_{Ny}, l' could be multiple values which result in different oversampling ratio w'_s and multiple choices for the implementation of the GSVA method. The weighted result has some difference for different choice. Later, we will give the explanation for this according to the simulation result.

We use a single matched filtering LFM signal sampled at 14.8 multiple of f_{Ny} to do the simulation. Then $l' = [8, 14]$. Figure 2.6 gives the simulation results before and after applying the GSVA method with all possible w'_s. Obviously, the GSVA method can suppress the sidelobes effectively without expanding the resolution. But there are some residual sidelobes that can not be completely eliminated and with bigger k, the residual sidelobe level goes higher. Although they are with very low intensity, but may appear as artifacts in the output imagery. Therefore, a robust SVA algorithm[26] is presented by Carlos Castillo-Rubio to improve the suppression performance.

2.2.3 Robust Spatially Variant Apodization

The idea for the robust SVA method is to increase the degree of freedom of the cosine-on-pedestal weighting function by extending it from three tap to five tap. Considering $N_i = 2$ in

the equation (2.5) and it becomes

$$A(f) = a + 2w_1 \cos\left(2\pi \frac{f}{f_s}\right) + 2w_2 \cos\left(2\pi \frac{2f}{f_s}\right) \tag{2.56}$$

Then equation (2.4) of RSVA method can be expressed as

$$\begin{aligned} g'_R[m] = g[m] + w_1 \left(-2\mathrm{sinc}(w'_s)g[m] + g[m+l'] + g[m-l']\right) \\ + w_2 \left(-2\mathrm{sinc}(w'_s)g[m] + g[m+2l'] + g[m-2l']\right) \end{aligned} \tag{2.57}$$

Similarly, the result of equation (2.57) can be obtained by solve the minimization problem $|g'_R[m]|^2$ subject to some constraints. Still considering the first constraint in equations (2.10), we can get

$$a = 1 - 2w_1 \mathrm{sinc}(w'_s) - 2w_2 \mathrm{sinc}(2w'_s) \tag{2.58}$$

The second constraint now should satisfy

$$\begin{cases} A(f) \geq 0, & f \in [-f_0/2, f_0/2] \\ \frac{\mathrm{d}A(f)}{\mathrm{d}f} < 0, & f \in [0, f_0/2] \end{cases} \tag{2.59}$$

Inserting (2.56) and (2.58) into the equation (2.59), we can get

$$\begin{gathered} 1 - 2\left(\mathrm{sinc}(w'_s) - \cos\left(\frac{2\pi f}{f_s}\right)\right) \cdot w_1 - 2\left(\mathrm{sinc}(2w'_s) - \cos\left(\frac{4\pi f}{f_s}\right)\right) \cdot w_2 < 0, \\ \text{s.t.} \quad f \in [-f_0/2, f_0/2] \end{gathered} \tag{2.60}$$

$$\begin{gathered} 1 - 2\left(\mathrm{sinc}(w'_s) + \frac{2\pi}{f_s}\sin\left(\frac{2\pi f}{f_s}\right)\right) \cdot w_1 - 2\left(\mathrm{sinc}(2w'_s) + \frac{4\pi}{f_s}\sin\left(\frac{4\pi f}{f_s}\right)\right) \cdot w_2 < 0, \\ \text{s.t.} \quad f \in [0, f_0/2] \end{gathered} \tag{2.61}$$

We can see that the constraints consist of a set of linear inequalities of $\{w_1, w_2\}$. And the valid weighting coefficient pairs lie in the polygon bounded by these straight lines in the $w_1 - w_2$ plane. The task is to find the optimal weighting coefficients w_1 and w_2 in the polygon that can achieve the minimum value of $g'_R[m]$ at each imaging pixel. Since the weighted result $g'_R[m]$ is linear for w_1 and w_2, the extrema can be obtained when $\{w_1, w_2\}$ is at the vertex of the polygon. If the weighted result at any two vertices is of different signs, there must be a pair of $\{w_1, w_2\}$ in the polygon that can make $g'_R[m]$ achieve the minimal value of zero. Otherwise, choose the one of minimum magnitude from the weighted results at all the vertices. However, this means that we should find out all the vertices. Moreover, the computation load will get very high. Therefore, to implement the RSVA method fast, we can do some relaxation on the constraints. After doing some mathematical manipulation, the constraints (2.60) and (2.61) are relaxed to equation (2.11) with some extra restrictions for w_i:

$$0 \leq w_1 \leq 1 \tag{2.62}$$

$$0 \leq w_2 \leq 1 \tag{2.63}$$

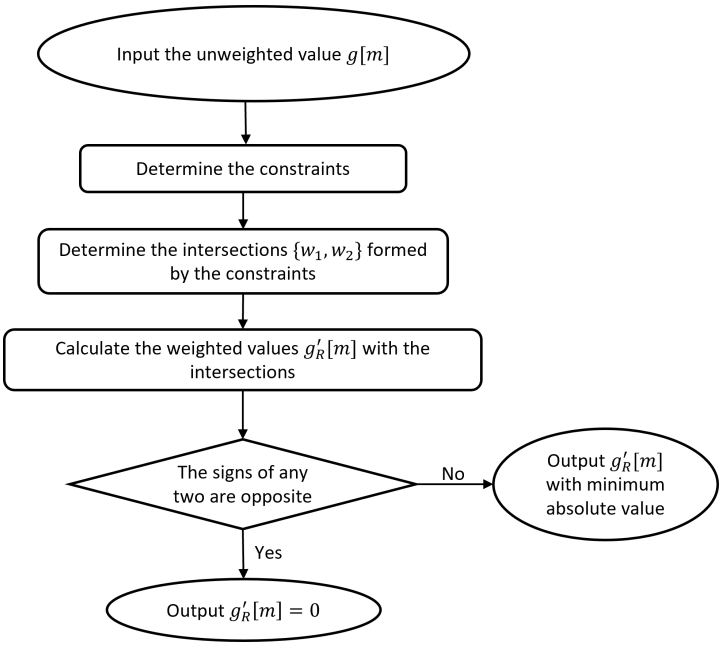

Figure 2.7: The flowchart of Robust SVA method

Then the whole constraints for the robust SVA method can be expressed as

$$w_2 \geq -w_1 \frac{\cos(\pi w'_s) - 1}{\cos(2\pi w'_s) - 1} \tag{2.64}$$

$$w_2 \leq \frac{0.5}{\text{sinc}(2w'_s) - \cos(2\pi w'_s)} - w_1 \frac{\text{sinc}(w'_s) - \cos(\pi w'_s)}{\text{sinc}(2w'_s) - \cos(2\pi w'_s)} \tag{2.65}$$

$$0 \leq w_1 \leq 1 \tag{2.66}$$

$$0 \leq w_2 \leq 1 \tag{2.67}$$

Now, we can solve the minimization problem $|g'_R[m]|^2$ subject to the constraints of equations (2.64) to (2.67). The flowchart of the robust SVA method is shown in Figure 2.7. Still do the simulation on the 14.8 multiple oversampled signal, the weighted result after applying the RSVA method is given in Figure 2.6 with all possible w'_s. Comparing it with Figure 2.6, the residual sidelobes are canceled out. Furthermore, the mainlobe resolution is improved, but the mainlobe energy is a little bit suppressed. Observing the enlarged part in Figure 2.8(a), we can see that with different w'_s, the mainlobe energy suppression is different, so the improved resolution is. In this case, the best choice is with $k = 1.35$ to get the best sidelobe suppression, best mainlobe resolution, and most minor mainlobe energy suppression. However, this does not mean that we can get the best mainlobe resolution and most minor mainlobe energy suppression at the same time. Figure 2.9 gives the simulation result with the same signal sampled at 19.7 multiple of f_{Ny}. Observing the enlarged part in Figure 2.9(a), we can see that the sidelobe suppression is still good, and with $k = 1.41$, we can get the best mainlobe resolution with the worst mainlobe energy. Furthermore, observing Figure 2.8(a) and 2.9(a), we can see that the mainlobe energy suppression is very small and can be ignored. Therefore, choosing the w_s with the best mainlobe resolution is much more critical for the RSVA method. According to the simulation, there is a simple conclusion that for fixed Nyquist frequency and sampling frequency, in general, when l' is equal to the middle integer of its interval, the mainlobe reso-

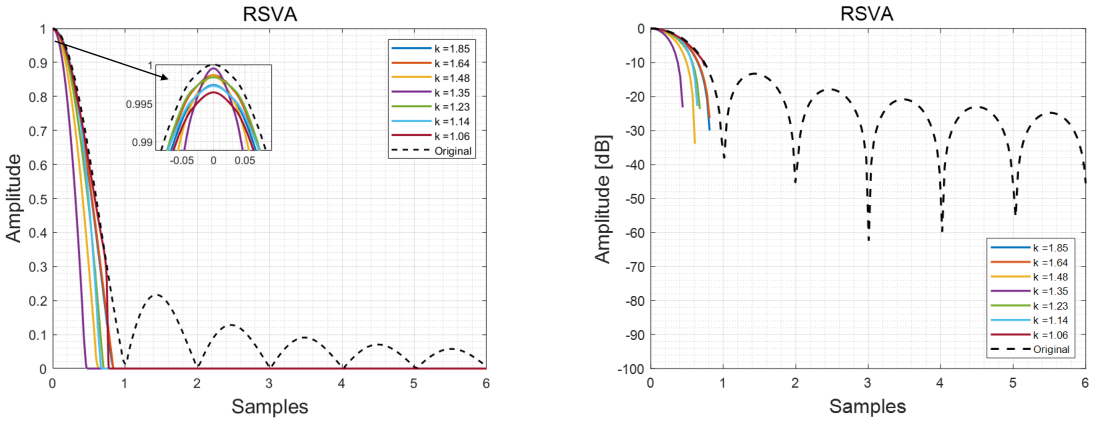

(a) (b)

Figure 2.8: Result of applying the RSVA method on the non-integer Nyquist sampled data with $f_s = 14.8 f_{Ny}$. (a) Absolute value, (b) dB.

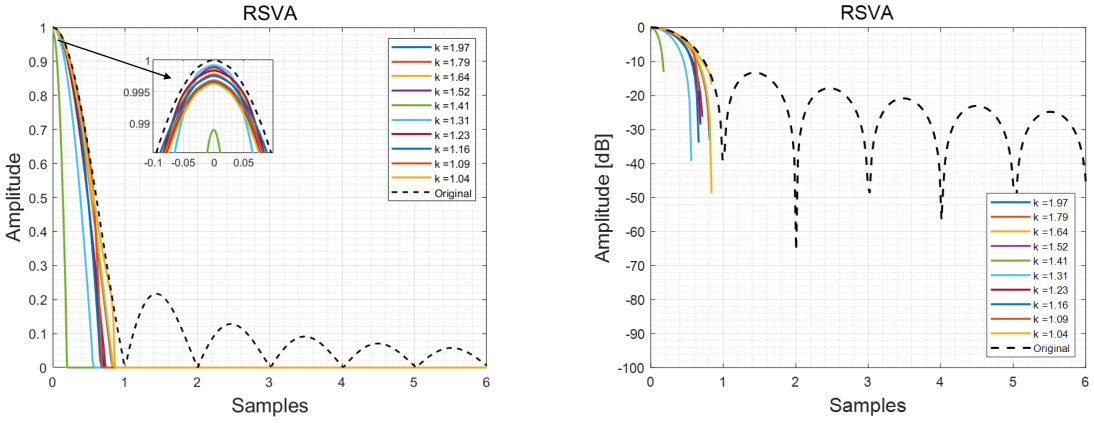

(a) (b)

Figure 2.9: Result of applying the RSVA method on the non-integer Nyquist sampled data with $f_s = 19.7 f_{Ny}$. (a) Absolute value, (b) dB.

lution can get to the best.

Actually, during the implementation of the RSVA method, the vertices of the polygon bounded by the constraints are obtained by calculating the intersections of any two straight lines of $\{w_1, w_2\}$ in the equations (2.64) to (2.67). However, some intersections are not in the polygon. When $g[m]$ is in the mainlobe, and the minimum value from the weighted result $g'_R[m]$ at all the vertices is smaller than the original one, the mainlobe energy will be reduced. Moreover, the RSVA method requires a strict sinc kernel. Otherwise, the mainlobe may deteriorate rapidly, and the target will disappear due to the relaxation of the constraints. Therefore, Chong Ni, et al. presented a modified SVA (MSVA) method based on the RSVA method.

2.2.4 Modified Spatially Variant Apodization

The MSVA method discusses different situations of the polygon to determine the valid vertices. For example, figure 2.10(a) and 2.10(b) show two possible polygons. Cons1 and Cons2

in the figures are the straight lines of taking the equality of the equation (2.64) and (2.65) respectively. The square bounded by two dashed lines shows the polygon of constraints (2.66) and (2.67).

Case 1 is under the situation that $k = 1.35$, while case 2 is with $k = 1.41$. The shadow shows the valid polygon of the weighting coefficient pair $\{w_1, w_2\}$. The orange points are the vertices of the valid polygon, while the purple points are the invalid intersections. The two figures show that the shape of the valid polygon is determined by the sampling frequency and the Nyquist frequency. Therefore, by discussing different cases, we can determine the valid intersections. This process is linear programming. And this method is called the modified SVA method.

The weighted result of applying the MSVA method on the data oversampled at 14.8 times of Nyquist sampling frequency is shown in figure 2.11. Comparing it with the weighted result of the RSVA method shown in Figure 2.8, we can see that the mainlobe energy is overall improved, although it is still a little bit reduced due to the relaxation of the constraints. And

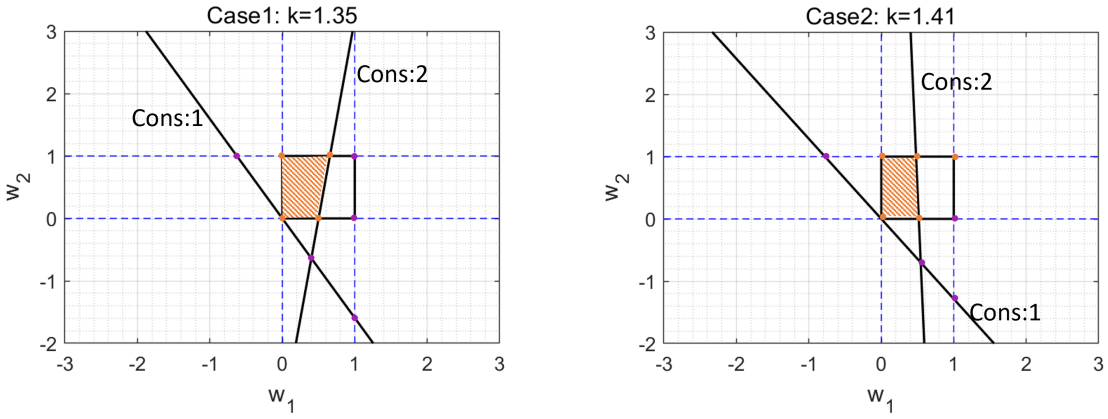

(a) (b)

Figure 2.10: The valid polygon of the weighting coefficients. (a) Case 1 with $k = 1.35$ for $f_s = 14.8 f_{Ny}$, (b) Case 2 with $k = 1.41$ for $f_s = 19.7 f_{Ny}$

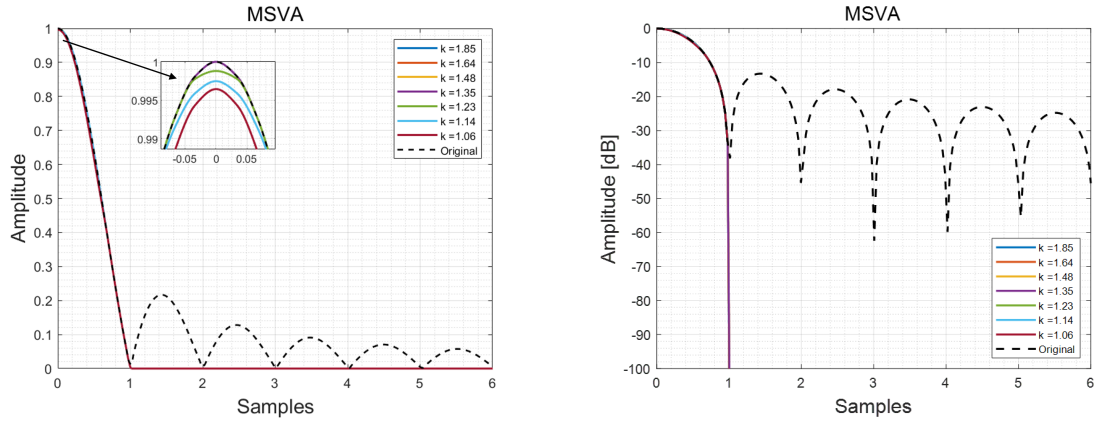

(a) (b)

Figure 2.11: Result of applying the MSVA method on the non-integer multiple Nyquist sampled data with $f_s = 14.8 f_{Ny}$. (a) Absolute value, (b) dB.

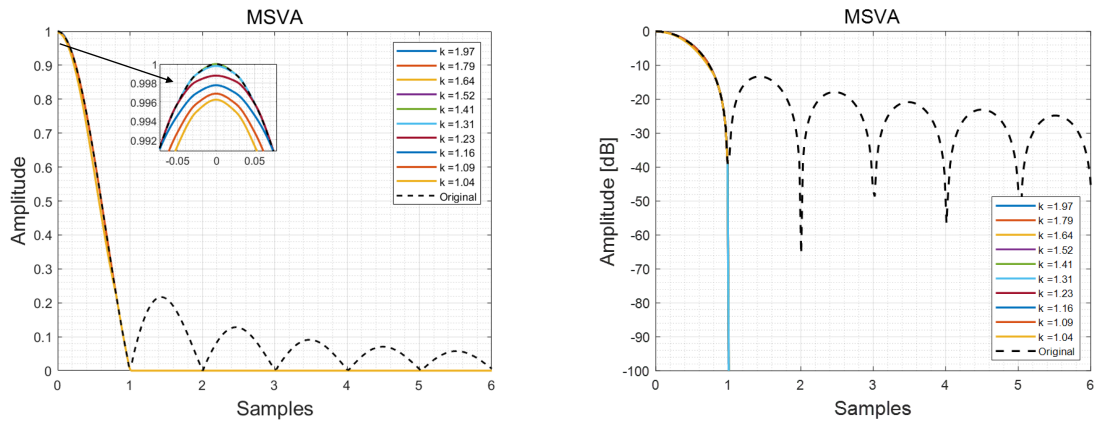

(a) (b)

Figure 2.12: Result of applying the MSVA method on the non-integer multiple Nyquist sampled data with $f_s = 19.7 f_{Ny}$. (a) Absolute value, (b) dB.

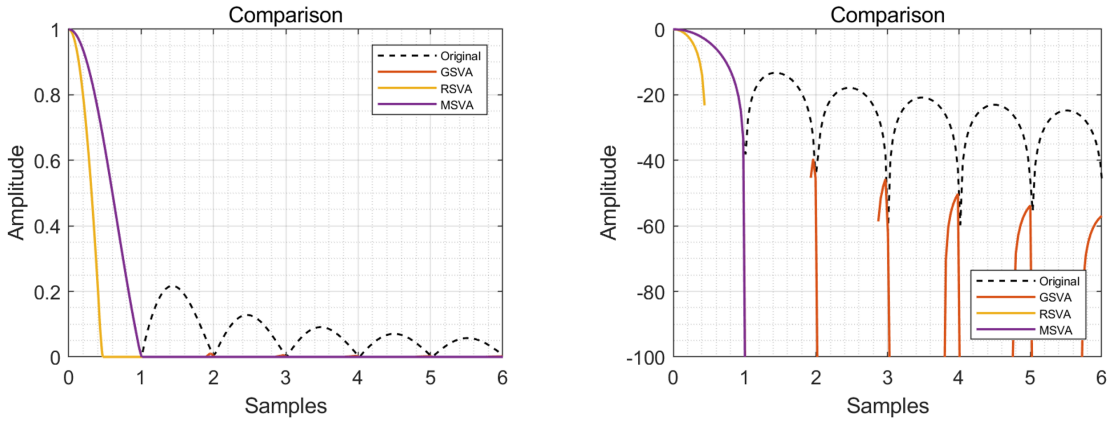

(a) (b)

Figure 2.13: Comparison of applying different methods on the non-integer multiple Nyquist sampled data with $f_s = 14.8 f_{Ny}$: the best choice of GSVA with $k = 1.06$; the best choice for RSVA, and MSVA with $k = 1.35$. (a) Absolute value, (b) dB.

there is no mainlobe resolution improvement, but it keeps unchanged compared with the original one. Still, we also give the simulation result of the RSVA method applied on the LFM signal sampled at 17.9 times of f_{Ny}, which is shown in Figure 2.12. According to large simulation for different f_s, we can simply conclude that when l' takes the median value of its interval, the mainlobe energy is the best and almost equal to the original value.

Observing Figure 2.8 and 2.11, we can see that the best choice of RSVA and MSVA method for signal sampled at $f_s = 14.8 f_{Ny}$ is with $k = 1.35$. Similarly, observing Figure 2.9 and 2.12, the best choice for $f_s = 19.7 f_{Ny}$ is with $k = 1.41$. The comparison of the GSVA, RSVA and MSVA method for the two cases is shown in Figure 2.11and 2.12 .

In conclusion, the amplitude weighting, BSVA, GSVA, RSVA, and MSVA methods all work for sidelobe suppression. The amplitude method has a limited suppression effect meanwhile broadening the mainlobe . The BSVA method can suppress the sidelobe completely without broadening the mainlobe but with the condition that the data should be sampled at an integer multiple of the Nyquist sampling frequency. Otherwise, the data must be up-sampled

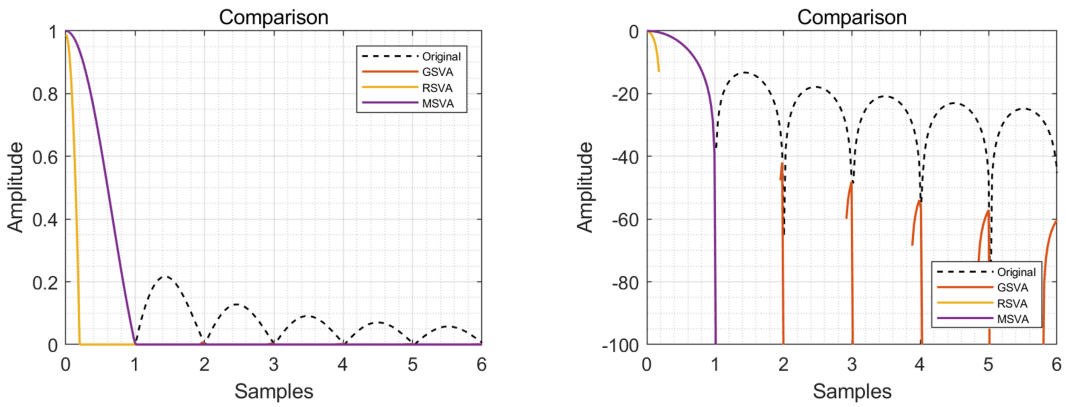

Figure 2.14: Comparison of applying different methods on the non-integer multiple Nyquist sampled data with $f_s = 19.7 f_{Ny}$: the best choice of GSVA with $k = 1.04$; the best choice for RSVA, and MSVA with $k = 1.31$. (a) Absolute value, (b) dB.

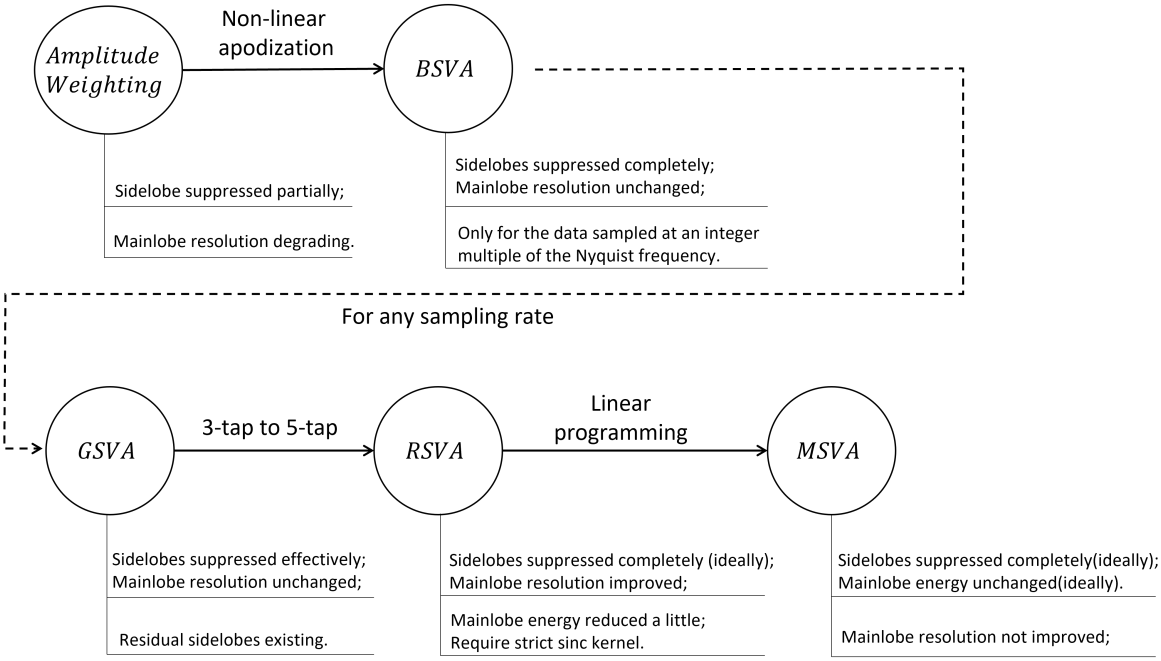

Figure 2.15: Comparison of different weighting methods

to an integer rate. To implement the SVA method at any sampling rate, the GSVA method was proposed, but some residual sidelobes exist. The RSVA method considers a more robust situation to solve the residual sidelobe by expanding 3-tap SVA to 5-tap. It gives better sidelobe suppression performance than the GSVA method, and with some w_s, it can improve the mainlobe resolution. However, it may reduce the mainlobe energy. In addition, the performance of the RSVA method relies on the information of the strict sinc kernel. Otherwise, the target may be disappearing due to the relaxed constraints. Therefore, based on the RSVA method, the MSVA method was proposed to maintain the mainlobe energy and give a more robust result. The relationships and characteristics of these methods are shown in Figure 2.15.

2.3 Spatially Variant Apodization for resolution improvement

Besides sidelobe suppression, the SVA method also can be applied to improve the resolution. This section will simply introduce two variants of the SVA methods that work for resolution improvement.

2.3.1 Super Spatially Variant Apodization

The super-SVA method improves the resolution for SAR imagery by extrapolating sparse sub-apertures into a full aperture without requiring any prior knowledge of scene content or point scatterer modeling [28], [29]. Actually, the super-SVA method is an iterative process of the SVA method [30]. From section 2.2, we know that after applying the SVA method, all the sidelobe in the image can be removed ideally and only maintain the mainlobe. Then perform an inverse Fourier transform on the SVA image. In this case, the frequency band is extended compared with the original. The next step is to apply inverse weighting and truncation to keep the total extrapolation below 60% of the original spectrum [31]. This is to avoid singularity over the extrapolated aperture. Then, replace the center portion with the original signal. Now, the new frequency spectrum is formed, and applying Fourier transform, a new sinc function with a narrower mainlobe can be obtained. Applying the SVA method again, the sidelobe suppressed and narrower mainlobe image can be achieved.

Furthermore, the above procedure can be repeated several times, and finally, we will get a super-resolved image. This is called the super-SVA method. Stankwitz et al. have pointed that if the extrapolation process is repeated n times by a factor k, the total extrapolation factor would be $K = k^n$. Therefore, two iterations with each extrapolation factor $k = \sqrt{2}$ can achieve an extrapolated aperture by a factor of two [31].

2.3.2 Three Quarter Spatially Variant Apodization

3/4 SVA method is also to improve the contrast and resolution for SAR imagery. The image data can be represented by an array of complex values. Here, the size of the array before processing with Fourier transform is referred to as the aperture. Generally, the oversampled image is preferred. Therefore, the aperture filling ratio is commonly 1/2 or higher, where the integer represents the amount of the oversampling. A larger integer means more zero filling and this requires more memory load. Furthermore, since the processing time is three times of the number of pixels with the SVA method, larger oversampling means a higher computation load. Therefore, 3/4 SVA is proposed to implement the SVA algorithm efficiently under a 3/4 aperture filling ratio. First, the data should be oversampled by a 4/3 ratio and zero-filled and then take Fourier transform to the space domain. Next, the data will be convolved with two 3x3 kernels spaced four samples apart and two samples apart respectively. And make a decision based on the results. The details of the super-SVA can be found in the patent [32].

2.4 Summary

This chapter introduces the non-linear apodization method from the dual apodization to the basic spatially variant apodization. The BSVA method is based on the integer multiple of Nyquist sampled data, and it can improve the image quality by suppressing the sidelobe level meanwhile maintaining the mainlobe resolution. Moreover, several SVA variants under non-

integer multiple of Nyquist sampling frequency are summarized and compared. The GSVA method retains some residual sidelobes, while the RSVA method suppresses the sidelobes completely and improves the resolution under some conditions. However, the peak magnitude is a little bit reduced. The MSVA method suppresses the sidelobes completely and maintains the peak magnitude (ideally) while the mainlobe resolution is not improved. Lastly, we introduce two other SVA variants for resolution improvement. In conclusion, the SVA method is efficient and easy to implement for high image quality.

3

SVA method for 1-D MIMO Array Imaging

For a MIMO array, the antenna elements are separated as transmitters and receivers that only transmit or receive signals. The analysis of the wavenumber domain spectrum for a MIMO array is therefore complicated compared with a uniformly linear array or synthetic aperture radar. However, when applying the SVA method, it is crucial to analyze the wavenumber domain spectrum. In addition, to suppress the sidelobe level in the cross-range and range directions, we need to perform wavenumber domain spectrum analysis in each direction. This chapter analyzes how to realize sidelobe suppression via the basic SVA method on 1-D MIMO array imaging. In section 3.1, the signal model and the imaging method of the generalized matched filtering (GMF) will be introduced. In section 3.2, based on GMF method, the analysis and simulation of the BSVA method in the cross-range direction will be discussed. An analysis and simulation of the BSVA method in the range direction will be discussed in section 3.3. Section 3.4 gives the implementation in both directions. The acceleration approach is provided in Section 3.5 via the BSVA, GSVA and MSVA methods. The conclusion is drawn in Section 3.6.

3.1 1-D MIMO Array Imaging

Linear sparse periodic array (SPA) is a commonly used 1-D MIMO array in near-field imaging application [33], [34]. For a properly configured SPA array with N_t transmit elements and N_r receive elements, if the transmit spacing is d_t, the receive spacing is $d_r = N_t \cdot d_t$. The equivalent virtual array consists of $N_{ev} = N_t \cdot N_r$ elements with a spacing of $d_{ev} = d_t$. Thus, it can achieve high resolution with a large virtual aperture. The geometry of SPA is shown in Figure 3.1.

3.1.1 Signal Model

Assume the sparse periodic array is on the x-axis. The position of the m_{th} transmit antenna is $u_m = (u_{mx}, 0)$, the n_{th} receive antenna is $v_n = (v_{nx}, 0)$. There is a point target $P = (x_p, y_p)$ in the spatial $x-y$ domain. Consider the linear frequency modulation (LFM) signal as the transmit signal and generate the echo signal in frequency domain:

$$s(f, u_m, v_n) = \sum_i \delta(f - f_i) e^{-j2\pi f \tau} \tag{3.1}$$

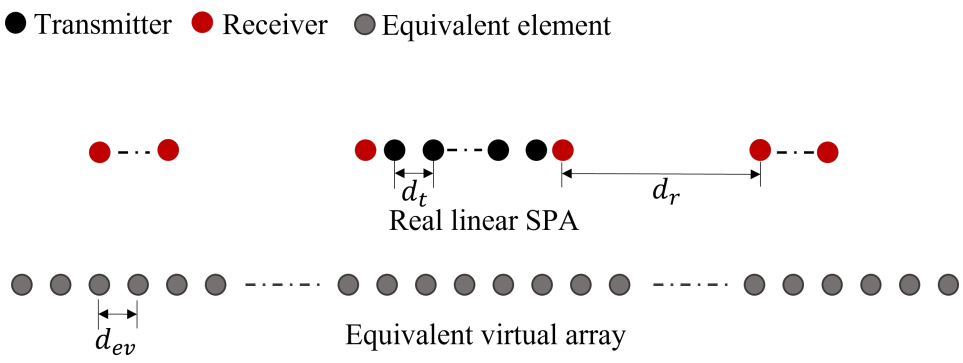

Figure 3.1: 1-D sparse periodic array

where $f_i = [f_{min}, f_{max}]$ is the signal frequency band, τ is the time delay from the target to the pair T/R antennas. And τ can be expressed as

$$\begin{aligned}\tau &= \left(\sqrt{(x_p - u_{mx})^2 + y_p^2} + \sqrt{(x_p - v_{nx})^2 + y_p^2}\right)/c \\ &= r_T/c + r_R/c\end{aligned} \tag{3.2}$$

Then, the echo signal can be denoted as

$$s(k, u_m, v_n) = \sum_i \delta(k - k_i) e^{-jkr_T} e^{-jkr_R} \tag{3.3}$$

where $k = [k_{min}, k_{max}]$ is the wavenumber under the wide-band measurement, r_T and r_R are the distances of the target w.r.t a transmitter and a receiver.

3.1.2 Generalized Matched Filtering

The Generalized matched filtering (GMF) method is a kind of novel imaging method [22] which is based on the original matched filtering (OMF) method. Assume the position of an arbitrary imaging pixel is $p_0 = (x_0, y_0)$. The imaging result of OMF can be expressed as

$$g(x_0, y_0) = \sum_k \sum_{u_m} \sum_{v_n} s(k, u_m, v_n) e^{jk\left(\sqrt{(u_{mx} - x_0)^2 + y_0^2} + \sqrt{(v_{nx} - x_0)^2 + y_0^2}\right)} \tag{3.4}$$

The phase term is the two-way phase delay of the signal between each pair T/R antennas to the imaging pixel.

For GMF method, we consider two different pixels at the same height $P_1(x_T, y_0)$ and $P_2(x_R, y_0)$. x_T and x_R denote the azimuth imaging positions corresponding to the transmit array and receive array, respectively. The imaging result of GMF is about one-way phase delay w.r.t. a transmitter or a receiver and can be formulated as

$$g(x_T, x_R|_{y=y_0}) = \sum_k \sum_{u_m} \sum_{v_n} s(k, u_m, v_n) e^{jk\left(\sqrt{(u_{mx} - x_T)^2 + y_0^2} + \sqrt{(v_{nx} - x_R)^2 + y_0^2}\right)} \tag{3.5}$$

In this case, at each height, the imaging result of the GMF method will form a 2-D plane about x_T and x_R as shown in Figure 3.2. The diagonal of the plane, namely $x_T = x_R = x$ is the imaging

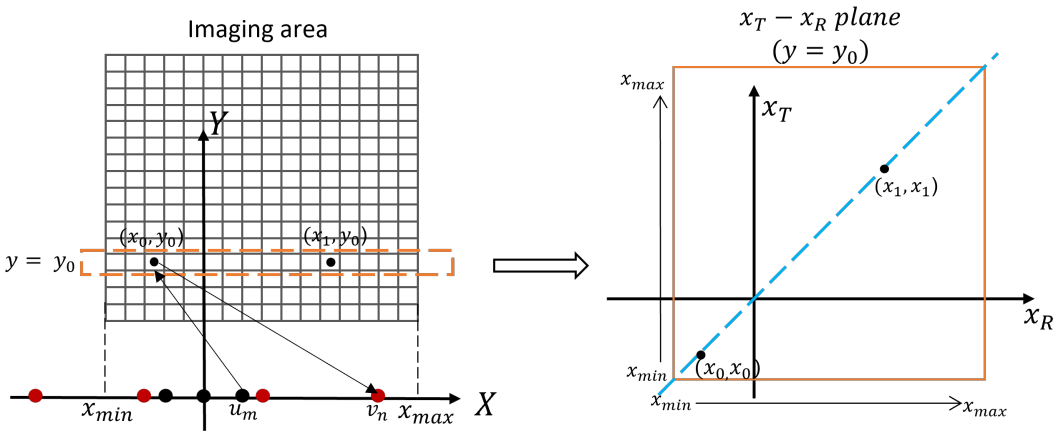

Figure 3.2: GMF imaging

result of the original matched filtering. Therefore, for the GMF imaging method about MIMO array, we can separately consider the matching about the transmit array and the receive array. This is of great benefit for the following wavenumber analysis and the application of the BSVA method.

3.2 BSVA in the Cross-range Direction

To suppress the grating lobes and side lobes via the BSVA method in the cross-range direction, we should first analyze the cross-range wavenumber spectrum and then deduce how to implement the BSVA method. Finally, verify the suppression effect by doing the numerical simulation in MATLAB.

3.2.1 Cross-range Wavenumber Spectrum Analysis

From the equation (3.5), we know that the imaging result of GMF is the sum related to each transmitter and receiver for each wavenumber. According to the discrete convolution principle [35], equation (3.5) can be expressed as

$$g\left(x_T, x_R|_{y=\ y_0}\right) = \sum_k s\left(k, x_T, x_R\right) \otimes_{x_T} e^{jk\sqrt{x_T^2+y_0^2}} \otimes_{x_R} e^{jk\sqrt{x_R^2+y_0^2}} \tag{3.6}$$

where $\otimes_{x_T}$ and $\otimes_{x_R}$ denote the convolution operation about x_T and x_R, respectively.

According to the Fourier transform [35], the convolution operation in the space domain is equal to the multiplication in the wavenumber domain. Thus, the corresponding wavenumber spectrum of equation (3.6) can be expressed as

$$G\left(k_{u_m}, k_{v_n}\right) = \mathscr{F}\left\{s\left(k, x_T, x_R\right)\right\} \cdot \mathscr{F}_{x_T}\left\{e^{jk\sqrt{x_T^2+y_0^2}}\right\} \cdot \mathscr{F}_{x_R}\left\{e^{jk\sqrt{x_R^2+y_0^2}}\right\} \tag{3.7}$$

where $\mathscr{F}$ represents Fourier transform. Considering the explicit expression of the above Fourier transform function, denote $\mathscr{F}\{s(k, x_T, x_R)\} = S(k, k_{u_m}, k_{v_n})$ and

$$\begin{aligned} \mathscr{F}_{x_T}\left(e^{jk\sqrt{x_T^2+y_0^2}}\right) &= \int_{-\infty}^{+\infty} e^{jk\sqrt{x_T^2+y_0^2}} \times e^{-jk_{u_m}x_T}\,\mathrm{d}x_T \\ &= \int_{-\infty}^{+\infty} e^{-j\left(k\sqrt{x_T^2+y_0^2}-k_{u_m}x_T\right)}\,\mathrm{d}x_T \end{aligned} \tag{3.8}$$

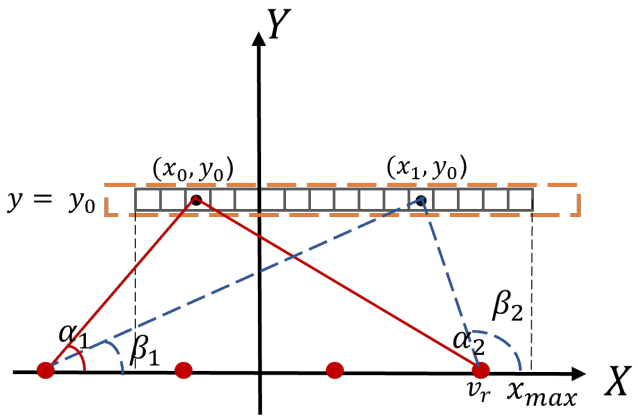

Figure 3.3: GMF of the receiving array

where k_{u_m} is the wavenumber domain variable of m_{th} transmitter corresponding to the cross-range imaging domain x_T. According to stationary phase principle [36], the above integral is significantly non-zero at the point where the phase variation rate is zero in the integral x_T domain, namely the phase is stationary. Denote this point as x'_T and it can be found by

$$\left.\frac{\partial\left[k\sqrt{x_T^2+y_0^2}-k_{u_m}x_T\right]}{\partial x_T}\right|_{x_T=x'_T}=0 \tag{3.9}$$

Then the explicit representation of the integral equation (3.8) can be obtained as follows:

$$\mathscr{F}_{x_T}\left(e^{jk\sqrt{x_T^2+y_0^2}}\right)=e^{-j\pi/4}\cdot\frac{e^{j\sqrt{k^2-k_{u_m}^2}y_0}}{\sqrt{k^2-k_{u_m}^2}} \tag{3.10}$$

Similarly considering stationary phase on x_R domain and ignoring the amplitude fluctuation, the equation (3.7) can be explicitly expressed as

$$G\left(k_{u_m},k_{v_n}\right)=S\left(k,k_{u_m},k_{v_n}\right)e^{j\sqrt{k^2-k_{u_m}^2}y_0}e^{j\sqrt{k^2-k_{v_n}^2}y_0} \tag{3.11}$$

with

$$k_{u_m}=k\cdot\frac{x_0-u_{mx}}{\sqrt{\left(x_0-u_{mx}\right)^2+y_0^2}} \tag{3.12}$$

$$k_{v_n}=k\cdot\frac{x_0-v_{nx}}{\sqrt{\left(x_0-v_{nx}\right)^2+y_0^2}} \tag{3.13}$$

From equation (3.12) and (3.13), we can know that the fraction term is the cosine value of the angle formed by the point and the m_{th} transmitter or n_{th} receiver concerning the positive direction of x-axis. Therefore, the value range of the cross-range wavenumber of transmit array k_u and receive array k_v are determined by the leftmost antenna u_{xl} and v_{xl} and the rightmost antenna u_{xr} and v_{xr} concerning the transmit array and receive array respectively. Figure 3.3 shows the angles formed by two different points concerning receive array, which determine the

minimum and maximum cross-range wavenumber value. Furthermore, since the wavenumber k is not a single value, therefore, to express the support of k_{u_m} and k_{v_n}, take $k_c = \frac{1}{2}(k_{min} + k_{max})$ to approximate:

$$\text{supp}\,(k_u) = \begin{cases} 1, & k_c \frac{x_0 - u_{xr}}{\sqrt{(x_0 - u_{xr})^2 + y_0^2}} \leq k_u \leq k_c \frac{x_0 - u_{xl}}{\sqrt{(x_0 - u_{xl})2 + y_0^2}} \\ 0, & \text{otherwise} \end{cases} \tag{3.14}$$

$$\text{supp}(k_v) = \begin{cases} 1, & k_c \frac{x_0 - v_{xr}}{\sqrt{(x_0 - v_{xr})^2 + y_0^2}} \leq k_v \leq k_c \frac{x_0 - v_{xl}}{\sqrt{(x_0 - v_{xl})^2 + y_0^2}} \\ 0, & \text{otherwise} \end{cases} \tag{3.15}$$

Then the widths of the cross-range wavenumber spectral of k_u and k_v can be obtained by

$$B_{k_u}(x_0) = k_c \left(\frac{x_0 - u_{xl}}{\sqrt{(x_0 - u_{xl})^2 - y_0^2}} - \frac{x_0 - u_{xr}}{\sqrt{(x_0 - u_{xr})^2 + y_0^2}} \right) \tag{3.16}$$

$$B_{k_v}(x_0) = k_c \left(\frac{x_0 - v_{xl}}{\sqrt{(x_0 - v_{xl})^2 + y_0^2}} - \frac{x_0 - v_{xr}}{\sqrt{(x_0 - v_{xr})^2 + y_0^2}} \right) \tag{3.17}$$

And the central positions of the two supports can be obtained by

$$k_{u,c}\,(x_0) = \frac{k_c}{2} \left(\frac{x_0 - u_{xl}}{\sqrt{(x_0 - u_{xl})^2 + y_0^2}} + \frac{x_0 - u_{xr}}{\sqrt{(x_0 - u_{xr})^2 + y_0^2}} \right) \tag{3.18}$$

$$k_{v,c}\,(x_0) = \frac{k_c}{2} \left(\frac{x_0 - v_{xl}}{\sqrt{(x_0 - v_{xl})^2 + y_0^2}} + \frac{x_0 - v_{xr}}{\sqrt{(x_0 - v_{xr})^2 + y_0^2}} \right) \tag{3.19}$$

From the above equations, it is clear that the width and the central position of the cross-range wavenumber spectrum are related to the point position. As shown in Figure 3.4, the widths of the cross-range wavenumber spectrum of point x_0 and x_1 w.r.t the receive array are different, so are central-wavenumber positions. This shows that the cross-range wavenumber spectrum of MIMO array imaging is spatially variant which is different from SAR imaging. And this is the key problem need to be solved when applying the BSVA method for MIMO array imaging.

3.2.2 Implementation

Phase compensation

From chapter 2, we know that the SVA method employs a cosine-on-pedestal weighting function in the frequency domain. The width of the window is determined by the frequency band, and the window is symmetric about zero-frequency. From the last section, we know how to calculate the width of the cross-range wavenumber spectrum. However, for those pixels not on the center line of the array, the central-wavenumber deviates from the zero-wavenumber position. Therefore, one crucial step is to shift the cross-range wavenumber spectrum to align the zero-wavenumber center as shown in Figure 3.5.

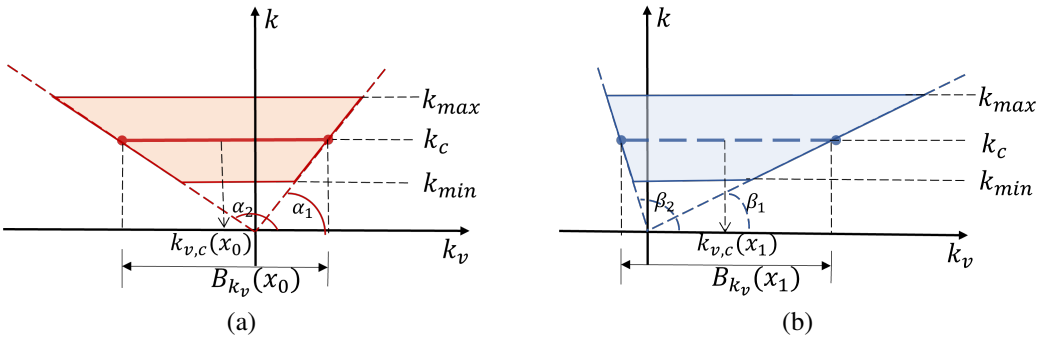

Figure 3.4: Cross-range wavenumber spectrum concerning receive array. (a) of point (x_0, y_0), (b) of point (x_1, y_0).

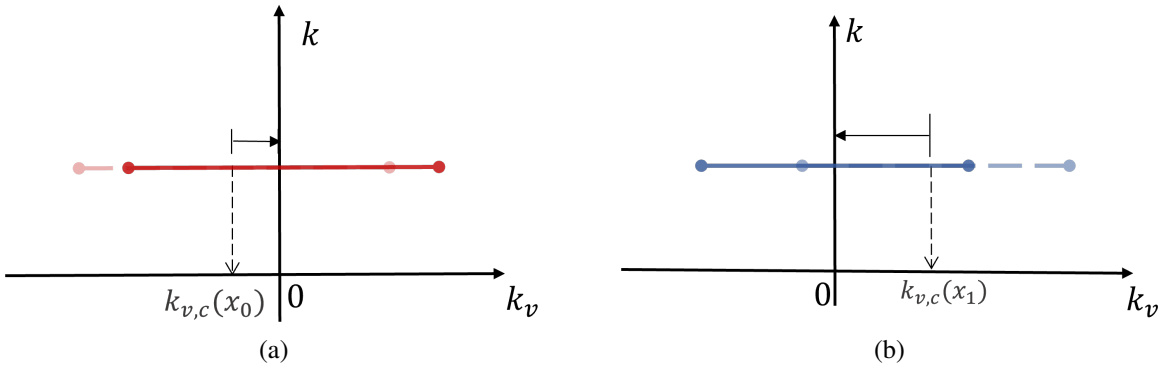

Figure 3.5: Alignment of the central wavenumber. (a) of point (x_0, y_0), (b) of point (x_1, y_0).

According to the Fourier transform pair

$$f(t)e^{j\omega_0 t} \overset{\mathscr{F}}{\Longleftrightarrow} F(\omega - \omega_0) \tag{3.20}$$

the shift in the frequency domain will lead to an exponential term in the time domain. Therefore, to apply the 2-D BSVA method in $x_T - x_R$ plane, we first need to compensate the following two exponential terms along the two axes in the space domain to align central-wavenumber to the zero-wavenumber position.

$$g(x_T)\, e^{-jk_{u,c}(x_0)x_T} \overset{\mathscr{F}}{\Longleftrightarrow} G\left(k_u(x_0) + k_{u,c}(x_0)\right) \tag{3.21}$$

$$g(x_R)\, e^{-jk_{v,c}(x_0)x_R} \overset{\mathscr{F}}{\Longleftrightarrow} G\left(k_v(x_0) + k_{v,c}(x_0)\right) \tag{3.22}$$

Denote the total compensating phase term as $\varphi(x_T, x_R)$, then the compensating exponential term can be expressed as

$$e^{-j\varphi(x_T,x_R)} = e^{-j[k_{u,c}(x_0)x_T + k_{v,c}(x_0)x_R]} \tag{3.23}$$

However, we cannot directly calculate its value, since each point at the same height of x_0 will generate an exponential term at the point (x_T, x_R). Therefore, considering Fourier series expansion to approximate, the compensating phase term can be obtained by satisfying the following conditions:

$$\begin{cases} \frac{\partial \varphi(x_T,x_R)}{\partial x_T}|_{x_T=x_0} = k_{u,c}(x_0), \\ \frac{\partial \varphi(x_T,x_R)}{\partial x_R}|_{x_R=x_0} = k_{v,c}(x_0). \end{cases} \tag{3.24}$$

Inserting equation (3.18) and (3.19) into the above equation (3.24), the compensating phase term can be solved as

$$\begin{aligned}\varphi\left(x_T,x_R\right) = & \frac{k_c}{2}\left[\sqrt{\left(x_T-u_{xr}\right)^2+y_0^2}+\sqrt{\left(x_T-u_{xl}\right)^2+y_0^2}\right] \\ & +\frac{k_c}{2}\left[\sqrt{\left(x_R-v_{xr}\right)^2+y_0^2}+\sqrt{\left(x_R-v_{xl}\right)^2+y_0^2}\right]\end{aligned} \tag{3.25}$$

Then the compensated imaging result can be obtained by

$$g_C\left(x_T,x_R|_{y=y_0}\right) = g\left(x_T,x_R|_{y=y_0}\right)e^{-j\varphi(x_T,x_R)} \tag{3.26}$$

Implementation of 2-D BSVA method

Now, the central position of the wavenumber spectra for different points are aligned at the zero-wavenumber position and we can deduce the 2-D BSVA method implementation in the space domain.

From the introduction of 2-D BSVA method in chapter 2, the cosine-on-pedestal weighting function can be expressed as

$$\begin{gathered}A\left(k_u,k_v\right) = \left[1+2w\left(x_T\right)\cos\left(\frac{2\pi k_u}{B_{k_u}\left(x_T\right)}\right)\right]\times\left[1+2w\left(x_R\right)\cos\left(\frac{2\pi k_v}{B_{k_v}\left(x_R\right)}\right)\right] \\ \text{s.t.}\quad 0<w(x_T)<0.5,\ 0<w(x_R)<0.5\end{gathered} \tag{3.27}$$

where $w(x_T)$ and $w(x_R)$ are weighting coefficients in domain k_u and k_v, respectively. Taking inverse Fourier transform(IFT) on the above weighting function yields:

$$a(x_T,x_R) = a(x_T)\otimes a(x_R) \tag{3.28}$$

with

$$\begin{aligned}a(x_T) = & \ \delta\left[x_T\right]+w(x_T)\delta\left[x_T-\frac{2\pi}{B_{k_u}(x_T)}\right]+w(x_T)\delta\left[x_T+\frac{2\pi}{B_{k_u}(x_T)}\right] \\ a(x_R) = & \ \delta[x_R]+w(x_R)\delta\left[x_R-\frac{2\pi}{B_{k_v}(x_R)}\right]+w(x_R)\delta\left[x_R+\frac{2\pi}{B_{k_v}(x_R)}\right]\end{aligned} \tag{3.29}$$

where $\otimes$ denotes the convolution operation. Then the weighted imaging result $\tilde{g}_C$ can be expressed as

$$\tilde{g}_C\left(x_T,x_R|_{y=\,y_0}\right) = g_C\left(x_T,x_R\right)+w\left(x_T\right)w\left(x_R\right)P+w\left(x_T\right)Q_T+w\left(x_R\right)Q_R \tag{3.30}$$

with

$$\begin{aligned}Q_T = & \ g_C\left(x_T-\frac{2\pi}{B_{k_u}\left(x_T\right)},x_R\right)+g_C\left(x_T+\frac{2\pi}{B_{k_u}\left(x_T\right)},x_R\right) \\ Q_R = & \ g_C\left(x_T,x_R-\frac{2\pi}{B_{k_v}\left(x_R\right)}\right)+g_C\left(x_T,x_R+\frac{2\pi}{B_{k_v}\left(x_R\right)}\right) \\ P = & \ g_C\left(x_T-\frac{2\pi}{B_{k_u}\left(x_T\right)},x_R-\frac{2\pi}{B_{k_v}\left(x_R\right)}\right)+g_C\left(x_T+\frac{2\pi}{B_{k_u}\left(x_T\right)},x_R+\frac{2\pi}{B_{k_v}\left(x_R\right)}\right) \\ & +g_C\left(x_T-\frac{2\pi}{B_{k_u}\left(x_T\right)},x_R+\frac{2\pi}{B_{k_v}\left(x_R\right)}\right)+g_C\left(x_T+\frac{2\pi}{B_{k_u}\left(x_T\right)},x_R-\frac{2\pi}{B_{k_v}\left(x_R\right)}\right)\end{aligned} \tag{3.31}$$

The task now is to find the minimum value of $\tilde{g}_C$ subject to its constraints. The constrained minimization problem is

$$\begin{aligned} \underset{w(x_T),w(x_R)}{\text{minimize}} \quad & \left|\tilde{g}_C\left(x_T,x_R|_{y=y_0}\right)\right|^2 \\ \text{s.t.} \quad & 0<w(x_T)<0.5, \\ & 0<w(x_R)<0.5 \end{aligned} \tag{3.32}$$

Considering I/Q separately, take the real component and imaginary component of the compensated imaging result in the problem respectively, and the output is

$$g_{\text{out}}\left(x_T,x_R|_{y=y_0}\right)=g_{\text{out}}^R\left(x_T,x_R|_{y=y_0}\right)+jg_{\text{out}}^I\left(x_T,x_R|_{y=y_0}\right) \tag{3.33}$$

with

$$g_{\text{out}}^R\left(x_T,x_R|_{y=y_0}\right)=\begin{cases} 0, & \text{if } \tilde{g}_C^R\left(x_T,x_R|_{y=y_0}\right)\cdot g_C^R\left(x_T,x_R|_{y=y_0}\right)<0 \quad \text{s.t. } (w(x_T),w(x_R))\in\Gamma \\ \min\left\{\tilde{g}_C^R\left(x_T,x_R|_{y=y_0}\right)||\,(w(x_T),w(x_R))\in\Gamma\right\}, & \text{others} \end{cases} \tag{3.34}$$

$$g_{\text{out}}^I\left(x_T,x_R|_{y=y_0}\right)=\begin{cases} 0, & \text{if } \tilde{g}_C^I\left(x_T,x_R|_{y=y_0}\right)\cdot g_C^I\left(x_T,x_R|_{y=y_0}\right)<0 \quad \text{s.t. } (w(x_T),w(x_R))\in\Gamma \\ \min\left\{\tilde{g}_C^I\left(x_T,x_R|_{y=y_0}\right)||\,(w(x_T),w(x_R))\in\Gamma\right\}, & \text{others} \end{cases} \tag{3.35}$$

where $\Gamma=\{(0,0),(0,0.5),(0.5,0),(0.5,0.5)\}$. Now,we can get the weighted result of x_T-x_R plane at height $y=y_0$. Taking $x_T=x_R=x_0$ which is on the diagonal line, the ultimate weighted imaging result at point (x_0,y_0) can be obtained by

$$g_{\text{out}}(x_0,y_0)=g_{\text{out}}\left(x_0,x_0|_{y=y_0}\right) \tag{3.36}$$

Similarly, taking other diagonal values in the x_T-x_R plane at height $y=y_0$, the weighted imaging result of MIMO array imaging at height $y=y_0$ via BSVA method can be obtained. Repeat the above operations at each height of the imaging area; the ultimate image after suppressing sidelobes and grating lobes can be obtained.

3.2.3 Numerical Simulation

Simulation Setup

The numerical simulation is carried out in MATLAB. The sparse periodic MIMO array consists of nine transmit elements with an interval of 2mm and ten receive elements with an interval of 18 mm. The structure of the MIMO array is shown in Figure 3.6(a). Seven point targets are distributed in the $x-y$ plane, and two of them are weak targets with 0.2 times the signal strength compared with others. The ground truth of the point targets is shown in Figure 3.6(b). These targets are illuminated by a stepped-frequency continuous wave (SFCW) signal from 120 GHz to 150 GHz with steps of 150 MHz. The imaging area is $0.3\,\text{m}\times 0.3\,\text{m}$ with 301×301 samples. All the parameters are listed in Table 3.1.

Table 3.1: Parameters of simulations

Parameters	**Values**
Frequency band f	120 – 150 GHz
Frequency interval df	150 MHz
Transmit interval d_{Tx}	2 mm
Receive interval d_{Rx}	18 mm
Number of transmitters N_{Tx}	9
Number of receivers N_{Rx}	10
Imaging area X	[-0.15 0.15]
Imaging area Y	[0.3 0.6]
Grid spacing d_X	1 mm
Grid spacing d_Y	1 mm
Image samples	301×301
Targets positions	(0.1,0.35); (0,0.35); (0,0.45); (0.01,0.45); (0,0.46); (0,0.55); (-0.1,0.55)
Targets power	[1; 1; 1; 0.2; 0.2; 1; 1]

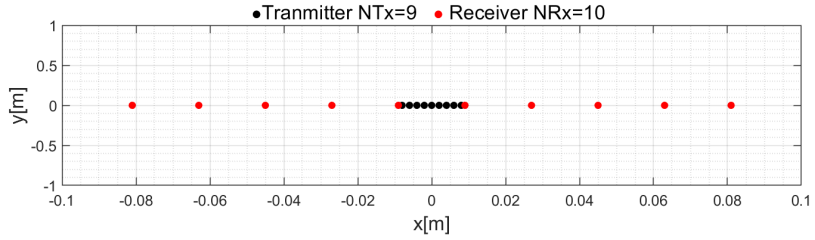

(a)

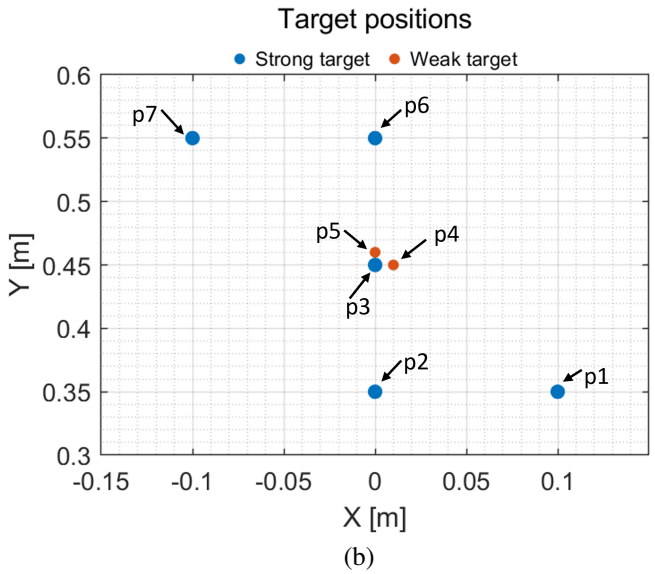

(b)

Figure 3.6: Simulation setup. (a) 1-D MIMO array Topology. (b) Target positions.

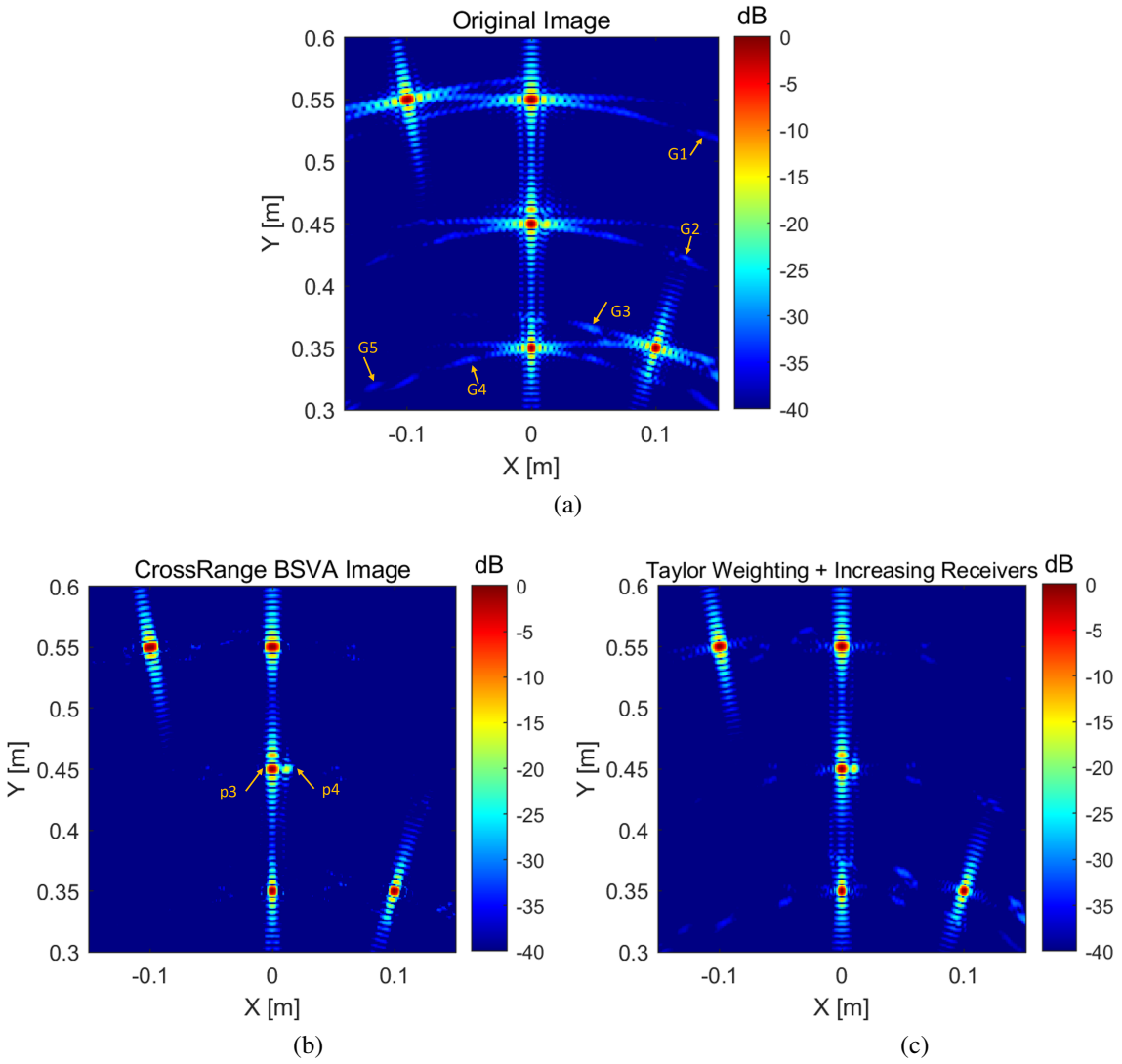

Figure 3.7: Imaging results. (a) The original image. (b) Cross-range sidelobe suppression via BSVA method. (c) Cross-range sidelobe suppression with Taylor weighting on the receiver array and increasing four receivers.

Simulation Result

The simulation result of the original image is shown in Figure 3.7(a). It can be seen that the grating lobes and the sidelobes are pretty high that the weak target p_4 is submerged in the sidelobe of the strong target p_3 and can not be distinguished. After applying the BSVA method in the cross-range direction as shown in Figure 3.7(b), the grating lobe level and the sidelobe level are significantly reduced without spreading the mainlobe, and the weak target p_4 can be resolved now.

Here, the aperture weighting method [13] with increasing four receivers to maintain the main lobe resolution is compared. The result is shown in Figure 3.7(c). Compared with the original imaging result, this method also shows a good sidelobe suppression effect. However, there are some residual sidelobes, and the grating lobe level is still pretty high compared with the SVA result.

In order to clearly illuminate this, the grating lobe level of four grating lobes is listed in Table 3.2. It shows that the BSVA method has a better grating lobe suppression effect. It has

Table 3.2: Grating lobe level

	Original	Aperture Weighting +Increasing receivers	BSVA
G_1 [dB]	-34.72	-37.93	-40.18
G_2 [dB]	-32.18	-35.00	-36.36
G_3 [dB]	-29.44	-31.18	-37.09
G_4 [dB]	-32.44	-35.20	-Inf
G_5 [dB]	-34.95	-37.27	-45.77

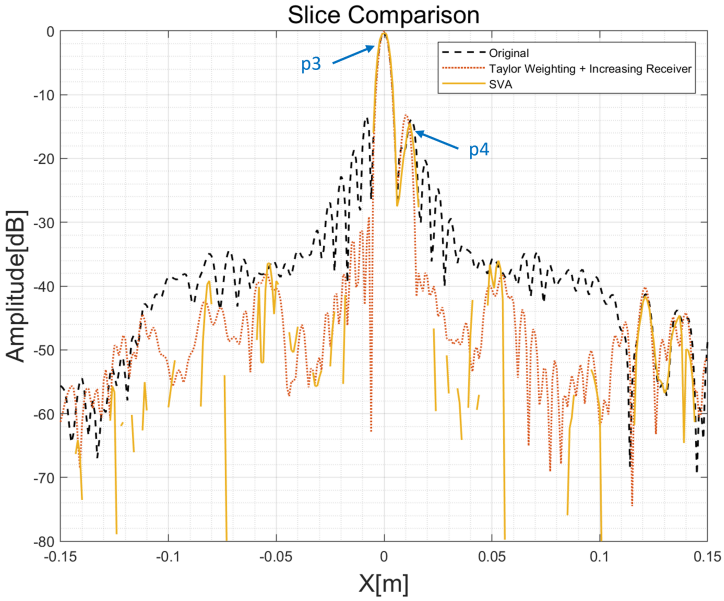

Figure 3.8: Slice comparison at $y = 0.45\,\text{m}$.

reduced by at least 4.18 dB with the BSVA method, compared with 1.74 dB with the aperture weighting method.

Furthermore, the slice along cross-range direction at height $y = 0.45\,\text{m}$ is given in Figure 3.8. The result shows that the sidelobe suppression effect of the SVA method is better than the aperture weighting method. What should be noted is that with the SVA method, the point p_3 is a little bit offset from its true position. The reason is that the SVA method relies on phase information, and the phase of the weak target is interfered by the strong closely spaced target destructively or constructively. Then its position may be a little bit offset, or even it may be split into two.

3.3 BSVA in the Range Direction

From the last section, we implement and verify the suppression effect of the BSVA method in the cross-range direction. Generally, for the range direction, we add a non-rectangular window function on the data to suppress the sidelobes. However, the price is sacrificing the range resolution, which also degrades the imaging quality, especially for close targets in the range direction.

Observing the imaging figures in the last section, we know that the sidelobes in the range

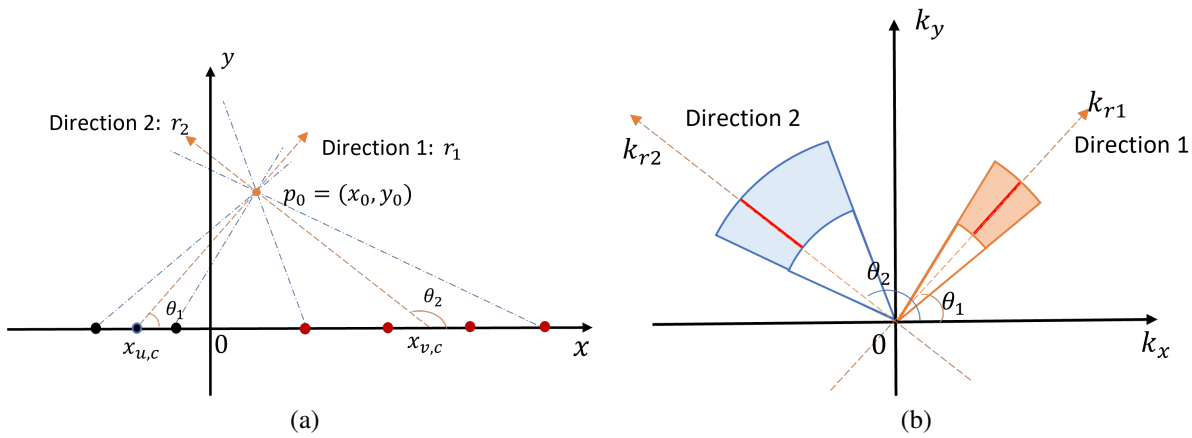

Figure 3.9: Range direction analysis. (a) 1-D MIMO array imaging of p_0. (b) Wavenumber spectrum of p_0.

direction are along with the directions from the center of the transmit array and receive array to the target. Therefore, in principle, the BSVA method can also be used in the range direction. From Figure 3.6(a), we can see that the center of transmit array and receive array are coincident at zero. Considering more general cases, assume they are located at different positions on the x-axis as shown in Figure 3.9a. In this section, we start by analyzing the wavenumber spectrum and then deduce the implementation of the BSVA method in the range direction. Lastly, do the numerical simulation in MATLAB.

3.3.1 Range Wavenumber Spectrum Analysis

Assume that an arbitrary point p_0 is located at (x_0, y_0). As shown in Figure 3.9(a), the sidelobe directions of p_0 will be along the direction 1 (r_1) with angle θ_1 and direction 2 (r_2) with angle θ_2. The whole wavenumber of the transmit and receive array about p_0 is shown in Figure 3.9(b). What should be noted is that here the wavenumber spectrum is about $k_x - k_y$ domain, which is different from the analysis of the cross-range wavenumber spectrum. The whole wavenumber spectrum of the MIMO array is complicated. However, as we know that the sidelobe is along the direction from the array center to the point, it makes sense to take the propagation direction from the array center (shown as the red line segment) to approximate. Furthermore, the support of the wavenumber spectrum along the range direction is the same for any point, but with different direction.

The support of wavenumber spectrum of the transmit array and the receive array are expressed as

$$\text{supp}(k_{r_1}) = \begin{cases} 1, & k_{min} < k_{r_1} < k_{max} \\ 0, & \text{otherwise} \end{cases} \tag{3.37}$$

$$\text{supp}(k_{r_2}) = \begin{cases} 1, & k_{min} < k_{r_2} < k_{max} \\ 0, & \text{otherwise} \end{cases} \tag{3.38}$$

where k_{min} and k_{max} are the minimum value and maximum value of the wavenumber. k_{r_1} and k_{r_2} are the wavenumber of the transmit and the receive array with directions determined by θ_1 and θ_2, respectively. Therefore, the widths of the wavenumber k_{r_1} and k_{r_2} are the same and

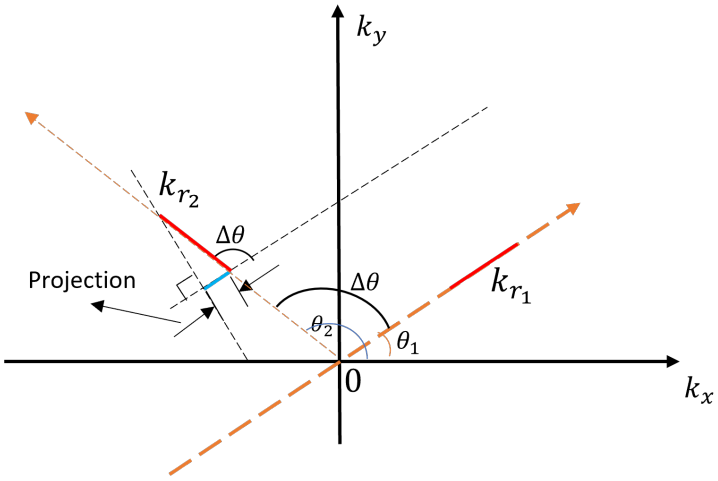

Figure 3.10: Wavenumber projection

denoted as B_{k_r}:

$$\begin{aligned} B_{k_r} &= B_{k_{r_1}} \\ &= B_{k_{r_2}} \\ &= k_{max} - k_{min} \end{aligned} \tag{3.39}$$

And the central-wavenumber can be obtained by

$$\begin{aligned} k_{r,c} &= k_{r_1,c} \\ &= k_{r_2,c} \\ &= (k_{max} + k_{min})/2 \end{aligned} \tag{3.40}$$

Since the wavenumber of the transmit and receive array are not orthogonal, one wavenumber will influence another one. For example, as shown in Figure 3.10, the projection of the wavenumber of receive array k_{r_2} to the direction r_1 will make the total width of wavenumber in the direction r_1 longer than $B_{k_{r_1}}$. The angle $\Delta\theta$ formed between the two directions is determined by

$$\Delta\theta = |\theta_2 - \theta_1| \tag{3.41}$$

Then the total width of the wavenumber spectrum in the direction r_1 can be obtained by

$$B'_{k_{r_1}} = B_{k_{r_1}} + \Delta B_{k_r} \tag{3.42}$$

with

$$\Delta B_{k_r} = B_{k_{r_2}} \times |\cos(\Delta\theta)| \tag{3.43}$$

Inserting (3.39) and (3.43) into equation (3.42), we can see that the width of the wavenumber spectrum along the two sidelobe directions are the same:

$$B'_{k_r} = B_{k_r} \times (1 + |\cos(\Delta\theta)|) \tag{3.44}$$

3.3.2 Implementation

Phase compensation

According to equation (3.40), it is obvious that the central position of the range wavenumber spectrum is not at zero-wavenumber position which need to be aligned before applying the BSVA method.

For an arbitrary point $p_0 = (x_0, y_0)$, the distances to the transmit and receive array center are

$$r_1 = \sqrt{(x_0 - x_{u,c})^2 + y_0^2} \tag{3.45}$$

$$r_2 = \sqrt{(x_0 - x_{v,c})^2 + y_0^2} \tag{3.46}$$

According to the analysis of phase compensation deduced in section 3.2.2, the compensating phase term can be formulated by

$$\varphi = k_{r,c} \cdot (r_1 + r_2) \tag{3.47}$$

Then the compensated imaging result is

$$g_C(x_0, y_0) = g(x_0, y_0) e^{-j\varphi} \tag{3.48}$$

Implementation of 2-D BSVA method

When dealing with the implementation in the cross-range direction, we apply I/Q separately, 2-D simultaneously, and uncoupled BSVA method to suppress the sidelobe and grating lobe level. For the range problem, since we have two sidelobe directions, in principle, we can also form a 2-D plane of r_1 and r_2. However, since the imaging area is constructed according to Cartesian coordinates and the two range directions are not orthogonal with the axes, the process will be complicated to operate. Combining the introduction of the multi-dimensional SVA method in section 2.2.1, the BSVA method in the two range directions can be implemented independently and in parallel.

Firstly, we deduce the BSVA implementation in the two range directions independently. The cosine-on-pedestal weighting function of 1-D BSVA method applying in the range directions is

$$A(k_{r_1}) = 1 + 2w_1(r_1)\cos\left(\frac{2\pi k_{r_1}}{B'_{k_r}}\right) \quad \text{s.t.} \quad 0 < w_1(r_1) < 0.5 \tag{3.49}$$

$$A(k_{r_2}) = 1 + 2w_2(r_2)\cos\left(\frac{2\pi k_{r_2}}{B'_{k_r}}\right) \quad \text{s.t.} \quad 0 < w_2(r_2) < 0.5 \tag{3.50}$$

Doing IFT of the above functions, the weighting function in the space domain are

$$a(r_1) = \delta[r_1] + w_1(r_1)\delta\left[r_1 - \frac{2\pi}{B'_{k_r}}\right] + w_1(r_1)\delta\left[r_1 + \frac{2\pi}{B'_{k_r}}\right] \tag{3.51}$$

$$a(r_2) = \delta[r_2] + w_2(r_2)\delta\left[r_2 - \frac{2\pi}{B'_{k_r}}\right] + w_2(r_2)\delta\left[r_2 + \frac{2\pi}{B'_{k_r}}\right] \tag{3.52}$$

Denote $d_r = \frac{2\pi}{B'_{k_r}}$, then the above weighting function can be expressed in Cartesian coordinates:

$$\begin{aligned} a_1(x_0,y_0) =& \delta[x_0,y_0] + w_1(x_0,y_0)\delta[x_0 - d_r\cos(\theta_1),\ y_0 - d_r\sin(\theta_1)] \\ &+ w_1(x_0,y_0)\delta[x_0 + d_r\cos(\theta_1),\ y_0 + d_r\sin(\theta_1)] \end{aligned} \tag{3.53}$$

$$\begin{aligned} a_2(x_0,y_0) =& \delta[x_0,y_0] + w_2(x_0,y_0)\delta[x_0 - d_r\cos(\theta_2),\ y_0 - d_r\sin(\theta_2)] \\ &+ w_2(x_0,y_0)\delta[x_0 + d_r\cos(\theta_2),\ y_0 + d_r\sin(\theta_2)] \end{aligned} \tag{3.54}$$

Then the weighted imaging result can be obtained by

$$\begin{aligned} g'_C(x_0,y_0) &= g_C(x_0,y_0) \otimes a_1(x_0,y_0) \\ &= g_C(x_0,y_0) + w_1(x_0,y_0)P_1 + w_1(x_0,y_0)P_2 \end{aligned} \tag{3.55}$$

$$\begin{aligned} g'_C(x_0,y_0) &= g_C(x_0,y_0) \otimes a_2(x_0,y_0) \\ &= g_C(x_0,y_0) + w_2(x_0,y_0)Q_1 + w_2(x_0,y_0)Q_2 \end{aligned} \tag{3.56}$$

with

$$\begin{aligned} P_1 &= g_C(x_0 - d_r\cos(\theta_1),\ y_0 - d_r\sin(\theta_1)) \\ P_2 &= g_C(x_0 + d_r\cos(\theta_1),\ y_0 + d_r\sin(\theta_1)) \end{aligned} \tag{3.57}$$

$$\begin{aligned} Q_1 &= g_C(x_0 - d_r\cos(\theta_2),\ y_0 - d_r\sin(\theta_2)) \\ Q_2 &= g_C(x_0 + d_r\cos(\theta_2),\ y_0 + d_r\sin(\theta_2)) \end{aligned} \tag{3.58}$$

Then combining equation (3.55) and (3.56), the BSVA method in the two range directions can be implemented simultaneously. The ultimate weighted imaging result can be expressed as

$$\tilde{g}_C(x_0,y_0) = g_C(x_0,y_0) + w_1(x_0,y_0)(P_1+P_2) + w_2(x_0,y_0)(Q_1+Q_2) \tag{3.59}$$

The task now is to solve the following problem:

$$\begin{aligned} \underset{w_1,w_2}{\text{minimize}} \quad & |\tilde{g}_C(x_0,y_0)|^2 \\ \text{s.t.} \quad & 0 < w_1(x_0,y_0) < 0.5, \\ & 0 < w_2(x_0,y_0) < 0.5 \end{aligned} \tag{3.60}$$

Still considering I/Q separately, the output of the above problem is

$$g_{\text{out}}(x_0,y_0) = g^R_{\text{out}}(x_0,y_0) + g^I_{\text{out}}(x_0,y_0) \tag{3.61}$$

with

$$g^R_{\text{out}}(x_0,y_0) = \begin{cases} 0, & \text{if } \tilde{g}^R_C(x_0,y_0)\cdot g^R_C(x_0,y_0) < 0, \quad \text{s.t. } (w_1,w_2) \in \Gamma_1 \\ \min\left\{\tilde{g}^R_C(x_0,y_0) || (w_1,w_2) \in \Gamma_2\right\}, & \text{otherwise} \end{cases} \tag{3.62}$$

$$g^I_{\text{out}}(x_0,y_0) = \begin{cases} 0, & \text{if } \tilde{g}^I_C(x_0,y_0)\cdot g^I_C(x_0,y_0) < 0, \quad \text{s.t. } (w_1,w_2) \in \Gamma_1 \\ \min\left\{\tilde{g}^I_C(x_0,y_0) || (w_1,w_2) \in \Gamma_2\right\}, & \text{otherwise} \end{cases} \tag{3.63}$$

where $\Gamma_1 = [(0,0.5),(0.5,0)]$ and $\Gamma_2 = [(0,0),(0.5,0),(0.5,0.5)]$. Repeat the above process on each pixels, then we can implement the sidelobe suppression along the range directions.

3.3.3 Numerical Simulation

The parameters for MATLAB simulation is the same as that in Table 3.1. The simulation result of the image applying the BSVA method in the range direction is shown in Figure 3.11(a). Furthermore, Hamming weighting method in the range direction is shown in Figure 3.11(b) as a comparison. Comparing the two figures with Figure 3.7(a), we can see that both methods can suppress the sidelobe in the range direction effectively. However, the weak target p_5 can not be distinguished due to the mainlobe spreading with Hamming window. While with the BSVA method, the mianlobe maintains unchanged, then p_5 can be resolved from the sidelobes of the strong target p_3.

To show this clearly, Figure 3.12 gives the slice at $X = 0\,\text{m}$. It is more clear that for the window method, the mianlobe is spreading. In contrast, the BSVA method maintains the mainlobe resolution unchanged. Therefore, the weak closely spaced target can be distinguished. Moreover, Table 3.3 gives the specific parameters to compare the performance of window method and BSVA method. We can see that the PSLR of the proposed method provides a sidelobe reduction of around 20 dB without degrading the range resolution, while the window method provides a sidelobe reduction of around 18 dB with the mainlobe spreading 1.49 times.

3.4 BSVA in Two Directions

Now, we implement the BSVA method in the cross-range direction and range direction, respectively. To suppress the sidelobes and grating lobes in the two dimensions, we need to

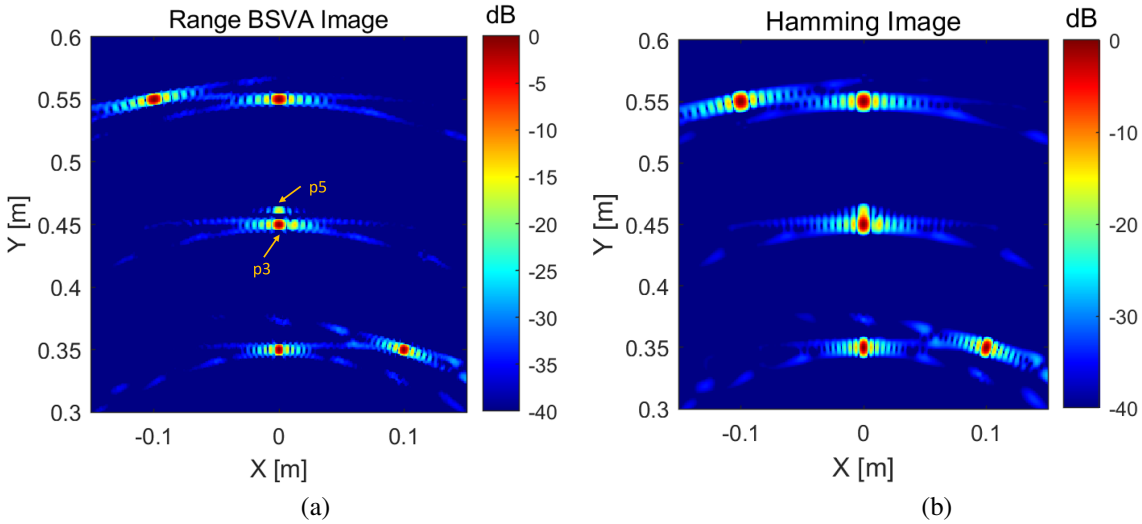

Figure 3.11: Images of sidelobe suppression in the range direction. (a) Image with BSVA method. (b) Image with Hamming weighting.

Table 3.3: Performance comparison

	Original	**Hamming**	**BSVA**
PSLR[dB]	-13.34	-31.76	-34.16
Resolution(-3dB) [mm]	4.3	6.4	4.3

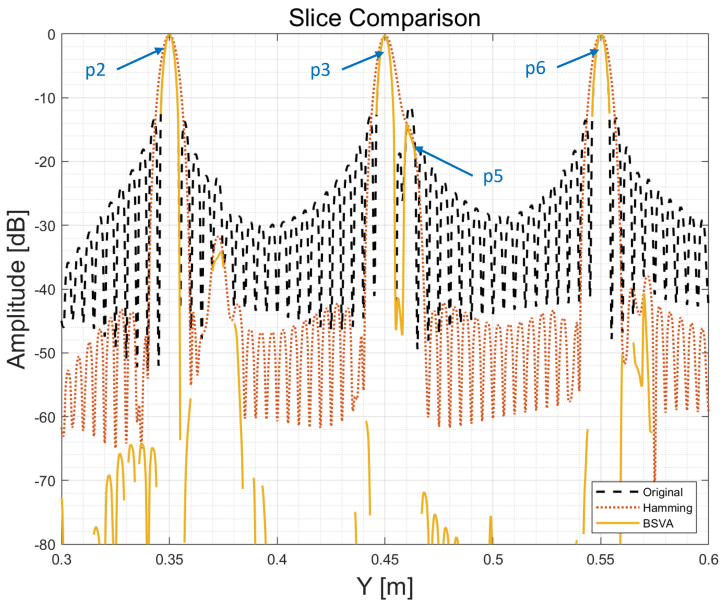

Figure 3.12: Comparison of slice at $X = 0\,\mathrm{m}$

apply the BSVA method in the two directions sequentially. However, since the BSVA method relies on the phase information and after applying the BSVA method in the cross-range direction, the phase information is different from the original ones. In this case, we can not directly apply the BSVA method in the range direction to get the image with sidelobe suppression in both directions.

Therefore, an essential step between applying the BSVA method in the cross-range direction and the range direction is to recover the phase information of the original image. Denote the image after applying the BSVA method in the cross-range direction as $g_a(x,y)$, the phase terms of the original image as $\varphi(g_o(x,y))$; thus, the phase-recovered image is

$$g_{pr}(x,y) = |g_a(x,y)|\, e^{j\varphi(g_o(x,y))} \tag{3.64}$$

Regard the phase recovered image as the new original image and then we can apply the BSVA method in the range direction as introduced in the last section.

3.4.1 Simulation Results

The simulation result of applying the BSVA method both in the cross-range direction and in the range direction is shown in Figure 3.13. Comparing this figure with the original imaging result of Figure 3.7(a), we can see that the two weak point target p_4 and p_5, which are submerged in the sidelobes of the strong closely spaced point target p_3 can be distinguished after applying the BSVA method in the two directions.

3.5 Acceleration

From above, we know that the weighted result of each pixel is related to the imaging values of its eight adjacent points when applying the BSVA method along the cross-range direction. And then, applying it in the range direction, the imaging results of four more adjacent points

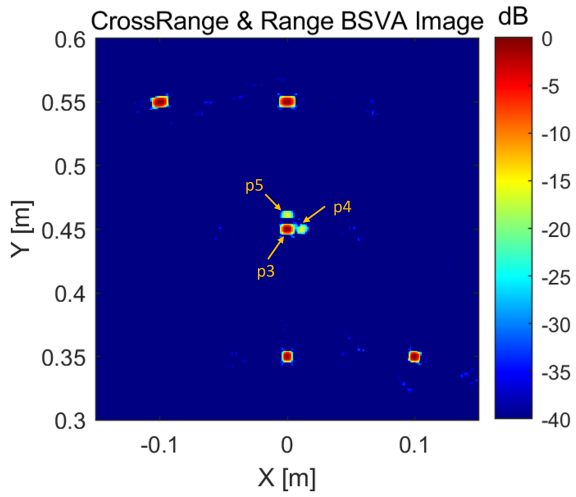

Figure 3.13: Image after applying the BSVA method in the cross-range and range directions

are needed. Generally, the twelve adjacent points are not located on the pixel, so we need to calculate their imaging values instead of directly getting from the original image. Therefore, the total processing time is approximately twelve times that of the original imaging, which results in a large computational burden. To speed up this process, the intuitive idea is to make use of the original imaging results. In other words, if these adjacent points are located in the imaging area, then we can approximate them to the nearest pixel.

3.5.1 Acceleration in the Range Direction

Consider the process acceleration in the range direction at first. From section 3.3, we know that when applying the BSVA method in the range direction, the four adjacent points are needed for each pixel. Denote the imaging grid spacing in the cross-range and down-range direction as d_X and d_Y, respectively. If the four adjacent points are located in the imaging area, we can make the following approximation.

First, combining with equation (3.57) and (3.58), calculate the number of pixels in the interval of the adjacent point and the target point (x_0, y_0).

$$\begin{aligned} N_{x_1} &= \left\lfloor \frac{d_r \cos(\theta_1)}{d_X} \right\rceil \\ N_{x_2} &= \left\lfloor \frac{d_r \cos(\theta_2)}{d_X} \right\rceil \end{aligned} \tag{3.65}$$

and

$$\begin{aligned} N_{y_1} &= \left\lfloor \frac{d_r \sin(\theta_1)}{d_Y} \right\rceil \\ N_{y_2} &= \left\lfloor \frac{d_r \sin(\theta_2)}{d_Y} \right\rceil \end{aligned} \tag{3.66}$$

where $\lfloor \rceil$ means rounding to an integer. Then the four adjacent points can be approximated as

$$\begin{aligned} p_1 &= (x_0 - N_{x_1} \cdot d_X, y_0 - N_{y_1} \cdot d_Y) \\ p_2 &= (x_0 + N_{x_1} \cdot d_X, y_0 + N_{y_1} \cdot d_Y) \end{aligned} \tag{3.67}$$

and

$$\begin{aligned} p_3 &= (x_0 - N_{x_2} \cdot d_X, y_0 - N_{y_2} \cdot d_Y) \\ p_4 &= (x_0 + N_{x_2} \cdot d_X, y_0 + N_{y_2} \cdot d_Y) \end{aligned} \tag{3.68}$$

Now, the four adjacent points are located on the pixels, and we can make use of the original imaging result to speed up the implementation of the BSVA method in the range direction. It should be noted that if the four points are located outside the imaging area, we still need to calculate their imaging result by any imaging method. Furthermore, there are some limitations for the grid spacing that d_X and d_Y should not be too large. The reason is that once N_x and N_y equals to zero due to large d_X and d_Y, the adjacent points p_1, p_2, p_3 and p_4 are coincident with the target point. Then for this point, there is no suppression effect with the SVA method. In addition, Large grid spacing and small imaging area mean that the adjacent points are more likely to locate outside the imaging area, and we can not make the approximation. Therefore, the effect of the acceleration is better for a large imaging area with small grid spacing.

3.5.2 Acceleration in the Cross-range Direction

From section 3.2, we know that in the cross-range direction, we use the GMF method to form a new 2-D imaging plane at each height and then apply the 2-D BSVA method. The eight adjacent points needed for each pixel in this process are in the new imaging plane, which means that we can not use the original imaging result to implement process acceleration. Fortunately, according to the wavenumber analysis in section 3.2.1, we have got the wavenumber spectrum of the transmit array and the receive array. If we consider the two jointly and regard the whole cross-range wavenumber spectrum as the sum of the two, we can implement the 1-D BSVA method in the cross-range direction. In this case, only two adjacent points are needed for each pixel and they are located in the original imaging plane. And if they are located in the imaging area, we can make some approximation to realize the process acceleration in the cross-range direction.

First, we should deduce the implementation of the 1-D BSVA method in the cross-range direction. The total wavenumber spectrum in the cross-range direction can be expressed as

$$k_x(x_0) = k_u(x_0) + k_v(x_0) \tag{3.69}$$

where $k_u(x_0)$ and $k_v(x_0)$ are defined in equation (3.12) and (3.13) respectively. Then its support can be expressed as

$$\begin{aligned} &\mathrm{supp}(k_x(x_0)) = \\ &\begin{cases} 1, & k_c\left(\frac{x_0-u_{xr}}{\sqrt{(x_0-u_{xr})^2+y_0^2}} + \frac{x_0-v_{xr}}{\sqrt{(x_0-v_{xr})^2+y_0^2}}\right) \le k_x \le k_c\left(\frac{x_0-u_{xl}}{\sqrt{(x_0-v_{xl})^2+y_0^2}} + \frac{x_0-v_{xl}}{\sqrt{(x_0-u_{xl})^2+y_0^2}}\right) \\ 0, & \text{otherwise.} \end{cases} \end{aligned} \tag{3.70}$$

Combining equation (3.16) and (3.17), the total wavenumber spectrum width is

$$B_{k_x}(x_0) = B_{k_u}(x_0) + B_{k_v}(x_0) \tag{3.71}$$

and the central wavenumber is

$$k_{x,c}(x_0) = k_{u,c}(x_0) + k_{v,c}(x_0) \tag{3.72}$$

According to the analysis of the compensating phase in section 3.2.2, the compensating phase term can be expressed as

$$\begin{aligned}\varphi(x_0,y_0) =& \frac{k_c}{2}\left[\sqrt{(x_0-u_{xl})^2+y_0^2}+\sqrt{(x_0-u_{xr})^2+y_0^2}\right] \\ &+\frac{k_c}{2}\left[\sqrt{(x_0-v_{xl})^2+y_0^2}+\sqrt{(x_0-v_{xr})^2+y_0^2}\right]\end{aligned} \tag{3.73}$$

Then the compensated image can be obtained by

$$g_C(x_0,y_0) = g(x_0,y_0)\mathrm{e}^{-j\varphi(x_0,y_0)} \tag{3.74}$$

Then we can apply the 1-D BSVA method in the cross-range direction. The weighting function can be expressed as

$$A(k_x) = 1 + w(x_0)\cos\left(\frac{2\pi k_x}{B_{k_x}(x_0)}\right) \tag{3.75}$$

Taking inverse Fourier transform on the above function yields:

$$a(x_0) = \delta[x_0] + w(x_0)\delta\left[x_0 - \frac{2\pi}{B_{k_x}(x_0)}\right] + w(x_0)\delta\left[x_0 + \frac{2\pi}{B_{k_x}(x_0)}\right] \tag{3.76}$$

Take the convolution of the above function with the compensated image, we can get the weighted imaging result:

$$\begin{aligned}\tilde{g}_C(x_0,y_0) &= g_C(x_0,y_0)\otimes a(x_0) \\ &= g_C(x_0,y_0) + w(x_0)\left[g_C\left(x_0-\frac{2\pi}{B_{k_x}(x_0)},y_0\right)+g_C\left(x_0+\frac{2\pi}{B_{k_x}(x_0)},y_0\right)\right]\end{aligned} \tag{3.77}$$

The optimal weighting result is also obtained by solving the minimization problem with the constraint:

$$\begin{aligned}\underset{w(x_0)}{\text{minimize}} \quad & |\tilde{g}_C(x_0,y_0)|^2 \\ \text{s.t.} \quad & 0 < w(x_0) < 0.5\end{aligned} \tag{3.78}$$

This is a typical 1-D BSVA problem and the solution can be found in section 2.2.1.

We can see that the weighted result of pixel (x_0,y_0) is related to the compensated imaging results of another two points $q_1 = \left(x_0 - \frac{2\pi}{B_{k_x}(x_0)},y_0\right)$ and $q_2 = \left(x_0 + \frac{2\pi}{B_{k_x}(x_0)},y_0\right)$. It is clear that the two points are in the imaging plane and if they are located in the imaging area, we can take some approximation to realize acceleration. And there are two kinds of considerations for process acceleration in the cross-range direction.

- **Approximation with 1-D BSVA method**
  We can still consider applying the BSVA method with directly approximating the two points q_1 and q_2 to the nearest pixel, similar to what we do in the range direction.

  The number of pixels in the interval of q_1 or q_2 to $p_0(x_0,y_0)$ is

$$N_q(x_0) = \left\lfloor \frac{2\pi}{B_{k_x}(x_0)\cdot d_X} \right\rfloor \tag{3.79}$$

Then q_1 and q_2 can be approximated as

$$\begin{aligned} q_1' &= (x_0 - N_q(x_0) \cdot d_X, y_0) \\ q_2' &= (x_0 + N_q(x_0) \cdot d_X, y_0) \end{aligned} \tag{3.80}$$

Now q_1' and q_2' are located on the pixels and we can make use of the original imaging result.

The weighted image can be expressed as

$$\tilde{g}_C(x_0, y_0) = g_C(x_0, y_0) + w(x_0) \left[g_C\left(q_1'\right) + g_C\left(q_2'\right) \right] \tag{3.81}$$

Still, if q_1 and q_2 are located outside the imaging area, there is no pixels to approximate and we need to calculate their imaging results.

- **Approximation with 1-D GSVA method**
  Still, we approximate q_1 and q_2 to the close pixel. Combining the introduction of non-integer multiple of Nyquist sampling case in chapter 2, this approximation can also be regarded as this situation. And then we can apply the 1-D GSVA method. $N_q(x_0)$ now is defined as

$$\left\lceil \frac{B_{k_x}(x_0)}{2B_{Ny}(x_0)} \right\rceil < N_q(x_0) < \left\lfloor \frac{B_{k_x}(x_0)}{B_{Ny}(x_0)} \right\rfloor \tag{3.82}$$

  where B_{Ny} is the space angular Nyquist frequency, $\lfloor\ \rfloor$ and $\lceil\ \rceil$ represent rounding down and rounding up to an integer. Solving this equation and only considering non-integer sampling case, we can get

$$\frac{B_k(x_0)}{2 \cdot N_p(x_0)} < B_{Ny}(x_0) < \frac{B_k(x_0)}{Np(x_0)} \tag{3.83}$$

  In this case, for $N_q(x_0) \geq 1$, we can always find a proper B_{Ny} that can make it be regarded as the oversampling case. And the oversampling ratio w_s is defined as

$$w_s = \frac{N_q(x_o) \cdot B_{Ny}}{B_{K_x}(x_0)} \tag{3.84}$$

  Therefore, w_s can be any value in the interval $(0.5, 1)$.

  Then the weighted image can be expressed as

$$\tilde{g}_C(x_0, y_0) = (1 - w(x_0)\mathrm{sinc}(w_s)) g_C(x_0, y_0) + w(x_0) \left(g_C(q_1') + g_C(q_2') \right) \tag{3.85}$$

  The solution of the above function can be found in section 2.2.2. Furthermore, according to the introduction of the GSVA method in section 2.2.2, we know that with bigger w_s, the residual sidelobe after applying the GSVA method is lower. Therefore, taking large value of w_s is a better choice.

  Furthermore, for non-integer multiple Nyquist sampling case, we can also consider the five-tap RSVA or MSVA method.

- **Approximation with 1-D MSVA method**
  In principle, we can choose either RSVA or MSVA method. However, for MIMO array imaging, due to the spatially variant wavenumber spectrum, the signal in the cross-range is not a strict sinc function but similar to the sinc function. Therefore, when we apply the

SVA method, we need to compensate the phase for aligning the wavenumber center of each point. But the compensated phase is an approximate result according to section 3.2.2. If we choose the more relaxed RSVA method compared with the MSVA method, we may miss the targets. Therefore, we consider applying the 5-tap MSVA method.

Compared with the BSVA method, two more adjacent points are needed for the MSVA method, which will increase the processing time. Fortunately, the increased time is still short enough compared with that before approximation.

The another two adjacent points are

$$\begin{aligned} q_3 &= \left(x_0 - \frac{4\pi}{B_{k_x}(x_0)}, y_0\right) \\ q_4 &= \left(x_0 + \frac{4\pi}{B_{k_x}(x_0)}, y_0\right) \end{aligned} \tag{3.86}$$

The number of pixels between q_3 or q_4 to the point target (x_0, y_0) is

$$N'_q(x_0) = \left\lfloor \frac{2 \cdot \pi}{B_{k_x}(x_0) \cdot d_X} \right\rceil \tag{3.87}$$

Then q_3 and q_4 can be approximated as

$$\begin{aligned} q'_3(x_0) &= x_0 - N'_q(x_0) \cdot d_X, y_0) \\ q'_4(x_0) &= x_0 + N'_q(x_0) \cdot d_X, y_0) \end{aligned} \tag{3.88}$$

The weighted image can be expressed as

$$\begin{aligned} \tilde{g}_C(x_0, y_0) =& g_C(x_0, y_0) \\ &+ w_1(x_0)\left(-2\mathrm{sinc}(w_s) g_C(x_0, y_0) + g_C(q'_1) + g_C(q'_2)\right) \\ &+ w_2(x_0)\left(-2\mathrm{sinc}(w_s) g_C(x_0, y_0) + g_C(q'_3) + g_C(q'_4)\right) \end{aligned} \tag{3.89}$$

where $w_s = (0.5, 1)$. The optimal weighted image can be formulated according to the introduction of the MSVA method in section 2.2.4.

To make sure the SVA method for each approximation considerations can be performed well in the cross-range direction, N_q should be bigger than and equal to one, namely

$$d_X \leq \frac{2 \cdot \pi}{B_{k_x}(x_0)} \tag{3.90}$$

The key is to determine the maximum wavenumber spectrum width B_{k_x} of the whole imaging area. From the equation (3.71), we know that $B_{k_x}(x_0)$ is related to the antenna position, the pixel position, and the central wavenumber. Therefore, it is complicated to determine its maximum value. Only for one situation that the transmit array center is coincident with the receive array center and the imaging area is in front of the array, it is easy to determine the maximum B_{k_x}. Denote the position of the array center as $Ac = (x_a, 0)$ and the minimum height of the imaging area as Y_{min}, then the maximum B_{k_x} for the whole imaging area can be obtained at the point (x_a, Y_{min}).

In our simulation setup, the maximum B_{k_x} is obtained at the pixel $(0, 0.3)$ and the maximum grid spacing in the cross-range direction could be 3.9 mm. Therefore, $d_X = 1$ mm satisfies this condition and we can consider the acceleration of SVA implementation and get good suppression effect in the cross-range direction.

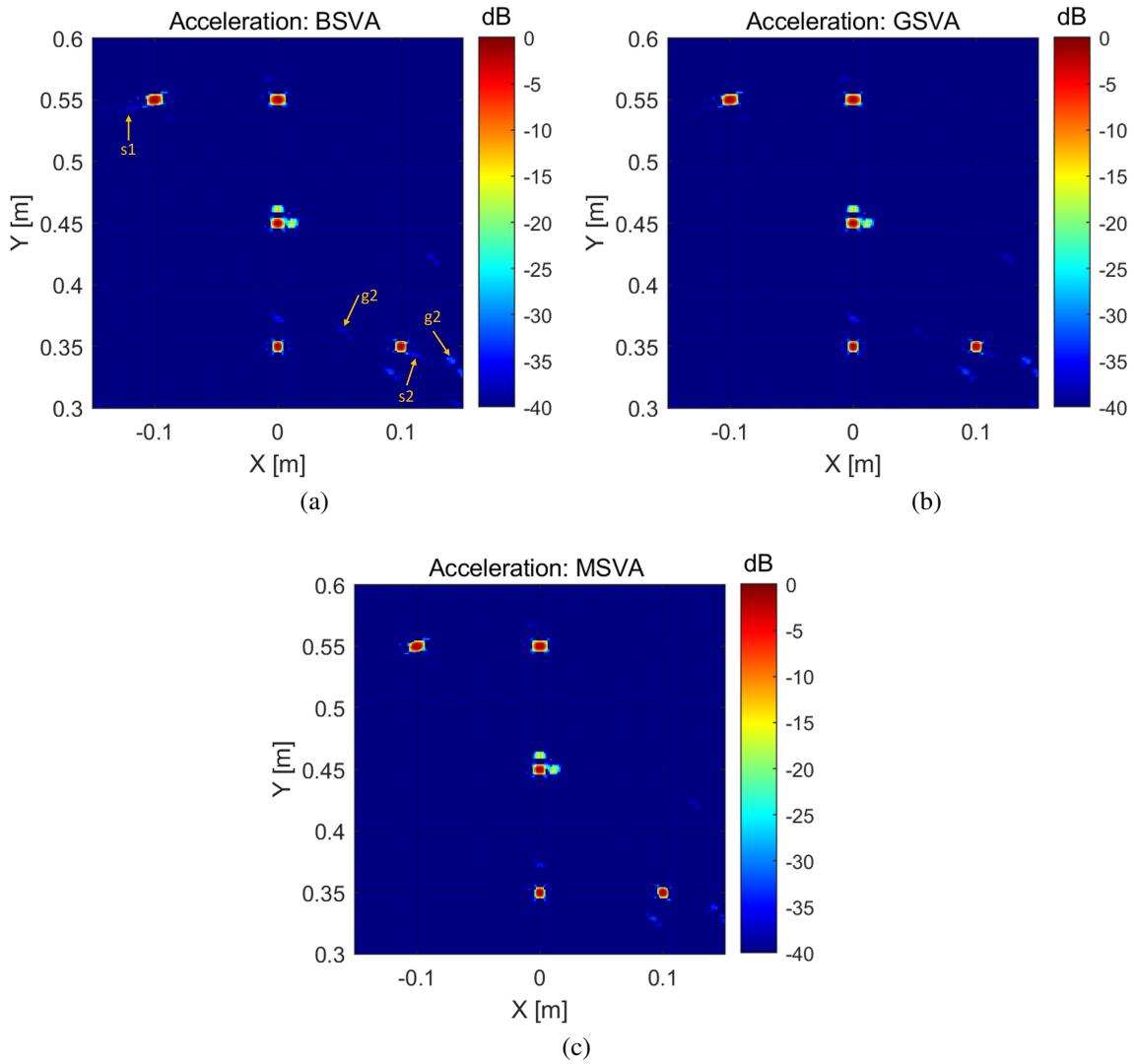

Figure 3.14: Results of acceleration implementation of SVA method. (a) Acceleration with BSVA method in the range direction and cross-range direction. (b) Acceleration with BSVA in the range direction and GSVA method in the cross-range direction. (c) Acceleration with BSVA in the range direction and MSVA method in the cross-range direction.

3.5.3 Simulation Result

Considering 1.1 times oversampling, then the oversampling ratio w_s is

$$w_s(x_0) = \frac{1}{1.1} = 0.909 \tag{3.91}$$

Figure 3.14 gives the simulation results of acceleration implementation with the BSVA method, GSVA method, and MSVA method in the cross-range direction and BSVA method in the range direction. Comparing it with the original image (Figure 3.7(a)) and the original SVA image (Figure 3.13), both the three acceleration methods can implement sidelobe suppression effectively. And comparing these acceleration methods, the MSVA method gives better sidelobe and grating lobe suppression.

Table 3.4 gives the comparison of the processing time, the amplitude of the sidelobe $s_1 = (-0.116\,\text{m}, 0.543\,\text{m})$ and $s_2 = (0.11\,\text{m}, 0.343\,\text{m})$, and the grating lobe $g_1 = (0.054\,\text{m}, 0.363\,\text{m})$

Table 3.4: Performance comparison

	Original	**BSVA**	**BSVA-acceleration**	**GSVA-acceleration**	**MSVA-acceleration**
Processing time [s]	6.76	90.23	9.28	9.4	10.38
s_1[dB]	-27.27	-41.95	-35.68	-37.14	-Inf
s_2[dB]	-27.52	-44.59	-34.34	-35.68	-Inf
g_1[dB]	-33.07	-Inf	-36.41	-37.78	-Inf
g_2[dB]	-30.12	-Inf	-31.11	-32.01	-34.32

and $g_2 = (0.142\,\mathrm{m}, 0.338\,\mathrm{m})$ before and after acceleration. We can see that the processing time is greatly reduced after acceleration and the suppression performance is still remarkable. Therefore, with proper imaging gird, the acceleration implementation of the SVA method can also give good suppression performance with much less processing time. Furthermore, the MSVA method is the best choice with comparable suppression performance with the original BSVA method, and the processing time only increases 53.55% that of the original imaging.

3.6 Conclusion

In this chapter, based on the GMF imaging method, we analyze the wavenumber spectrum in the cross-range direction and range direction and propose a method to perform the BSVA method in the two directions for 1-D MIMO array imaging. Then by numerical simulation, we verify that this method can realize sidelobe suppression in the two directions without sacrificing the mainlobe resolution. The sidelobe level is suppressed by at least 22.59 dB in the cross-range direction, and the grating lobe level is suppressed by at least 4.18 dB. In the range direction, the sidelobe is suppressed by at least 20.82 dB. Both in the two directions, the mainlobe resolution remains unchanged. Therefore, it can improve the image quality.

In addition, to address the problem of large computational burden, we propose three acceleration implementations of this method. And they all can work well under some conditions of imaging grid. In our simulation, the BSVA and GSVA acceleration method has reduced the processing time to 10.28% and 10.42% of the original SVA method, while the suppression effect has also been reduced slightly. The MSVA acceleration method has reduced the processing time to 11.50% and provided a comparable suppression effect of the original SVA method.

4

SVA Method for 2-D MIMO Array Imaging

In this chapter, we consider the application of the BSVA method on 2-D planar MIMO array imaging. We are still considering the implementation in the cross-range and range directions. But the cross-range directions include horizontal and vertical directions. Therefore, in the cross-range directions, we need to apply the BSVA method two times. The structure of this chapter is as follows. In section 4.1, the signal model and the GMF implementation of 2-D MIMO array imaging are given. In section 4.2, the analysis and simulation of the BSVA method in the cross-range plane are discussed. The analysis and simulation of the BSVA method in the range direction are discussed in section 4.3. The complete implementation of the BSVA method in cross-range and range directions for 2-D MIMO array imaging is given in section 4.4. The acceleration implementation of the SVA approach is provided in section 4.5. Lastly, the conclusion is drawn in section 4.6.

4.1 2-D MIMO Array Imaging

Assume the antenna elements of a 2-D MIMO array are uniformly distributed in the *xoz* plane. As shown in Figure 4.1, the black points are transmitters and the red points denote receivers.

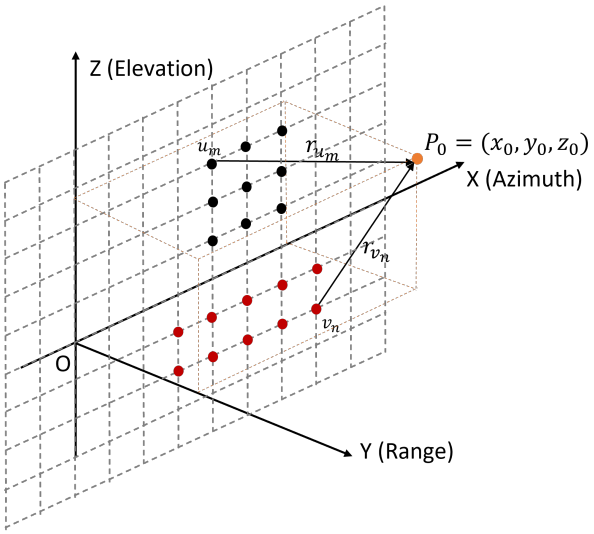

Figure 4.1: 2-D MIMO array topology

Assume the position of the m_{th} transmit element is $u_m = (u_{mx}, 0, u_{mz})$ and the n_{th} receive element is $v_n = (v_{nx}, 0, v_{nz})$. An arbitrary point target $p_0 = (x_0, y_0, z_0)$ is located in front of the MIMO array. Denote the one-way distance from the m_{th} transmitter and the n_{th} receiver to the point target p_0 as r_{u_m} and r_{v_n} respectively and they can be expressed as

$$\begin{aligned} r_{u_m} &= \sqrt{(x_0 - u_{mx})^2 + y_0^2 + (z_0 - u_{mz})^2} \\ r_{v_n} &= \sqrt{(x_0 - v_{nx})^2 + y_0^2 + (z_0 - v_{nz})^2} \end{aligned} \tag{4.1}$$

4.1.1 Signal Model

The signal model is the same as that for 1-D MIMO array imaging. According to equation (3.3) and (4.1), the echo signal can be expressed as

$$s(k, u_m, v_n) = \sum_i \delta(k - k_i) e^{-jkr_{u_m}} e^{-jkr_{v_n}} \tag{4.2}$$

4.1.2 Generalized Matching Filtering

Similar to the expression of GMF for 1-D MIMO array imaging, for 2-D MIMO array imaging, considering at a specific range $y = y_0$ and considering the generalized matched filtering of x and z, the imaging result of point p_0 can be formulated as

$$\begin{aligned} &g\left(x_T, z_T, x_R, z_R|_{y=y_0}\right) = \\ &\sum_k \sum_{u_n} \sum_{v_m} s(k, u_n, v_m) e^{jk\sqrt{(x_T - u_{mx})^2 + y_0^2 + (z_T - u_{mz})^2}} e^{jk\sqrt{(x_R - v_{nx})^2 + y_0^2 + (z_R - v_{nz})^2}} \end{aligned} \tag{4.3}$$

When $x_T = x_R = x_0$ and $z_T = z_R = z_0$, the imaging result of the GMF is the same as the original matched filtering.

4.2 BSVA in the Cross-range Plane

4.2.1 Cross-range Wavenumber Spectrum Analysis

Express the equation (4.3) in convolution form,

$$g\left(x_T, z_T, x_R, z_R|_{y=y_0}\right) = \sum_k s(k, x_T, z_T, x_R, z_R) \otimes_{x_T, z_T} e^{jk\sqrt{x_T^2 + z_T^2 + y_0^2}} \otimes_{x_R, z_R} e^{jk\sqrt{x_R^2 + z_R^2 + y_0^2}} \tag{4.4}$$

here, $\otimes_{x_T, z_T}$ means the 2-D convolution in domain x_T, z_T; $\otimes_{x_R, z_R}$ means the 2-D convolution in domain x_R, z_R.

Take 2-D Fourier transform on x_T, z_T, z_R, z_R, the corresponding wavenumber spectrum of equation (4.4) can be expressed as

$$\begin{aligned} G\left(k_{u_{mx}}, k_{u_{mz}}, k_{v_{nx}}, k_{v_{nz}}\Big|_{y=y_0}\right) =& \mathscr{F}_{x_T, z_T, x_R, z_R}\left\{s(k, x_T, z_T, x_R, z_R)\right\} \\ & \cdot \mathscr{F}_{x_T, z_T}\left\{e^{jk\sqrt{x_T^2 + z_T^2 + y_0^2}}\right\} \cdot \mathscr{F}_{x_R, z_R}\left\{e^{jk\sqrt{x_R^2 + z_R^2 + y_0^2}}\right\} \end{aligned} \tag{4.5}$$

According to stationary phase principle [36], the above equation can be denoted as

$$G\left(k_{u_{mx}},k_{u_{mz}},k_{v_{nx}},k_{v_{nz}}\big|_{y=y_0}\right)=S(k_{u_{mx}},k_{u_{mz}},k_{v_{nx}},k_{v_{nz}})e^{j\sqrt{k^2-k_{u_{mx}}^2-k_{u_{mz}}^2}y_0}e^{j\sqrt{k^2-k_{v_{nx}}^2-k_{v_{nz}}^2}y_0} \tag{4.6}$$

with

$$S(k_{u_{mx}},k_{u_{mz}},k_{v_{nx}},k_{v_{nz}})=\mathscr{F}\{s(k,x_T,z_T,x_R,z_R)\} \tag{4.7}$$

and the corresponding wavenumber along x-axis and z-axis are

$$\begin{aligned}
k_{u_{mx}}&=k\frac{x_0-u_{mx}}{\sqrt{(x_0-u_{mx})^2+(z_0-u_{mz})^2+y_0^2}}\\
k_{v_{nx}}&=k\frac{x_0-v_{nx}}{\sqrt{(x_0-v_{nx})^2+(z_0-v_{nz})^2+y_0^2}}\\
k_{u_{mz}}&=k\frac{z_0-u_{mz}}{\sqrt{(x_0-u_{mx})^2+(z_0-u_{mz})^2+y_0^2}}\\
k_{v_{nz}}&=k\frac{z_0-v_{nx}}{\sqrt{(x_0-v_{nz})^2+(z_0-v_{nz})^2+y_0^2}}
\end{aligned} \tag{4.8}$$

Denote the fraction terms as $\mu_{mx},\gamma_{nx},\mu_{nz},\gamma_{nz}$ respectively and for wide-band measurement, take the central wavenumber $k_c=(k_{min}+k_{max})/2$ to approximate. The supports of the wavenumber spectra can be denoted as

$$\text{supp}\,(k_{u_x})=\begin{cases}1, & k_c\cdot\mu_{x,min}<k_{u_x}<k_c\cdot\mu_{x,max}\\ 0, & \text{others}\end{cases} \tag{4.9}$$

$$\text{supp}\,(k_{v_x})=\begin{cases}1, & k_c\cdot\gamma_{x,min}<k_{v_x}<k_c\cdot\gamma_{x,max}\\ 0, & \text{others}\end{cases} \tag{4.10}$$

$$\text{supp}(k_{u_z})=\begin{cases}1, & k_c\cdot\mu_{z,min}<k_{u_z}<k_c\cdot\mu_{z,max}\\ 0, & \text{others}\end{cases} \tag{4.11}$$

$$\text{supp}(k_{v_z})=\begin{cases}1, & k_c\cdot\gamma_{z,min}<k_{v_z}<k_c\cdot\gamma_{z,max}\\ 0, & \text{others}\end{cases} \tag{4.12}$$

Here, the value ranges of k_{u_x},k_{v_x},k_{u_z} and k_{v_z} are limited by the minimum and maximum value of the fraction terms, which are determined by the corner positions of the antenna array. Therefore, corresponding to a rectangular antenna array, in order to obtain the support of the wavenumber spectrum, we need to insert the four corner positions of the antenna array into the equation (4.8) to calculate the minimum and maximum value of the fraction terms. The relations of the fraction values and the corner points are listed in Table 4.1.

Then the widths of the wavenumber spectral are

$$\begin{aligned}
B_{k_{u_x}}(x_0)&=k_c\,(\mu_{x,max}-\mu_{x,min})\\
B_{k_{v_x}}(x_0)&=k_c\,(\gamma_{x,max}-\gamma_{x,min})\\
B_{k_{u_z}}(z_0)&=k_c\,(\mu_{z,max}-\mu_{z,min})\\
B_{k_{v_z}}(z_0)&=k_c\,(\gamma_{z,max}-\gamma_{z,min})
\end{aligned} \tag{4.13}$$

Table 4.1: Corner Points

Fraction values	Corner points
$\mu_{x,min}$	P_{T1}
$\mu_{x,max}$	P_{T2}
$\gamma_{x,min}$	P_{R1}
$\gamma_{x,max}$	P_{R2}
$\mu_{z,min}$	Q_{T1}
$\mu_{z,max}$	Q_{T2}
$\gamma_{z,min}$	Q_{R1}
$\gamma_{z,max}$	Q_{R2}

The central positions of the wavenumber spectral are

$$\begin{aligned} k_{u_{x,c}}(x_0) &= \frac{k_c}{2}(\mu_{x,max}+\mu_{x,min}) \\ k_{v_{x,c}}(x_0) &= \frac{k_c}{2}(\gamma_{x,max}+\gamma_{x,min}) \\ k_{u_{z,c}}(z_0) &= \frac{k_c}{2}(\mu_{z,max}+\mu_{z,min}) \\ k_{v_{z,c}}(z_0) &= \frac{k_c}{2}(\gamma_{z,max}+\gamma_{z,min}) \end{aligned} \tag{4.14}$$

According to Table 4.1, we can know that at which antenna the minimum or maximum value of the wavenumber spectrum is obtained.

4.2.2 Implementation

Phase compensation

Similarly, in general, the central wavenumber is not at the zero-wavenumber position. Therefore, we need to compensate a phase term in the space domain, and the compensating phase term can be formulated by

$$\begin{aligned} \varphi(x_T,x_R) = & \\ & \frac{k_c}{2}\left[\sqrt{(x_T-x_{P_{T1}})^2+(z_0-z_{P_{T1}})^2+y_0^2}+\sqrt{(x_T-x_{P_{T2}})^2+(z_0-z_{P_{T2}})^2+y_0^2}\right] \\ & +\frac{k_c}{2}\left[\sqrt{(x_R-x_{P_{R1}})^2+(z_0-z_{P_{R1}})^2+y_0^2}+\sqrt{(x_R-x_{P_{R2}})^2+(z_0-z_{P_{R2}})^2+y_0^2}\right] \end{aligned} \tag{4.15}$$

and

$$\begin{aligned} \varphi(z_T,z_R) = & \\ & \frac{k_c}{2}\left[\sqrt{(x_0-x_{Q_{T1}})^2+(z_T-z_{Q_{T1}})^2+y_0^2}+\sqrt{(x_0-x_{Q_{T2}})^2+(z_T-z_{Q_{T2}})^2+y_0^2}\right] \\ & +\frac{k_c}{2}\left[\sqrt{(x_0-x_{Q_{R1}})^2+(z_R-z_{Q_{R1}})^2+y_0^2}+\sqrt{(x_0-x_{Q_{R2}})^2+(z_R-z_{Q_{R2}})^2+y_0^2}\right] \end{aligned} \tag{4.16}$$

Then the compensated imaging results can be obtained by

$$g_C(x_T,x_R) = g\left(x_T,x_R|_{\substack{y=y_0\\z=z_0}}\right)e^{-j\varphi(x_T,x_R)} \tag{4.17}$$

and

$$g_C(z_T,z_R) = g\left(z_T,z_R|_{\substack{x=x_0\\y=y_0}}\right)e^{-j\varphi(z_T,z_R)} \tag{4.18}$$

Implementation of 2-D BSVA method

The implementation of the BSVA method in the cross-range plane for 2-D MIMO array imaging is almost the same as that for 1-D MIMO array imaging. The only difference is that for 2-D MIMO array imaging, we need to apply the 2-D BSVA method in $k_{u_x}-k_{v_x}$ plane and $k_{u_z}-k_{v_z}$ plane, respectively. And then take the minimum value between the output results of the two.

In $k_{u_x}-k_{v_x}$ plane, the cosine-on-pedestal weighting function is

$$\begin{aligned} A(k_{u_x},k_{v_x}) = &\left[1+2w_{u_x}(x_0)\cos\left(\frac{2\pi k_{u_x}(x_0)}{B_{k_{u_x}}(x_0)}\right)\right]\cdot\left[1+2w_{v_x}(x_0)\cos\left(\frac{2\pi k_{v_x}(x_0)}{B_{k_{v_x}}(x_0)}\right)\right] \\ &\text{s.t.}\quad 0<w_{u_x}(x_0)<0.5,\quad 0<w_{v_x}(x_0)<0.5 \end{aligned} \tag{4.19}$$

where $w_{u_x}(x_0)$ adn $w_{v_x}(x_0)$ are the weighting coefficients in domain $k_{u_x}(x_0)$ and $k_{v_x}(x_0)$ respectively.

In $k_{u_z}-k_{v_z}$ plane, the cosine-on-pedestal weighting function is

$$\begin{aligned} A(k_{u_z},k_{v_z}) = &\left[1+2w_{u_z}(z_0)\cos\left(\frac{2\pi k_{u_z}(z_0)}{B_{k_{u_z}}(z_0)}\right)\right]\cdot\left[1+2w_{v_z}(z_0)\cos\left(\frac{2\pi k_{v_z}(z_0)}{B_{k_{v_z}}(z_0)}\right)\right] \\ &\text{s.t.}\quad 0<w_{u_z}(z_0)<0.5,\quad 0<w_{v_z}(z_0)<0.5 \end{aligned} \tag{4.20}$$

where $w_{u_z}(z_0)$ and $w_{v_z}(z_0)$ are the weighting coefficients in domain $k_{u_z}(z_0)$ and $k_{v_z}(z_0)$ respectively.

Taking IFT on the above weighting functions yields:

$$a(x_T,x_R) = a(x_T)\otimes a(x_R) \tag{4.21}$$

$$a(z_T,z_R) = a(z_T)\otimes a(z_R) \tag{4.22}$$

with

$$a(x_T) = \delta[x_T] + w_{u_x}(x_0)\delta\left[x_T-\frac{2\pi}{B_{k_{u_x}}(x_0)}\right] + w_{u_x}(x_0)\delta\left[x_T+\frac{2\pi}{B_{k_{u_x}}(x_0)}\right] \tag{4.23}$$

$$a(x_R) = \delta[x_R] + w_{v_x}(x_0)\delta\left[x_R-\frac{2\pi}{B_{k_{v_x}}(x_0)}\right] + w_{v_x}(x_0)\delta\left[x_R+\frac{2\pi}{B_{k_{v_x}}(x_0)}\right] \tag{4.24}$$

and

$$a(z_T) = \delta[z_T] + w_{u_z}(z_0)\delta\left[z_T-\frac{2\pi}{B_{k_{u_z}}(z_0)}\right] + w_{u_z}(z_0)\delta\left[z_T+\frac{2\pi}{B_{k_{u_z}}(z_0)}\right] \tag{4.25}$$

$$a(z_R) = \delta[z_R] + w_{v_z}(z_0)\delta\left[z_R-\frac{2\pi}{B_{k_{v_z}}(z_0)}\right] + w_{v_z}(z_0)\delta\left[z_R+\frac{2\pi}{B_{k_{v_z}}(z_0)}\right] \tag{4.26}$$

Then the weighted imaging results $\tilde{g}_C$ about the GMF in the two plane are

$$\tilde{g}_C\left(x_T, x_R|_{\substack{y=y_0\\z=z_0}}\right) = g_C(x_T, x_R) + w_{u_x}(x_0)w_{v_x}(x_0)P_x + w_{u_x}(x_0)Q_{T_x} + w_{v_x}(x_0)Q_{R_x} \tag{4.27}$$

$$\tilde{g}_C\left(z_T, z_R|_{\substack{x=x_0\\y=y_0}}\right) = g_C(z_T, z_R) + w_{u_z}(z_0)w_{v_z}(z_0)P_z + w_{u_z}(z_0)Q_{T_z} + w_{v_z}(z_0)Q_{R_z} \tag{4.28}$$

with

$$Q_{T_x} = g_C\left(x_T - \frac{2\pi}{B_{k_{u_x}}(x_0)}, x_R\right) + g_C\left(x_T + \frac{2\pi}{B_{k_{u_x}}(x_0)}, x_R\right) \tag{4.29}$$

$$Q_{R_x} = g_C\left(x_T, x_R - \frac{2\pi}{B_{k_{v_x}}(x_0)}\right) + g_C\left(x_T, x_R + \frac{2\pi}{B_{k_{v_x}}(x_0)}\right) \tag{4.30}$$

$$P_x = g_C\left(x_T - \frac{2\pi}{B_{k_{u_x}}(x_0)}, x_R - \frac{2\pi}{B_{k_{v_x}}(x_0)}\right) + g_C\left(x_T - \frac{2\pi}{B_{k_{u_x}}(x_0)}, x_R + \frac{2\pi}{B_{k_{v_x}}(x_0)}\right) \tag{4.31}$$

$$+ g_C\left(x_T + \frac{2\pi}{B_{k_{u_x}}(x_0)}, x_R - \frac{2\pi}{B_{k_{v_x}}(x_0)}\right) + g_C\left(x_T + \frac{2\pi}{B_{k_{u_x}}(x_0)}, x_R + \frac{2\pi}{B_{k_{v_x}}(x_0)}\right) \tag{4.32}$$

and

$$Q_{T_z} = g_C\left(z_T - \frac{2\pi}{B_{k_{u_z}}(z_0)}, z_R\right) + g_C\left(z_T + \frac{2\pi}{B_{k_{u_z}}(z_0)}, z_R\right) \tag{4.33}$$

$$Q_{R_z} = g_C\left(z_T, z_R - \frac{2\pi}{B_{k_{v_z}}(z_0)}\right) + g_C\left(z_T, z_R + \frac{2\pi}{B_{k_{v_z}}(z_0)}\right) \tag{4.34}$$

$$P_z = g_C\left(z_T - \frac{2\pi}{B_{k_{u_z}}(z_0)}, z_R - \frac{2\pi}{B_{k_{v_z}}(z_0)}\right) + g_C\left(z_T - \frac{2\pi}{B_{k_{u_z}}(z_0)}, z_R + \frac{2\pi}{B_{k_{v_z}}(z_0)}\right) \tag{4.35}$$

$$+ g_C\left(z_T + \frac{2\pi}{B_{k_{u_z}}(z_0)}, z_R - \frac{2\pi}{B_{k_{v_z}}(z_0)}\right) + g_C\left(z_T + \frac{2\pi}{B_{k_{u_z}}(z_0)}, z_R + \frac{2\pi}{B_{k_{v_z}}(z_0)}\right) \tag{4.36}$$

Now, the task is to find the minimum value of $\tilde{g}_C\left(x_T, x_R|_{\substack{y=y_0\\z=z_0}}\right)$ and $\tilde{g}_C\left(z_T, z_R|_{\substack{x=x_0\\y=y_0}}\right)$ subject to the constraints.

$$\begin{aligned} \underset{w_{u_x}, w_{v_x}}{\text{minimize}} \quad & \left|\tilde{g}_C\left(x_T, x_R|_{\substack{y=y_0\\z=z_0}}\right)\right|^2 \\ \text{s.t.} \quad & 0 < w_{u_x}(x_0) < 0.5, \\ & 0 < w_{v_x}(x_0) < 0.5 \end{aligned} \tag{4.37}$$

$$\begin{aligned} \underset{w_{u_z}, w_{v_z}}{\text{minimize}} \quad & \left|\tilde{g}_C\left(z_T, z_R|_{\substack{x=x_0\\y=y_0}}\right)\right|^2 \\ \text{s.t.} \quad & 0 < w_{u_z}(z_0) < 0.5, \\ & 0 < w_{v_z}(z_0) < 0.5 \end{aligned} \tag{4.38}$$

We still consider I and Q separately, take the real component in the two constrained problem and we will get

$$g_1^R\left(x_T, x_R|_{\substack{y=y_0\\z=z_0}}\right) = \begin{cases} 0, & \text{if } \tilde{g}_C^R\left(x_T, x_R|_{\substack{y=y_0\\z=z_0}}\right) \cdot g_C^R\left(x_T, x_R|_{\substack{y=y_0\\z=z_0}}\right) < 0, \\ & \text{s.t. } (w(x_T), w(x_R)) \in \Gamma \\ \min\left\{\tilde{g}_C^R\left(x_T, x_R|_{\substack{y=y_0\\z=z_0}}\right) || \, (w(x_T), w(x_R)) \in \Gamma\right\}, & \text{others} \end{cases} \tag{4.39}$$

$$g_2^R\left(z_T,z_R|_{\substack{x=x_0\\y=y_0}}\right)=\begin{cases}0, & \text{if } \tilde{g}_C^R\left(z_T,z_R|_{\substack{x=x_0\\y=y_0}}\right)\cdot g_C^R\left(z_T,z_R|_{\substack{x=x_0\\y=y_0}}\right)<0,\\ & \text{s.t. } (w(z_T),w(z_R))\in\Gamma\\ \min\left\{\tilde{g}_C^R\left(z_T,z_R|_{\substack{x=x_0\\y=y_0}}\right)\,||\,(w(z_T),w(z_R))\in\Gamma\right\}, & \text{others}\end{cases} \tag{4.40}$$

where $\Gamma=\{(0,0),(0.5,0),(0,0.5),(0.5,0.5)\}$.

Now, we get the real component of the whole weighted imaging result of GMF in the plane x_T-x_R and z_T-z_R. Then, taking $x_T=x_R=x_0$ and $z_T=z_R=z_0$ respectively, we can get two weighted imaging results at point (x_0,y_0,z_0). The last step is to take the min function on the amplitude of the two:

$$g_{\text{out}}^R(x_0,y_0,z_0)=\text{sign}(a)\cdot\min\left(\left|g_1^R\left(x_0,x_0|_{\substack{y=y_0\\z=z_0}}\right)\right|,\ \left|g_2^R\left(z_0,z_0|_{\substack{x=x_0\\y=y_0}}\right)\right|\right) \tag{4.41}$$

where $\text{sign}(a)$ means taking the sign of the two weighted results which has the minimum amplitude.

In the same way, take the imaginary component in the two constrained problem in equation (4.39) and (4.40), and taking $x_T=x_R=x_0$ and $z_T=z_R=z_0$, we will get $g_1^I\left(x_0,x_0|_{\substack{y=y_0\\z=z_0}}\right)$ and $g_2^I\left(z_0,z_0|_{\substack{x=x_0\\y=y_0}}\right)$. And then we can get the imaginary component of the ultimate imaging result:

$$g_{\text{out}}^I(x_0,y_0,z_0)=\text{sign}(b)\cdot\min\left(\left|g_1^I\left(x_0,x_0|_{\substack{y=y_0\\z=z_0}}\right)\right|,\ \left|g_2^I\left(z_0,z_0|_{\substack{x=x_0\\y=y_0}}\right)\right|\right) \tag{4.42}$$

where $\text{sign}(b)$ means taking the sign of the two imaginary component which has the minimum amplitude.

Then the ultimate complex-valued weighted result after applying 2-D BSVA method in the cross-range plane is

$$g_{\text{out}}(x_0,y_0,z_0)=g_{\text{out}}^R(x_0,y_0,z_0)+j\cdot g_{\text{out}}^I(x_0,y_0,z_0) \tag{4.43}$$

Repeat the above process for each imaging pixel, then we can get the whole weighted 3-D imaging result.

Table 4.2: Parameters of simulations

Parameters	**Values**
Frequency band f	120 – 150 GHz
Frequency interval df	150 MHz
Transmit interval d_{Tx}	2 mm
Receive interval d_{Rx}	6 mm
Number of transmitters N_{Tx}	9
Number of receivers N_{Rx}	36
Imaging area X range	[-0.07 0.07]
Imaging area Y range	[0.07 0.13]
Imaging area Z range	[-0.07 0.07]
Image samples	$141\times61\times141$
Targets positions	(0,0.11,0); (0,0.11,0.02); (0.02,0.11,0); (0,0.095,0); (0.04,0.11,0.04); (0.04,0.095,0.04); (-0.04,0.11,-0.04); (-0.04,0.095,-0.04);
Targets power	[1; 0.2; 0.2; 0.2; 1; 0.2; 0.2; 1]

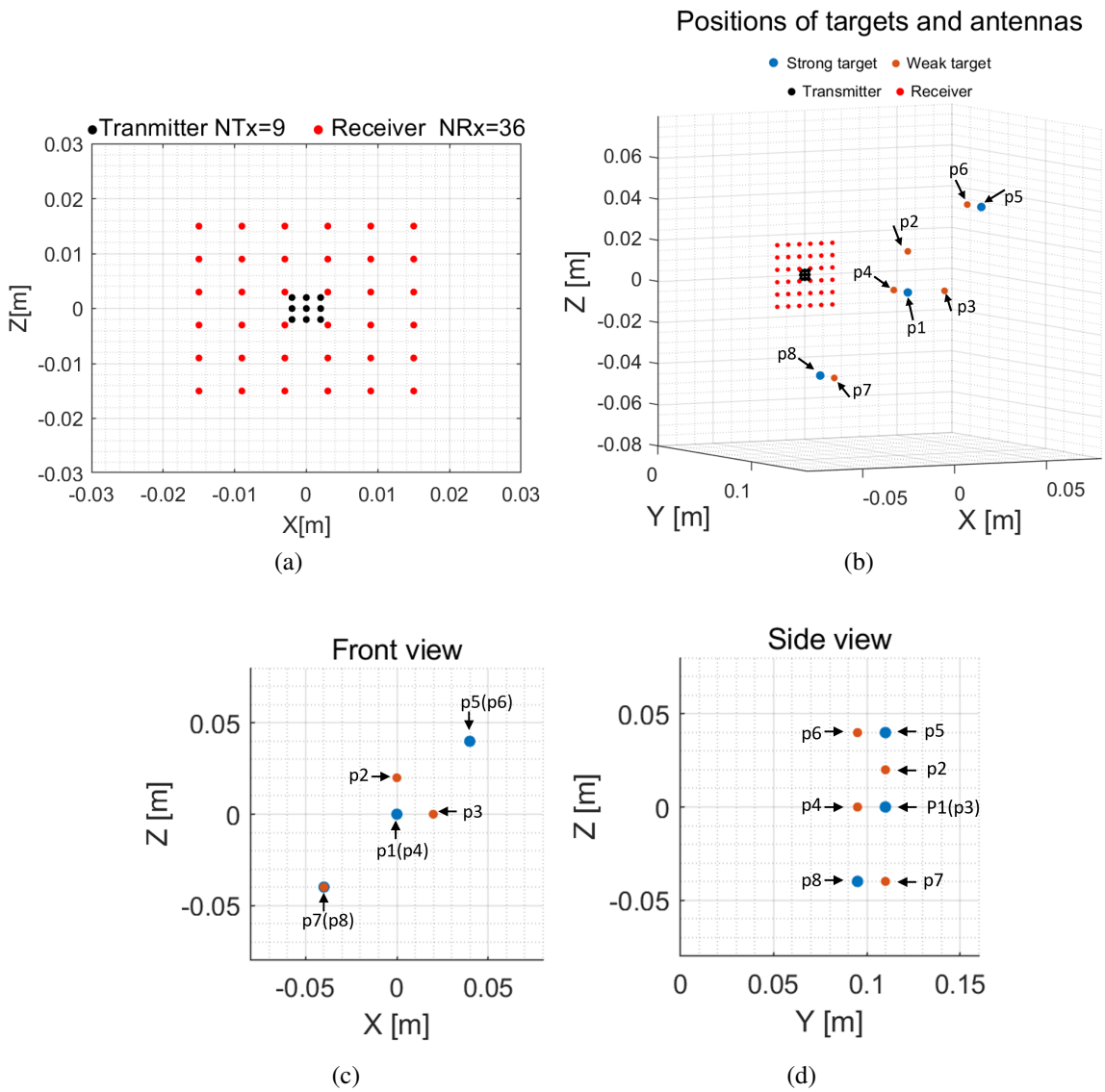

Figure 4.2: Simulation setup of 2-D MIMO array. (a) The 2-D MIMO array Topology. (b) The position of the MIMO array and point targets. (c) The front view of the target positions. (d) The side view of the target positions.

4.2.3 Numerical Simulation

Simulation Setup

The 2-D MIMO array consists of nine transmit elements with the interval of 2 mm and thirty-six receive elements with 6 mm and distributed in *xoz* plane. The structure of the MIMO array is shown in Figure 4.2(a). Six-point targets are distributed in the 3-D space, and three of them are weak targets with 0.2 times the signal strength of others. The ground truth of the point targets relative to the MIMO array is shown in Figure 4.2(b). The front view and the side view of the point targets are shown in Figure 4.2(c) and 4.2(d) . These targets are illuminated by a stepped-frequency continuous wave (SFCW) signal from 120 GHz to 150 GHz with an interval of 150 MHz. The imaging area is $0.14\text{m} \times 0.06\text{m} \times 0.14\text{m}$ with $141 \times 61 \times 141$ samples. All the parameters are listed in Table 4.2.

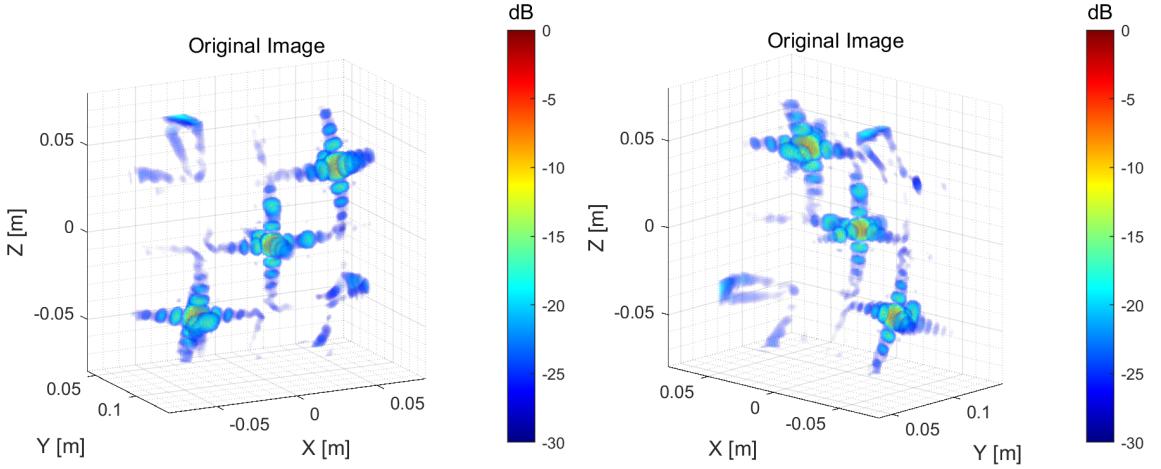

(a) (b)

Figure 4.3: The original imaging result of 2-D MIMO array imaging. (a) The front view of the original image. (b) The back view of the original image.

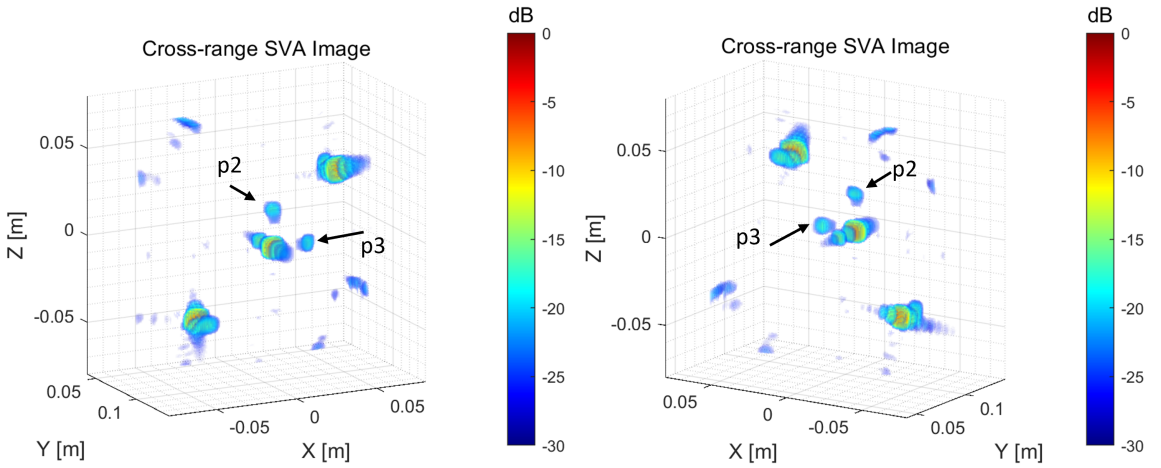

(a) (b)

Figure 4.4: Cross-range BSVA result of 2-D MIMO array imaging. (a) The front view of the cross-range BSVA image. (b) The back view of the cross-range BSVA image.

Imaging Result

The original image and the image after applying the BSVA method in the cross-range *xoz* plane are shown in Figure 4.3 and 4.4 respectively. The original image shows that the sidelobes are pretty high, and we can only identify three strong targets while the weak targets are submerged. After applying the BSVA method, the sidelobes are suppressed effectively. Then the weak target p_2 and p_3 submerged in the sidelobes in the original image, can be distinguished now. Furthermore, the grating lobes are also suppressed.

To go details of the suppression performance, Figure 4.5(a) and 4.5(b) give the slices of the original 3D image and the cross-range BSVA 3D image at $y = 0.11$m along *xoz* plane. Figure 4.5(c) and 4.5(d) give the slices along x-axis and z-axis of Figure 4.5(a) and 4.5(b) respectively. From the figures, we can see that the mainlobe of the strong target p_1 is not

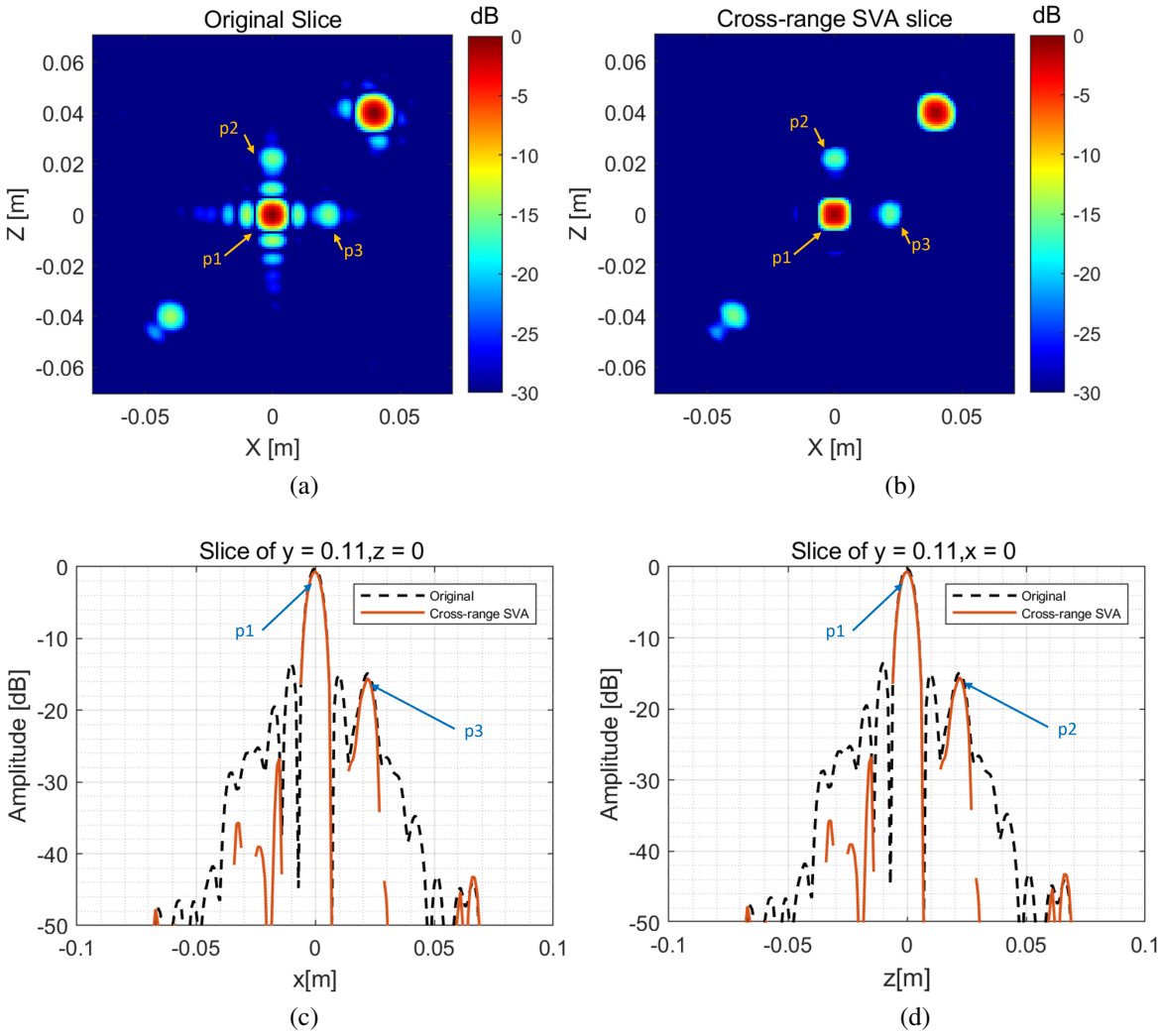

Figure 4.5: Slices. (a) Slice of the original 3D image at $y = 0.11$m; (b) Slice of the cross-range SVA 3D image at $y = 0.11$m; (c) Slice at $y = 0.11$m, $z = 0$m (along the x-axis); (d) Slice at $y = 0.11$m, $x = 0$m (along the z-axis).

broadened and the sidelobes are suppressed. The first side lobe level has been suppressed from -13.41 dB to -26.68 dB. Therefore, the weak target with comparable amplitude of the first sidelobe of the strong target can be distinguished.

4.3 BSVA in the Range Direction

The analysis of the BSVA method in the range direction for 2-D MIMO array imaging is similar to that for 1-D case. Denote the center antenna of the transmit array as $u_c = (x_{c,T}, 0, z_{c,T})$ and the center antenna of the receive array as $v_c = (x_{c,R}, 0, z_{c,R})$. An arbitrary pixel p_0 is located at (x_0, y_0, z_0). The analysis along range direction is shown in Figure 4.6(a).

4.3.1 Range Wavenumber Spectrum Analysis

According to the deduction in section 3.3.1, the sidelobe along range direction for 2-D MIMO array imaging is also from the transmit center to the target point and from the receive center to

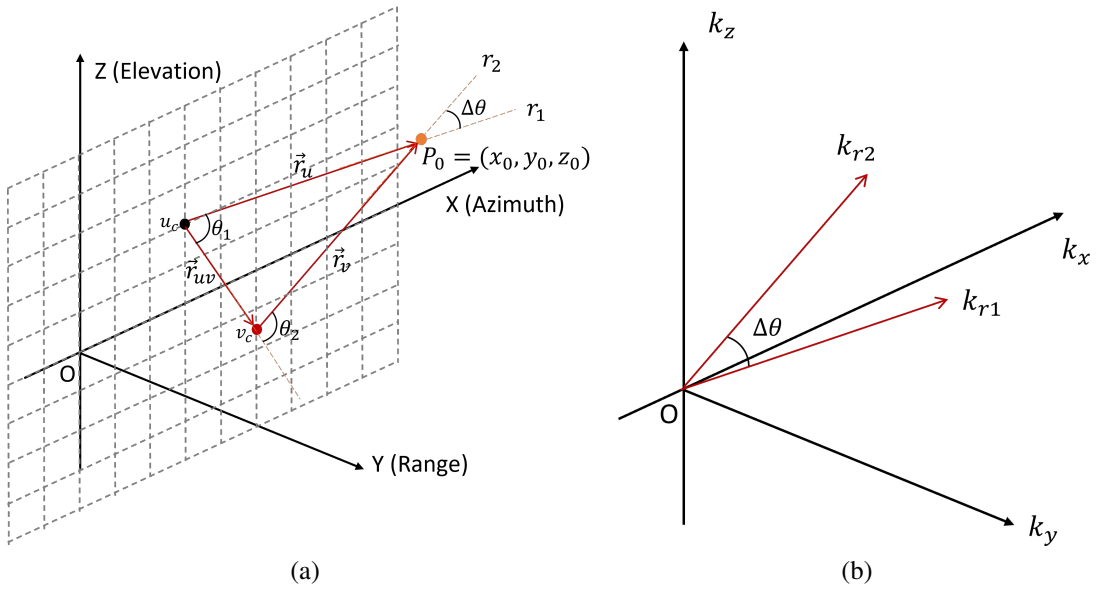

(a) (b)

Figure 4.6: Range direction analysis. (a) The imaging domain. (b) The wavenumber spectrum

the target point. The only difference is that it is about 3-D space. Denote the wavenumber in the two directions as k_{r_u} and k_{r_v} as shown in Figure 4.6(b). Then, the analysis of the wavenumber spectrum along range direction for 2-D MIMO array can be simplified by analyzing k_{r_u} and k_{r_v}.

The support of k_{r_u} and k_{r_v} can be formulated as

$$k_{r_u} = \begin{cases} 1, & k_{min} < k_{r_u} < k_{max} \\ 0, & \text{otherwise} \end{cases} \tag{4.44}$$

$$k_{r_v} = \begin{cases} 1, & k_{min} < k_{r_v} < k_{max} \\ 0, & \text{otherwise} \end{cases} \tag{4.45}$$

where k_{min} and k_{max} are the minimum and maximum values of the wavenumber under wideband measurement. The directions are determined by θ_1 and θ_2 respectively.

The width of the two supports are the same and can be expressed as

$$\begin{aligned} B_{k_r} &= B_{k_{r_u}} \\ &= B_{k_{r_v}} \\ &= k_{max} - k_{min} \end{aligned} \tag{4.46}$$

The central wavenumber of the supports are

$$\begin{aligned} k_{r,c} &= k_{r_u,c} \\ &= k_{r_v,c} \\ &= \frac{k_{max} + k_{min}}{2} \end{aligned} \tag{4.47}$$

The angle $\Delta\theta$ formed between the two directions is determined by

$$\Delta\theta = |\theta_2 - \theta_1| \tag{4.48}$$

Thus, the projection of wavenumber support of receive array r_2 in that of transmit array r_1 is expressed as

$$\Delta B_k = B_k \cdot |\cos(\Delta\theta)| \tag{4.49}$$

Considering the whole MIMO array and the sidelobes suppression in the direction r_1, the width of the wavenumber spectrum is

$$B'_k = B_k + \Delta B_k \tag{4.50}$$

which is the same in direction r_2.

Now, the problem is to calculate the angle $\Delta\theta$ and the key is to calculate θ_1 and θ_2. Since the positions of the central transmit antenna, the central receive antenna and pixel are known, we can form three vectors. Denote the transmit array center as $p_{c,T} = (x_{c,T}, y_{c,T}, z_{c,T})$, and the receive array center as $p_{c,R} = (x_{c,R}, y_{c,R}, z_{c,R})$.

The vector from the transmit center to p_0 is denoted as

$$\mathbf{r_u} = (x_0 - x_{c,T},\ y_0,\ z_0 - z_{c,T}) \tag{4.51}$$

The vector from the receive center to p_0 is denoted as

$$\mathbf{r_v} = (x_0 - x_{c,R},\ y_0,\ z_0 - z_{c,R}) \tag{4.52}$$

The vector from the transmit center to the receive center is denoted as

$$\mathbf{r_{uv}} = (x_{c,R} - x_{c,T},\ 0,\ z_{c,R} - z_{c,T}) \tag{4.53}$$

According to the definition of the dot product, the cosine value of the angle between two vectors can be calculated

$$\cos(\theta_1) = \frac{\mathbf{r_u} \cdot \mathbf{r_{uv}}}{\|\mathbf{r_u}\|\|\mathbf{r_{uv}}\|} \tag{4.54}$$

$$\cos(\theta_2) = \frac{\mathbf{r_v} \cdot \mathbf{r_{uv}}}{\|\mathbf{r_v}\|\|\mathbf{r_{uv}}\|} \tag{4.55}$$

Then by taking inverse cosine functions, we can get the values of θ_1 and θ_2. And the $\Delta\theta$ can be formulated by

$$\Delta\theta = |\cos^{-1}(\theta_2) - \cos^{-1}(\theta_1)| \tag{4.56}$$

4.3.2 Implementation

Phase compensation

Similarly, according to the equation (4.47), it is clear that the central wavenumber is not at the zero-wavenumber position. For the arbitrary point $p_0 = (x_0, y_0, z_0)$, the distances to the array centers are

$$\begin{aligned} \|\mathbf{r_u}\| &= \sqrt{(x_0 - x_{c,T})^2 + (z_0 - z_{c,T})^2 + y_0^2} \\ \|\mathbf{r_v}\| &= \sqrt{(x_0 - x_{c,R})^2 + (z_0 - z_{c,R})^2 + y_0^2} \end{aligned} \tag{4.57}$$

Thus, the compensating phase term is

$$\varphi = k_{r,c} \cdot (\|\mathbf{r_u}\| + \|\mathbf{r_v}\|) \tag{4.58}$$

The compensated result is denoted as

$$g_C(x_0, y_0, z_0) = g(x_0, y_0, z_0) e^{-j\varphi} \tag{4.59}$$

Implementation of 2-D BSVA method

Firstly, considering applying the 1-D BSVA method in the direction r_1 , the cosine-on-pedestal weighting function is

$$\begin{aligned} A_1(k_{r_1}) &= 1 + w_1(r_1)\cos\left(\frac{2\pi k_{r_1}}{B'_k}\right) \\ \text{s.t.} \quad & 0 \le w_1(r_1) \le 0.5 \end{aligned} \tag{4.60}$$

Taking IFT on the above function,

$$a_1(r_1) = \delta[r_1] + w_1(r_1)\delta\left[r_1 - \frac{2\pi}{B'_k}\right] + w_1(r_1)\delta\left[r_1 + \frac{2\pi}{B'_k}\right] \tag{4.61}$$

Now, the problem is to express the above function in Cartesian coordinates.

Set $d_r = \frac{2\pi}{B'_k}$, denote the angle formed by the vector $\mathbf{r_u}$ with the positive directions of x-axis, y-axis, and z-axis as α_x, α_y and α_z. The cosine values of the three angles can be formulated by

$$\begin{aligned} \cos(\alpha_x) &= \frac{x_0 - x_{c,T}}{\|\mathbf{r_u}\|} \\ \cos(\alpha_y) &= \frac{y_0}{\|\mathbf{r_u}\|} \\ \cos(\alpha_z) &= \frac{z_0 - z_{c,T}}{\|\mathbf{r_u}\|} \end{aligned} \tag{4.62}$$

Denote the two points along the direction r_1 for 1-D BSVA method as $p_1 = (x_{p_1}, y_{p_1}, z_{p_1})$ and $p_2 = (x_{p_2}, y_{p_2}, z_{p_2})$, then the position of the two points can be formulated by

$$\begin{aligned} x_{p_1} &= x_0 - d_r \cdot \cos(\alpha_x) \\ y_{p_1} &= y_0 - d_r \cdot \cos(\alpha_y) \\ z_{p_1} &= z_0 - d_r \cdot \cos(\alpha_z) \end{aligned} \tag{4.63}$$

and

$$\begin{aligned} x_{p_2} &= x_0 + d_r \cdot \cos(\alpha_x) \\ y_{p_2} &= y_0 + d_r \cdot \cos(\alpha_y) \\ z_{p_2} &= z_0 + d_r \cdot \cos(\alpha_z) \end{aligned} \tag{4.64}$$

Then the function of equation (4.61) can be expressed as

$$a_1(x_0, y_0, z_0) = \delta[x_0, y_0, z_0] + w_1\delta[x_{p_1}, y_{p_1}, z_{p_1}] + w_1\delta[x_{p_2}, y_{p_2}, z_{p_2}] \tag{4.65}$$

The weighted imaging result can be denoted as

$$\begin{aligned} g'_C(x_0, y_0, z_0) &= g_C(x_0, y_0, z_0) \otimes a_1(x_0, y_0, z_0) \\ &= g_C(x_0, y_0, z_0) + w_1 g_C(x_{p_1}, y_{p_1}, z_{p_1}) + w_1 g_C(x_{p_2}, y_{p_2}, z_{p_2}) \end{aligned} \tag{4.66}$$

Similarly, applying the 1-D BSVA method in the direction r_2, the cosine-on-pedestal weighting function is

$$\begin{aligned} A_2(k_{r_2}) &= 1 + w_2(r_2)\cos\left(\frac{2\pi k_{r_2}}{B'_k}\right) \\ \text{s.t.} \quad & 0 \le w_2(r_2) \le 0.5 \end{aligned} \tag{4.67}$$

Taking IFT on the above function,

$$a_2(r_2) = \delta[r_2] + w_2(r_2)\delta\left[r_2 - \frac{2\pi}{B_k'}\right] + w_2(r_2)\delta\left[r_2 + \frac{2\pi}{B_k'}\right] \tag{4.68}$$

denote the angle formed by the vector $\mathbf{r_v}$ with the positive directions of x-axis, y-axis, and z-axis as β_x, β_y and β_z. The cosine values of the three angles can be formulated by

$$\begin{aligned} \cos(\beta_x) &= \frac{x_0 - x_{c,R}}{\|\mathbf{r_v}\|} \\ \cos(\beta_y) &= \frac{y_0}{\|\mathbf{r_v}\|} \\ \cos(\beta_z) &= \frac{z_0 - z_{c,R}}{\|\mathbf{r_v}\|} \end{aligned} \tag{4.69}$$

Denote the two points along the direction r_2 for 1-D BSVA method as $p_3 = (x_{p_3}, y_{p_3}, z_{p_3})$ and $p_4 = (x_{p_4}, y_{p_4}, z_{p_4})$, then the position of the two points can be formulated by

$$\begin{aligned} x_{p_3} &= x_0 - d_r \cdot \cos(\beta_x) \\ y_{p_3} &= y_0 - d_r \cdot \cos(\beta_y) \\ z_{p_3} &= z_0 - d_r \cdot \cos(\beta_z) \end{aligned} \tag{4.70}$$

and

$$\begin{aligned} x_{p_4} &= x_0 + d_r \cdot \cos(\beta_x) \\ y_{p_4} &= y_0 + d_r \cdot \cos(\beta_y) \\ z_{p_4} &= z_0 + d_r \cdot \cos(\beta_z) \end{aligned} \tag{4.71}$$

Then the function of equation (4.68) can be expressed as

$$a_2(x_0, y_0, z_0) = \delta[x_0, y_0, z_0] + w_2\delta[x_{p_3}, y_{p_3}, z_{p_3}] + w_2\delta[x_{p_4}, y_{p_4}, z_{p_4}] \tag{4.72}$$

The weighted imaging result can be denoted as

$$\begin{aligned} g_C'(x_0, y_0, z_0) &= g_C(x_0, y_0, z_0) \otimes a_2(x_0, y_0, z_0) \\ &= g_C(x_0, y_0, z_0) + w_2 g_C(x_{p_3}, y_{p_3}, z_{p_3}) + w_2 g_C(x_{p_4}, y_{p_4}, z_{p_4}) \end{aligned} \tag{4.73}$$

Now, considering the two 1-D BSVA methods are applied in parallel and simultaneously, the weighted imaging result can be expressed as

$$\begin{aligned} \tilde{g}_C(x_0, y_0, z_0) = g_C(x_0, y_0, z_0) &+ w_1(g_C[x_{p1}, y_{p1}, z_{p1}] + g_C[x_{p2}, y_{p2}, z_{p2}]) \\ &+ w_2(g_C[x_{p_3}, y_{p_3}, z_{p_3}] + g_C[x_{p_4}, y_{p_4}, z_{p_4}]) \end{aligned} \tag{4.74}$$

Then the task is to solve the constrained problem

$$\begin{aligned} \underset{w_1, w_2}{\text{minimize}} \quad & |\tilde{g}_C(x_0, y_0, z_0)|^2 \\ \text{s.t.} \quad & 0 < w_1 < 0.5 \\ & 0 < w_2 < 0.5 \end{aligned} \tag{4.75}$$

Still considering I/Q separately, the output of the above problem is

$$g_{\text{out}}(x_0, y_0, z_0) = g_{\text{out}}^R(x_0, y_0, z_0) + g_{\text{out}}^I(x_0, y_0, z_0) \tag{4.76}$$

with

$$g_{\text{out}}^{R}(x_0,y_0,z_0)=\begin{cases}0, & \text{if } \tilde{g}_C^R(x_0,y_0,z_0)\cdot g_C^R(x_0,y_0,z_0)<0 \quad \text{s.t. } (w_1,w_2)\in\Gamma_1\\ \min\left\{\tilde{g}_C^R(x_0,y_0,z_0)||(w_1,w_2)\in\Gamma_2\right\}, & \text{otherwise}\end{cases} \tag{4.77}$$

$$g_{\text{out}}^{I}(x_0,y_0,z_0)=\begin{cases}0, & \text{if } \tilde{g}_C^I(x_0,y_0,z_0)\cdot g_C^I(x_0,y_0,z_0)<0, \quad \text{s.t. } (w_1,w_2)\in\Gamma_1\\ \min\left\{\tilde{g}_C^I(x_0,y_0,z_0)||(w_1,w_2)\in\Gamma_2\right\}, & \text{otherwise}\end{cases} \tag{4.78}$$

where $\Gamma_1=[(0,0.5),(0.5,0)]$ and $\Gamma_2=[(0,0),(0.5,0),(0.5,0.5)]$. Repeat the above process for each pixel, we can get the ultimate optimal weighted result of BSVA method applied in the range direction.

4.3.3 Numerical Simulation

The parameters for MATLAB simulation is the same as that in Table 4.2. The imaging result of applying the BSVA method along the range direction is shown in Figure 4.7. Comparing the figure with the original imaging result (Figure 4.3), we can see that the weak targets p_4, p_6 and p_7 which are submerged in the original image can be distinguished.

To go details of the suppression performance, Figure 4.8(a) and 4.8(b) give the slices of the original 3D image and the range BSVA 3D image at $x=0\,\text{m}$ along the *yoz* plane. Figure 4.8(c) gives the slice along the *y*-axis of Figure 4.8(a) and 4.8(b). From the figures, we can see that the mainlobe of the strong target p_1 is not broadened and the first sidelobe level is suppressed form -13.13 dB to -32.06 dB. Therefore, the weak target p_4 with comparable amplitude of the first sidelobe of the strong target p_1 can be distinguished.

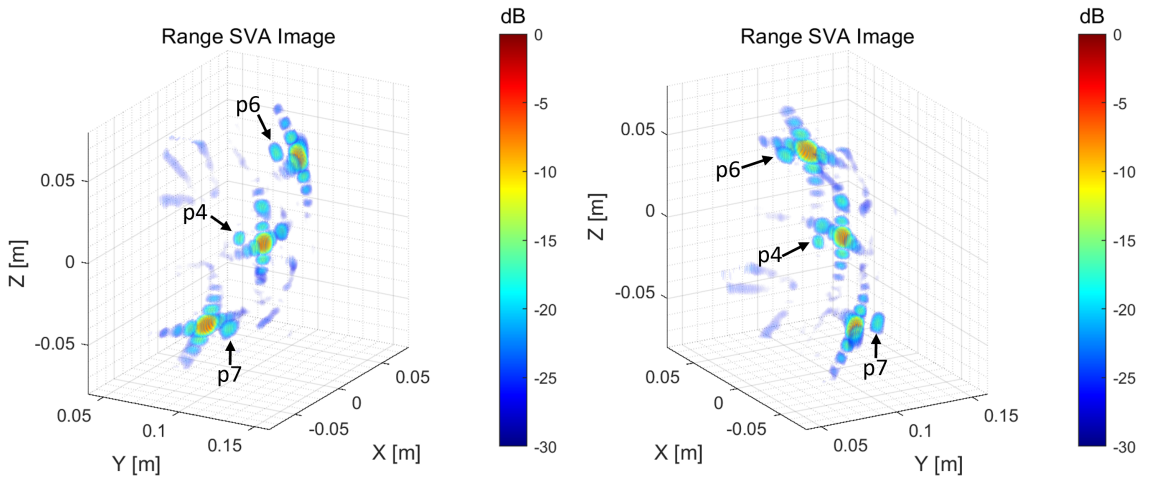

(a) (b)

Figure 4.7: Range BSVA result of 2-D MIMO array imaging. (a) The front view of the range SVA image, (b) The back view of the range SVA image.

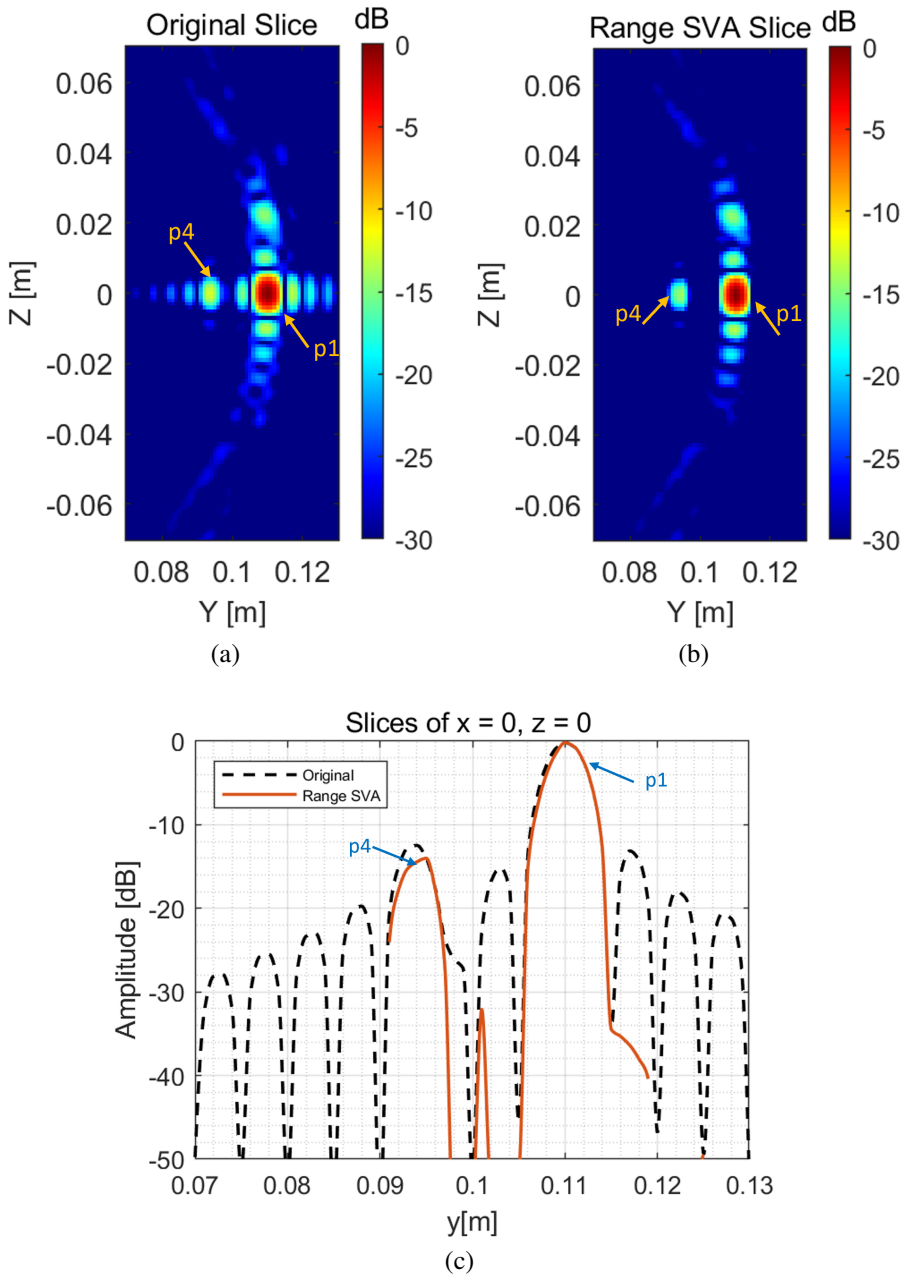

Figure 4.8: Slices. (a) Slice of the original 3D image at $x = 0$m. (b) Slice of the range BSVA 3D image at $x = 0$m. (c) Slice at $x = 0$m, $z = 0$m (along y-axis).

4.4 BSVA Applied on Two Directions

Similar to the 1-D MIMO case, after performing BSVA method in the cross-range plane, we should recover the phase information of the original image:

$$g_{pr}(x,y,z) = |g_{cr}(x,y,z)|\, e^{j(\varphi g_o(x,y,z))} \tag{4.79}$$

where $g_{cr}(x,y,z)$ is the magnitude of the image after applying BSVA in the cross-range plane and $\varphi(g_o(x,y,z))$ is the phase terms of the original image.

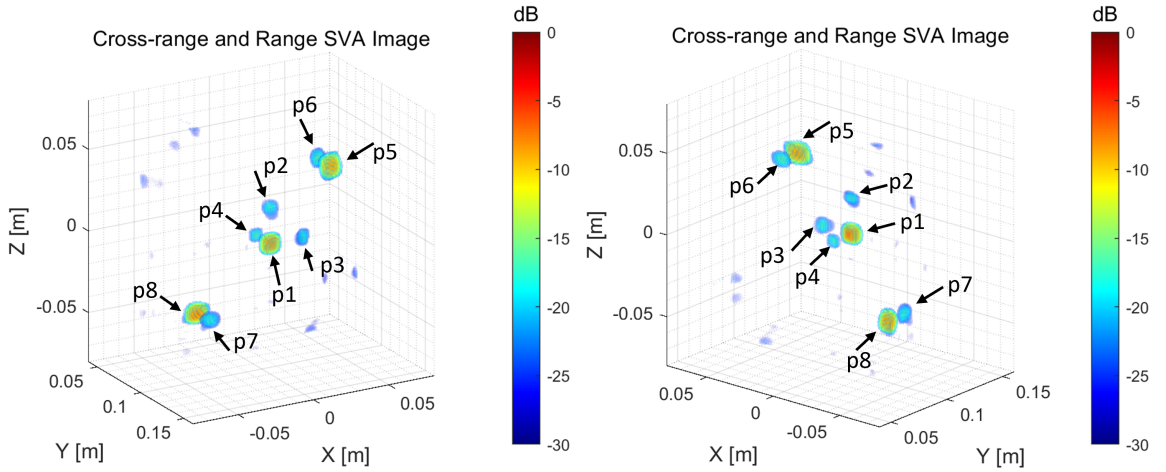

(a) (b)

Figure 4.9: Cross-range and range BSVA result of 2-D MIMO array imaging. (a) The front view of the cross-range and range SVA image. (b) The back view of the cross-range and range SVA image.

4.4.1 Simulation Results

The result of applying BSVA method both in the cross-range plane and in the range direction is shown in Figure 4.9. Comparing the figure with the original 3D image (Figure 4.3), it is clear that the sidelobes are suppressed, therefore all the weak targets submerged in the sidelobes of the close strong targets in the original image can be distinguished. Furthermore, the grating lobes are also suppressed.

4.5 Acceleration

Similar to the acceleration of the SVA method for 1-D MIMO array imaging. We also can deduce the acceleration of the SVA method for 2-D MIMO array imaging.

4.5.1 Acceleration in the Range Direction

Combining with equation (4.63), (4.64), (4.70) and (4.71), we can calculate the number of pixels in the interval of the adjacent point p_1 to the target $P_0(x_0, y_0)$ and p_3 to the target $P_0(x_0, y_0)$, respectively.

$$\begin{aligned} N_x(p_1) &= \left\lfloor \frac{d_r \cos(\alpha_x)}{d_X} \right\rceil \\ N_y(p_1) &= \left\lfloor \frac{d_r \cos(\alpha_y)}{d_Y} \right\rceil \\ N_z(p_1) &= \left\lfloor \frac{d_r \cos(\alpha_z)}{d_Z} \right\rceil \end{aligned} \tag{4.80}$$

and

$$\begin{aligned} N_x(p_3) &= \left\lfloor \frac{d_r \cos(\beta_x)}{d_X} \right\rceil \\ N_y(p_3) &= \left\lfloor \frac{d_r \cos(\beta_y)}{d_Y} \right\rceil \\ N_z(p_3) &= \left\lfloor \frac{d_r \cos(\beta_z)}{d_Z} \right\rceil \end{aligned} \tag{4.81}$$

Then the four adjacent point can be approximated as

$$\begin{aligned} p_1' &= (x_0 - N_x(p_1)\cdot d_X, y_0 - N_y(p_1)\cdot d_Y, z_0 - N_z(p_1)\cdot d_Z) \\ p_2' &= (x_0 + N_x(p_1)\cdot d_X, y_0 + N_y(p_1)\cdot d_Y, z_0 + N_z(p_1)\cdot d_Z) \end{aligned} \tag{4.82}$$

and

$$\begin{aligned} p_3' &= (x_0 - N_x(p_3)\cdot d_X, y_0 - N_y(p_3)\cdot d_Y, z_0 - N_z(p_3)\cdot d_Z) \\ p_4' &= (x_0 + N_x(p_3)\cdot d_X, y_0 + N_y(p_3)\cdot d_Y, z_0 + N_z(p_3)\cdot d_Z) \end{aligned} \tag{4.83}$$

Then the weighted image of applying BSVA method (4.74) in the range direction can be expressed as

$$\tilde{g}_C(x_0, y_0, z_0) = g_C(x_0, y_0, z_0) + w_1(g_C(p_1') + g_C(p_2')) + w_2(g_C(p_3') + g_C(p_4')) \tag{4.84}$$

Still, if p_1', p_2', p_3' and p_4' are located outside of the imaging area, we need to calculate their imaging results according to the imaging method.

4.5.2 Acceleration in the Cross-range Direction

For the cross-range sidelobe suppression of 2-D MIMO array imaging, we use two times 2-D BSVA method along x-axis and z-axis, respectively. Same as the acceleration method used in 1-D MIMO array imaging, firstly, we need to implement 1-D BSVA method to replace the 2-D BSVA method.

According to the deduction of 1-D BSVA method in the cross-range direction of 1-D MIMO array imaging in section 3.5.2 and combining equation (4.13), the total equivalent wavenumber spectrum width along x-axis and z-axis can be expressed as

$$\begin{aligned} B_{k_x}(x_0) &= B_{k_{ux}}(x_0) + B_{k_{vx}}(x_0) \\ B_{k_z}(z_0) &= B_{k_{uz}}(z_0) + B_{k_{vz}}(z_0) \end{aligned} \tag{4.85}$$

The compensating phase term $\varphi(x_0)$ and $\varphi(z_0)$ can be obtained according to equation (4.15) and (4.16) by taking $x_T = x_R = x_0$ and $z_T = z_R = z_0$, respectively. Then the compensated image along x-axis and z-axis can be expressed as

$$\begin{aligned} g_1(x_0, y_0, z_0) &= g(x_0, y_0, z_0) e^{-j\varphi(x_0)} \\ g_2(x_0, y_0, z_0) &= g(x_0, y_0, z_0) e^{-j\varphi(z_0)} \end{aligned} \tag{4.86}$$

According 1-D BSVA method, the adjacent two points along each axis can be expressed as

$$\begin{aligned} q_{x_1} &= \left(x_0 - \frac{2\pi}{B_{k_x}(x_0)}, y_0, z_0 \right) \\ q_{x_2} &= \left(x_0 + \frac{2\pi}{B_{k_x}(x_0)}, y_0, z_0 \right) \end{aligned} \tag{4.87}$$

and

$$\begin{aligned} q_{z_1} &= \left(x_0, y_0, z_0 - \frac{2\pi}{B_{k_z}(z_0)}\right) \\ q_{z_2} &= \left(x_0, y_0, z_0 + \frac{2\pi}{B_{k_z}(z_0)}\right) \end{aligned} \tag{4.88}$$

Then the corresponding weighted image with 1-D BSVA method can be expressed as

$$\begin{aligned} \tilde{g}_1(x_0, y_0, z_0) &= g_1(x_0, y_0, z_0) + w_{11}(x_0)(g_1(q_{x_1}) + g_1(q_{x_2})) \\ \tilde{g}_2(x_0, y_0, z_0) &= g_2(x_0, y_0, z_0) + w_{21}(z_0)(g_2(q_{z_1}) + g_2(q_{z_2})) \end{aligned} \tag{4.89}$$

The above functions can be solved according to the introduction of 1-D BSVA method in section 2.2.1, we will get two complex values for each pixel, then choose the one with smaller magnitude as the final weighted result. In this way, we can implement sidelobe suppression via 1-D BSVA method for 2-D MIMO array imaging.

To speed up the implementation of SVA method by making use of the original imaging values, we also need to approximate the points to the nearest pixels.

- **Approximation with 1-D BSVA method**
  Considering BSVA method, the number of pixels for the point target and its adjacent points can be formulated by

$$\begin{aligned} N_{11}(x_0) &= \left\lfloor \frac{2\pi}{B_{k_x}(x_0) \cdot d_X} \right\rceil \\ N_{21}(z_0) &= \left\lfloor \frac{2\pi}{B_{k_z}(z_0) \cdot d_Z} \right\rceil \end{aligned} \tag{4.90}$$

  The adjacent points can be approximated as

$$\begin{aligned} q'_{x_1} &= (x_0 - N_{11}(x_0) \cdot d_X,\ y_0,\ z_0) \\ q'_{x_2} &= (x_0 + N_{11}(x_0) \cdot d_X,\ y_0,\ z_0) \\ q'_{z_1} &= (x_0,\ y_0,\ z_0 - N_{21}(z_0) \cdot d_Z) \\ q'_{z_2} &= (x_0,\ y_0,\ z_0 + N_{21}(z_0) \cdot d_Z) \end{aligned} \tag{4.91}$$

  The equation (4.89) can be expressed as

$$\begin{aligned} \tilde{g}'_1(x_0, y_0, z_0) &= g_1(x_0, y_0, z_0) + w_{11}(x_0)[g_1(q'_{x_1}) + g_1(q'_{x_2})] \\ \tilde{g}'_2(x_0, y_0, z_0) &= g_2(x_0, y_0, z_0) + w_{21}(z_0)[g_2(q'_{z_1}) + g_2(q'_{z_2})] \end{aligned} \tag{4.92}$$

  Then we can implement acceleration of 1-D BSVA method.

- **Approximation with 1-D GSVA method**
  Similarly, we can apply GSVA method. The equation (4.89) can be expressed according to the GSVA method

$$\begin{aligned} \tilde{g}'_1(x_0, y_0, z_0) &= (1 - w_{11}(x_0)\mathrm{sinc}(w_s))g_1(x_0, y_0, z_0) + w_{11}(x_0)[g_1(q'_{x_1}) + g_1(q'_{x_2})] \\ \tilde{g}'_2(x_0, y_0, z_0) &= (1 - w_{21}(z_0)\mathrm{sinc}(w_s))g_2(x_0, y_0, z_0) + w_{21}(z_0)[g_2(q'_{z_1}) + g_2(q'_{z_2})] \end{aligned} \tag{4.93}$$

  The above functions can be solved according to the introduction of 1-D GSVA method in section 2.2.2. And choose the result with smaller magnitude of the two functions as the final optimal weighted result.

- **Approximation with 1-D MSVA method**
  Similarly, we can apply MSVA method. Then the another two adjacent points along each axis are

$$\begin{aligned} q_{x_3} &= \left(x_0 - \frac{4\pi}{B_{k_x}(x_0)},\ y_0,\ z_0\right) \\ q_{x_4} &= \left(x_0 + \frac{4\pi}{B_{k_x}(x_0)},\ y_0,\ z_0\right) \end{aligned} \tag{4.94}$$

$$\begin{aligned} q_{z_3} &= \left(x_0,\ y_0,\ z_0 - \frac{4\pi}{B_{k_z}(z_0)}\right) \\ q_{z_4} &= \left(x_0,\ y_0,\ z_0 + \frac{4\pi}{B_{k_z}(z_0)}\right) \end{aligned} \tag{4.95}$$

  The number of the pixels between the point target and the new adjacent points are

$$\begin{aligned} N_{12}(x_0) &= \left\lfloor \frac{4\pi}{B_{k_x}(x_0)\cdot d_X} \right\rceil \\ N_{22}(z_0) &= \left\lfloor \frac{4\pi}{B_{k_z}(z_0)\cdot d_Z} \right\rceil \end{aligned} \tag{4.96}$$

  The new adjacent points can be approximated as

$$\begin{aligned} q'_{x_3} &= (x_0 - N_{12}(x_0)\cdot d_X,\ y_0,\ z_0) \\ q'_{x_4} &= (x_0 + N_{12}(x_0)\cdot d_X,\ y_0,\ z_0) \\ q'_{z_3} &= (x_0,\ y_0,\ z_0 - N_{22}(z_0)\cdot d_Z) \\ q'_{z_4} &= (x_0,\ y_0,\ z_0 + N_{22}(z_0)\cdot d_Z) \end{aligned} \tag{4.97}$$

  The weighted image can be expressed as

$$\begin{aligned} \tilde{g}'_1(x_0,y_0,z_0) &= g_1(x_0,y_0,z_0) + w_{11}(x_0)[-2\mathrm{sinc}(w_s)g_1(x_0,y_0,z_0) + g_1(q'_{x_1}) + g_1(q'_{x_2})] \\ &\quad + w_{12}(x_0)[-2\mathrm{sinc}(w_s)g_1(x_0,y_0,z_0) + g_1(q'_{x_3}) + g_1(q'_{x_4})] \\ \tilde{g}'_2(x_0,y_0,z_0) &= g_2(x_0,y_0,z_0) + w_{21}(z_0)[-2\mathrm{sinc}(w_s)g_2(x_0,y_0,z_0) + (g_2(q'_{z_1}) + g_1(q'_{z_2})] \\ &\quad + w_{22}(z_0)[-2\mathrm{sinc}(w_s)g_2(x_0,y_0,z_0) + g_2(q'_{z_3}) + g_2(q'_{z_4})] \end{aligned} \tag{4.98}$$

  Then we can implement acceleration of 1-D MSVA method.

4.5.3 Simulation Result

Still, set $w_s = 0.909$, and we get the following simulation results. Figure 4.10 gives the acceleration result with the BSVA, GSVA and MSVA method in the cross-range direction. Compared with the original image (Figure 4.3), the sidelobe suppression is effective. However, compared with the original SVA image (Figure 4.9), there are some residual sidelobes, especially for the targets located at the corner of the imaging area. But the MSVA method gives better performance among the three acceleration implementations.

Table 4.3 compares the processing time, the amplitude of the first and second sidelobes and two grating lobes. $s_1 = (0.051\,\mathrm{m}, 0.105\,\mathrm{m}, 0.04\,\mathrm{m})$ and $s_2 = (0.059\,\mathrm{m}, 0.101\,\mathrm{m}, 0.04\,\mathrm{m})$ are the

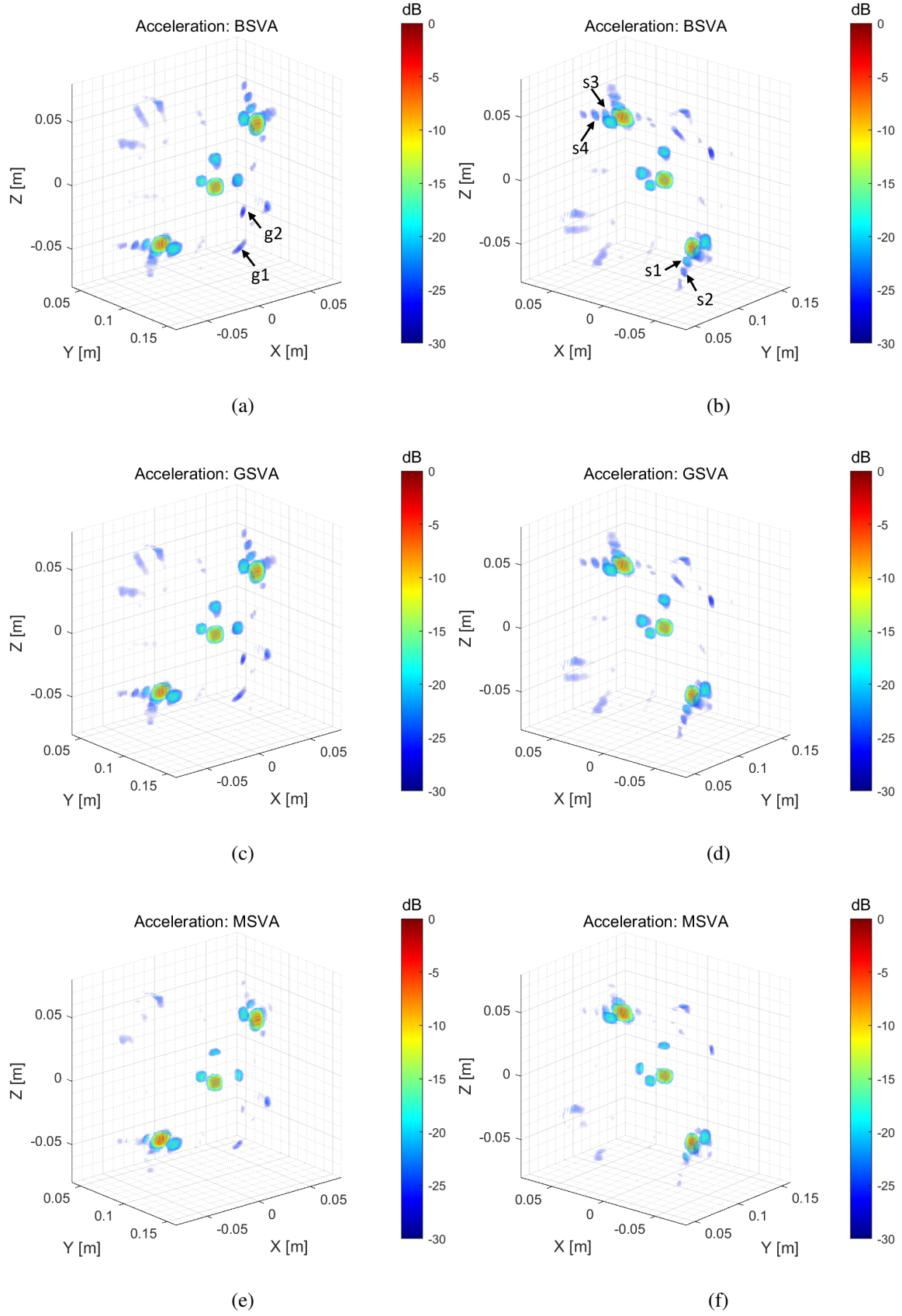

Figure 4.10: Acceleration results with different SVA method in the cross-range direction and BSVA in the range direction. (a) Front view with BSVA method, (b) back view with BSVA method; (c) Front view with GSVA method, (d) back view with GSVA method; (e) Front view with MSVA method, (f) back view with MSVA method.

Table 4.3: Performance comparison

	Original	**BSVA**	**BSVA-acceleration**	**GSVA-acceleration**	**MSVA-acceleration**
Processing time [min]	5.30	106.6	11.09	11.07	14.04
s_1[dB]	-13.53	-Inf	-21.33	-22.41	-32.21
s_2[dB]	-18.68	-32.21	-21.50	-22.24	-Inf
s_3[dB]	-13.51	-Inf	-21.68	-22.82	-Inf
s_4[dB]	-18.78	-33.86	-22.70	-23.52	-43.66
g_1[dB]	-23.31	-23.79	-24.02	-24.30	-25.02
g_2[dB]	-22.14	-34.59	-22.34	-22.82	-28.07

first and second sidelobes of the strong target p_5 along x-axis. $s_3 = (-0.04\,\text{m}, 0.09\,\text{m}, -0.05\,\text{m})$ and $s_4 = (-0.04\,\text{m}, 0.086\,\text{m}, -0.057\,\text{m})$ are the first and second sidelobes of the strong target p_8 along z-axis. $g_1 = (0.042\,\text{m}, 0.086\,\text{m}, -0.069\,\text{m})$ and $g_2 = (0.062\,\text{m}, 0.07\,\text{m}, -0.042\,\text{m})$ are the grating lobes of p_8 along x-axis and p_5 along z-axis respectively. From the table, we can see that the processing time is significantly reduced with acceleration methods. With BSVA and GSVA acceleration method, it has been reduced to around 10% of the original SVA method. With MSVA acceleration method, it has been reduced to 13.17%. The suppression performance of BSVA-acceleration method and GSVA-acceleration method is similar. But due to the approximation, some errors are introduced, then the suppression performance is not as good as that of the original SVA method. While the suppression effect of the MSVA-acceleration method is almost comparable with that of the original SVA method, the processing time only increases 1.65 times that of the original imaging, much less than 20 times for the original SVA method. Therefore, with a proper imaging grid, the MSVA-acceleration method is a good choice to implement sidelobe and grating lobe suppression effectively and quickly.

4.6 Experimental Validation

4.6.1 Measurement Setup

The experimental measurement campaign was performed in the anechoic chamber in the Delft University of Technology (TU Delft). And the method is implemented in MATLAB using the Server 2 of Group MS3 , EEMCS, TU Delft.

The operating frequency is from 1 GHz to 26 GHz with steps of 100 MHz. The MIMO array composes of 16 transmitters and 9 receivers. And a target is placed in front of the array around 0.5 m. The imaging area is $0.495\,\text{m} \times 0.59\,\text{m} \times 0.495\,\text{m}$ with $100 \times 60 \times 100$ samples. All the parameters are listed in the table 4.4. The structure of the MIMO array is shown in Figure 4.11. What should be noted is that here we choose a irregular MIMO array to verify the general case. When dealing with the cross-range SVA method, the corner antenna is determined by calculating the wavenumber width of all antennas corresponding to the current pixel and choosing the antenna pair that getting the maximum wavenumber width. When dealing with the range SVA method, the central position of the transmit array and the receive array is determined with k-mean clustering method.

Table 4.4: Parameters of Experimental Validation

Parameters	**Values**
Frequency band f	1 – 26 GHz
Frequency interval df	100 MHz
Number of transmitters N_{Tx}	16
Number of receivers N_{Rx}	9
Imaging area X	[-0.25 0.245]
Imaging area Y	[0 0.59]
Imaging area Z	[-0.25 0.245]
Grid spacing d_X	5 mm
Grid spacing d_Y	10 mm
Grid spacing d_Z	5 mm
Image samples	$100 \times 60 \times 100$

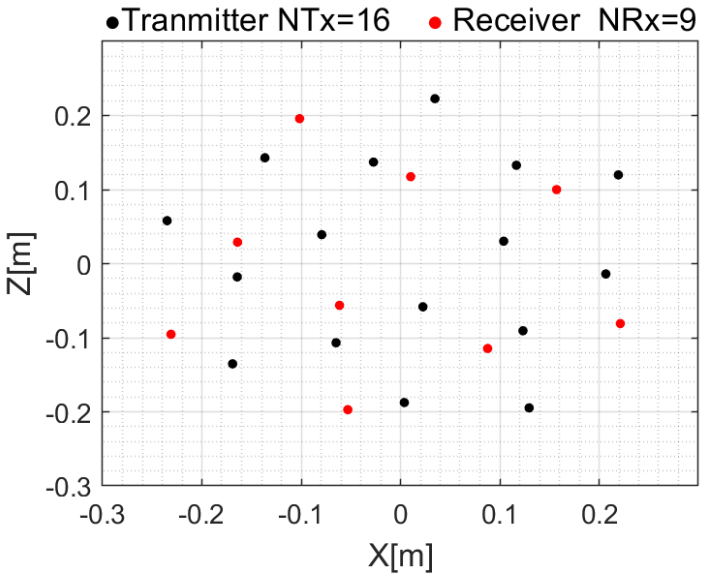

Figure 4.11: MIMO array topology of experimental validation

4.6.2 Experimental Results

The original imaging result is shown in Figure 4.12(a) and the image after performing SVA method is given in Figure 4.12(b). The sidelobes are greatly suppressed with the SVA method in Figure 4.12(b), compared with the original image.

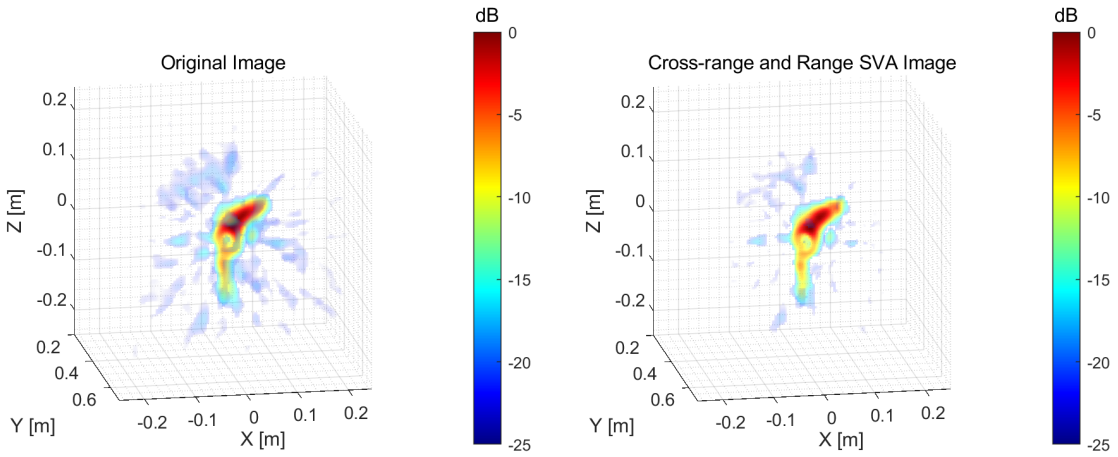

(a) (b)

Figure 4.12: Images of experimental data. (a) The original image. (b) The SVA image.

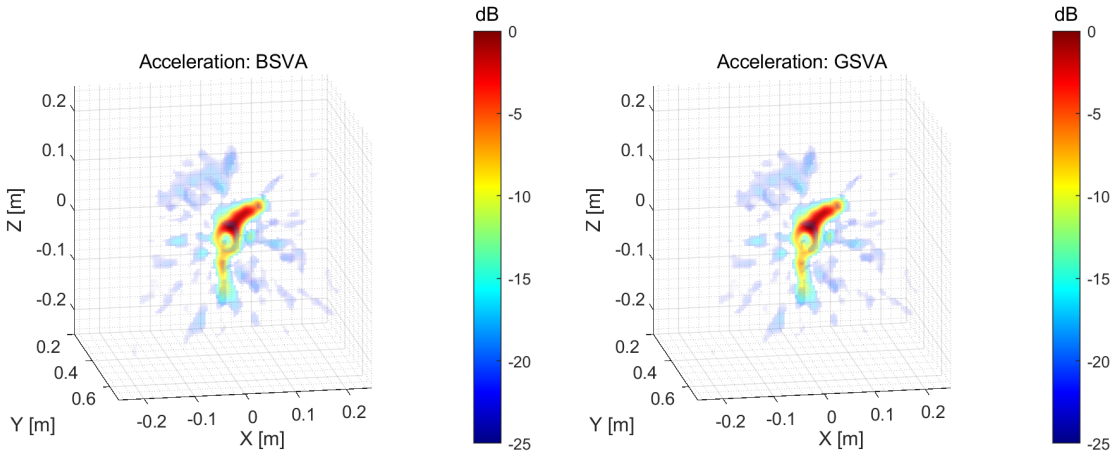

(a) (b)

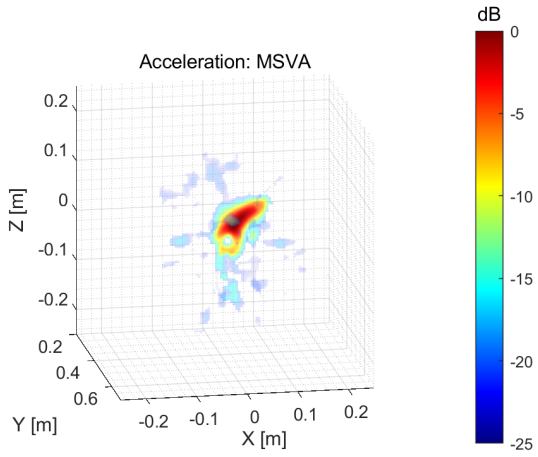

(c)

Figure 4.13: The acceleration implementation of the experimental measurement. (a) with BSVA method in the cross-range plane; (b) with GSVA method in the cross-range plane; (c) with MSVA method in the cross-range plane.

Table 4.5: Processing time comparison

	Original	**BSVA**	**BSVA-acceleration**	**GSVA-acceleration**	**MSVA-acceleration**
Processing time [min]	1.69	33.34	3.19	3.19	4.07

The comparison of the processing time is listed in Table 4.5. The acceleration implementation results are given in Figure 4.13(a), 4.13(b) and 4.13(c) . Compared with the original image, the three acceleration implementations can suppress the sidelobe level. The BSVA and GSVA acceleration implementation show the similar suppression effect but not that good. The MSVA implementation show better sidelobe suppression effect but also loss part of the distributed target due to the relaxation of the constraints. In this case, the MSVA method is not a good choice to accelerate the SVA implementation. And this is what need to solve in the future, to find a more robust and low-computation constraints of the MSVA method.

4.7 Conclusion

In this chapter, based on the SVA applied on 1-D MIMO array imaging in chapter 3, we give the deduction and implementation of the BSVA method for 2-D MIMO array imaging in the cross-range plane (x-axis direction and z-axis direction) and range direction separately. Furthermore, we propose a method to implement the BSVA method in the three directions simultaneously.

Besides, we propose three acceleration implementations of the SVA method. And they can work well under some conditions of imaging grid and the oversampling ratio.

The numerical simulation verifies the effectiveness of the SVA method and the acceleration implementations of the SVA method based on a uniformly spaced 2-D MIMO array. The sidelobe level in the cross-range plane has been suppressed at least 13.27 dB, and the sidelobe suppression in the range direction of 18.93 dB has been achieved. Furthermore, the mainlobe in the cross-range and range directions are not been broadened. With the BSVA and GSVA acceleration method, the computational time has been reduced to around 10% of the original SVA method, while the suppression effect has been weakened slightly. With the MSVA acceleration method, the processing time has been reduced to 13.17% of the original SVA method, while the suppression effect is comparable with that before acceleration.

Lastly, we verify the SVA method with the experimental measurement. The result shows that the SVA method can be performed on the irregular 2-D MIMO array imaging to improve the image quality by suppressing the sidelobe level without sacrificing the mainlobe resolution. Besides, the result of the acceleration shows the limitation of the three acceleration methods. the BSVA and GSVA acceleration provide limited suppression effect and the MSVA acceleration loss part of the distributed target due to the relaxation of the constraints. Therefore, investigating a more robust and effective acceleration method is the future work.

5

Conclusion and Future Work

5.1 Conclusion

This thesis project aims to enhance the image quality of the short-range MIMO array imaging by suppressing the sidelobe and grating lobe level via non-linear apodization method. The traditional method is to apply a non-rectangular weighting function on the array aperture or the data. However, all weighting methods result in the mainlobe spreading, which reduces the resolution. Furthermore, through the literature review of the main methods applied on MIMO array imaging, we can see some limitations, for example, only suitable for the specific array topology, the limited suppression effect, or the complex implementation. Through the research, we find that the non-linear apodization method used for SAR imagery could effectively suppress the sidelobe level without sacrificing the mainlobe resolution. Furthermore, it is easy to implement due to the unique spatial property of the cosine-on-pedestal weighting function. The optimal weighting results can be obtained pixel by pixel with a three-point convolver. Therefore, it seems a good choice for MIMO array imaging. However, the challenge is that the wavenumber spectrum of a MIMO array is complicated and spatially variant that we cannot directly apply the SVA method on a MIMO array imaging.

The analysis of the wavenumber spectrum is the key point to address the problem. By utilizing the imaging method of generalized matched filtering in the cross-range direction, we can separately analyze the cross-range wavenumber spectrum of the transmit array and the receive array. In this way, the complicated wavenumber spectrum analysis of MIMO array imaging is simplified. Then, we can make some approximations to obtain the support of the wavenumber spectrum of the separate sub-array in the cross-range direction and form a new imaging plane at each imaging height. By analyzing the wavenumber spectrum support, we find its width is spatially variant and related to the imaging point. Therefore, when applying the SVA method, the spatial sampling frequency for each pixel is different, which results in the different sampling spacing in the space domain. Furthermore, for the pixel not on the line of the array center, its central wavenumber deviates from the zero-wavenumber position. Thus, a phase term is compensated in the space domain to eliminate the deviation of the central wavenumber. Then we can implement the 2-D BSVA pixel by pixel. In the range direction, the support width of the sub-array does not change. However, the wavenumber in one range direction will project on another range direction due to the non-orthogonality of the two range directions. Therefore, the total wavenumber consists of two parts. Furthermore, the

central wavenumber is also not at the zero-wavenumber position. A phase term is needed to compensate in the space domain. Then two 1-D BSVA methods can be applied independently and in parallel.

In this thesis, the SVA method is first applied to suppress the sidelobes in the range direction of the 1-D MIMO array imaging. And the complete implementation of the SVA method both in the cross-range and range direction is provided. Besides, the SVA method for 2-D MIMO array imaging is also proposed to reduce the sidelobe level in the cross-range plane and the range direction. Furthermore, three acceleration approaches are proposed to reduce the computational time.

For 1-D case, the numerical simulation is based on a sparse periodic array. The result shows that the sidelobe level has been suppressed by at least 22.59 dB in the cross-range direction; the grating lobe level has been suppressed by at least 4.18 dB. In the range direction, at least 20.82 dB suppression of the sidelobe has been achieved. Besides, the mainlobe has not been broadened in the two directions. Therefore, the small closely spaced targets can be resolved from the strong closely spaced targets with this method since the main lobe resolution remains unchanged and the sidelobe level is effectively suppressed. Then to address the much-increased processing time, we propose several acceleration implementations of the SVA method. Among them, the BSVA and GSVA acceleration method has reduced the processing time to around 10% that of the original SVA method, while the suppression effect has been weakened slightly. The MSVA-acceleration method shows a better suppression effect, which is comparable with the original SVA method. At the same time, the processing time is only 11.50% that of the original SVA method. What should be noted is that the acceleration methods have the requirement of the imaging grid. Once the grid is too dense, the suppression effect of acceleration methods would degrade rapidly.

For 2-D case, the numerical simulation is based on a uniformly spaced rectangular MIMO array. The result shows that the proposed method provides a sidelobe reduction of at least 13.27 dB in the cross-range plane and 18.93 dB in the range direction. At the same time, the grating lobe level has been reduced slightly. Besides, the cross-range resolution and range resolution remains unchanged. Therefore, the proposed method can enhance the image quality of 2-D MIMO array imaging by providing a large dynamic range without degrading the main lobe width. Furthermore, several acceleration implementations are also proposed and implemented. The processing time with BSVA and GSVA acceleration method has been reduced to around 10% that of the original SVA method, while the suppression effect has been weakened slightly. The MSVA-acceleration method shows a better suppression effect, and the processing time is 13.17% that of the original SVA method. Besides, experimental validation is also given to verify the performance of the proposed method. The experimental validation is based on an irregular MIMO array to illustrate the generality of the proposed method. The result shows that the proposed method can also be applied on the irregular array and achieve a sidelobe reduction of 8 dB with preserving the mainlobe resolution. Moreover, the acceleration implementations are also provided. However, the experimental results show the limited suppression performance with the BSVA and GSVA acceleration methods. The suppression effect gets better with the MSVA acceleration method, while part of the distributed targets are suppressed and even lost. And this is what we need to address in the future.

In conclusion, the proposed method is suitable for arbitrary MIMO array. For the 1-D and 2-D cases, the sidelobe level is suppressed to below -26 dB in the cross-range and range directions with the proposed method. Therefore, the proposed method is highly effective for a

MIMO array to provide better suppression performance than a full array in the same aperture size. Furthermore, with acceleration approaches under a dense imaging grid, the sidelobe level can also be reduced to below -26 dB, at the same time, the computational time is reduced to around 10% that before acceleration.

5.2 Recommendation and Future Work

Though the acceleration implementations of the proposed method work well for simulation, it shows the limitation in the experimental validation. Once the imaging grid is too sparse, the acceleration implementations would not achieve a good sidelobe suppression effect. Furthermore, the MSVA acceleration implementation may result in the loss of the targets. Therefore, some work can be carried in the future.

Firstly, go a step further in the detailed conditions and effect of acceleration implementation with the BSVA and GSVA method. Try to give a robust consideration and implementation to achieve the compromise between the less processing time and better suppression effect.

Secondly, redefine the constraints of the MSVA method for the MIMO array imaging. The constraints of the 5-tap SVA method is relaxed to reduce the complicated computation. Therefore, it requires a strict sinc kernel of the point spread function (PSF) to avoid the loss of the target. However, the PSF of the MIMO array is only similar to the sinc kernel due to the spatially variant wavenumber spectrum. Furthermore, combined with the approximation of the wavenumber width and the compensated phase, the error would be enlarged, and the uncontrolled risk of losing the targets would increase. To avoid the loss, we need to tighten the excessive relaxed constraints.

Thirdly, we can investigate the acceleration implementation of the SVA method with machine learning. The key idea for acceleration is to make use of the original imaging result. By machine learning, we may implement the acceleration fast and accurate.

Acknowledgements

How time flies, the two-year study and life in **TU Delft** went so fast. I will always miss the time I spent here though it was different from what I imagined due to the COVID-19.

The thesis was not just a graduation project to get the degree. I really learned a lot and made rapid progress. Analyzing the problem, doing the research, and solving it with the knowledge I learned was challenging but worthy to experience. I think I will be confident and not afraid anymore when difficulties and challenges come in my future career.

I would like to thank many people for their help and support. First of all, I would like to express my great gratitude to my supervisor, **Prof. Alexander Yarovoy**, for his valuable guidance, suggestions, and encouragement. The detailed comments on the report and the constructive suggestions of the mid-term presentation gave me a lot of help. His patience and encouragement in every meeting gave me much confidence about my thesis.

I would like to give my deep appreciation to my daily supervisor **Dr. Jianping Wang**. His profound knowledge and excellent insight gave me a lot of expert suggestions and support for my thesis and inspired me to have higher requirements for myself. Furthermore, he gave me valuable career advice and experiences on how to think logically, seek resources, and deal with problems. These will influence me throughout my whole life.

I would like to thank all the members of **Group MS3** that offered their help and support. Having the chance to be a part of this warm group was very enjoyable.

I would also like to thank my friends Huaiyang Gong and Yi Mi. The two-year life spent with them in Delft and Den Haag was happy and full of joy. And thank you to my best friend Yi'er He. I know you always support and encourage me, and congratulations on your marriage. Lastly, I would like to thank my family for their unconditional love and support. Whenever I was depressed and sad, I always received encouragement and care from them.

Thanks to all! I learned a lot and became better!

Ying Zhang
Delft, November 2021

Bibliography

[1] M. Guarnieri, "The early history of radar [historical]," IEEE Industrial Electronics Magazine, vol. 4, no. 3, pp. 36–42, 2010.

[2] R. J. James, "A history of radar," IEE Review, vol. 35, no. 9, pp. 343–349, 1989.

[3] S. S. Ahmed, A. Schiessl, F. Gumbmann, M. Tiebout, S. Methfessel, and L.-P. Schmidt, "Advanced microwave imaging," IEEE microwave magazine, vol. 13, no. 6, pp. 26–43, 2012.

[4] L. Cutrona, "Synthetic aperture radar," Radar handbook, vol. 2, pp. 2333–2346, 1990.

[5] E. Fishler, A. Haimovich, R. Blum, D. Chizhik, L. Cimini, and R. Valenzuela, "Mimo radar: An idea whose time has come," in Proceedings of the 2004 IEEE Radar Conference (IEEE Cat. No. 04CH37509), IEEE, 2004, pp. 71–78.

[6] R. Herschel, S. A. Lang, and N. Pohl, "Mimo imaging for next generation passenger security systems," in Proceedings of EUSAR 2016: 11th European Conference on Synthetic Aperture Radar, VDE, 2016, pp. 1–4.

[7] R. Demirli, X. Rivenq, Y. D. Zhang, C. Ioana, and M. G. Amin, "Mimo array imaging for ultrasonic nondestructive testing," in Nondestructive Characterization for Composite Materials, Aerospace Engineering, Civil Infrastructure, and Homeland Security 2011, International Society for Optics and Photonics, vol. 7983, 2011, p. 798 338.

[8] F. Gumbmann and L.-P. Schmidt, "Millimeter-wave imaging with optimized sparse periodic array for short-range applications," IEEE Transactions on Geoscience and Remote Sensing, vol. 49, no. 10, pp. 3629–3638, 2011. DOI: 10.1109/TGRS.2011.2164616.

[9] X. P. Masbernat, M. G. Amin, F. Ahmad, and C. Ioana, "An mimo-mti approach for through-the-wall radar imaging applications," in 2010 International Waveform Diversity and Design Conference, IEEE, 2010, pp. 000 188–000 192.

[10] X. Zhuge, "Short-range ultra-wideband imaging with multiple-input multiple-output arrays," 2010.

[11] X. Tu, G. Zhu, X. Hu, and X. Huang, "Grating lobe suppression in sparse array-based ultrawideband through-wall imaging radar," IEEE Antennas and Wireless Propagation Letters, vol. 15, pp. 1020–1023, 2015.

[12] T. Ge, L. Zhao, Y. Cai, and J. Zhou, "A grating lobes suppression technique for near-field sparse linear mimo array imaging," in 2016 CIE International Conference on Radar (RADAR), IEEE, 2016, pp. 1–4.

[13] W. Tian, Y. Li, J. Wang, C. Hu, and T. Zeng, "Design of mimo array with low grating lobes in near-field imaging," in 2017 XXXIInd General Assembly and Scientific Symposium of the International Union of Radio Science (URSI GASS), IEEE, 2017, pp. 1–4.

[14] X. Zhuge, A. Yarovoy, and L. Ligthart, “A sidelobe reduction technique for enhancing images of uwb sparse mimo array,” in 2009 International Radar Conference" Surveillance for a Safer World"(RADAR 2009), IEEE, 2009, pp. 1–6.

[15] Y. Liu and X. Xu, “Azimuth sidelobe suppression technique for near-field mimo radar imaging,” in Image and Signal Processing for Remote Sensing XXI, International Society for Optics and Photonics, vol. 9643, 2015, 96431E.

[16] R. J. Burkholder and K. E. Browne, “Coherence factor enhancement of through-wall radar images,” IEEE Antennas and Wireless Propagation Letters, vol. 9, pp. 842–845, 2010.

[17] Y. Jiang, Y. Qin, H. Wang, B. Deng, K. Liu, and B. Cheng, “A side-lobe suppression method based on coherence factor for terahertz array imaging,” IEEE Access, vol. 6, pp. 5584–5588, 2018.

[18] J. Camacho, M. Parrilla, and C. Fritsch, “Grating-lobes reduction by application of phase coherence factors,” in 2009 IEEE International Ultrasonics Symposium, IEEE, 2009, pp. 341–344.

[19] X. Tu, G. Zhu, J. Hu, X. Huang, and Z. Zhou, “A sidelobes/grating lobes suppression method for ultrawindeband ultrasparse array through-the-wall imaging radar,” in 2014 IEEE China Summit & International Conference on Signal and Information Processing (ChinaSIP), IEEE, 2014, pp. 199–202.

[20] J. Liu, Y. Jia, L. Kong, X. Yang, and Q. H. Liu, “Sign-coherence-factor-based suppression for grating lobes in through-wall radar imaging,” IEEE Geoscience and Remote Sensing Letters, vol. 13, no. 11, pp. 1681–1685, 2016.

[21] R. Zhu, J. Zhou, G. Jiang, B. Cheng, and Q. Fu, “Grating lobe suppression in near range mimo array imaging using zero migration,” IEEE Transactions on microwave theory and techniques, vol. 68, no. 1, pp. 387–397, 2019.

[22] ——, “Grating lobe suppression in near range mimo array imaging using zero migration,” IEEE Transactions on microwave theory and techniques, vol. 68, no. 1, pp. 387–397, 2019.

[23] R. Zhu, J. Zhou, Q. Fu, and G. Jiang, “Spatially variant apodization for grating and sidelobe suppression in near-range mimo array imaging,” IEEE Transactions on Microwave Theory and Techniques, vol. 68, no. 11, pp. 4662–4671, 2020.

[24] H. Stankwitz, R. Dallaire, and J. Fienup, “Nonlinear apodization for sidelobe control in sar imagery,” IEEE Transactions on Aerospace and Electronic Systems, vol. 31, no. 1, pp. 267–279, 1995. DOI: 10.1109/7.366309.

[25] B. H. Smith, “Generalization of spatially variant apodization to noninteger nyquist sampling rates,” IEEE Transactions on Image Processing, vol. 9, no. 6, pp. 1088–1093, 2000.

[26] C. Castillo-Rubio, S. Llorente-Romano, and M. Burgos-Garcia, “Robust sva method for every sampling rate condition,” IEEE Transactions on Aerospace and Electronic Systems, vol. 43, no. 2, pp. 571–580, 2007.

[27] C. Ni, Y. Wang, X. Xu, C. Zhou, and P. Cui, “A sar sidelobe suppression algorithm based on modified spatially variant apodization,” Science China Technological Sciences, vol. 53, no. 9, pp. 2542–2551, 2010.

[28] L. Zhuang, X. Liu, and Z. Zhou, "Enhanced resolution for sparse aperture radar imaging using super-sva," in 2007 Asia-Pacific Microwave Conference, IEEE, 2007, pp. 1–4.

[29] K. M. R. Stankwitz Herbert C., "Super spatially variant apodization (super - sva)," 5 686 922, Nov. 1997.

[30] X. Xu and R. M. Narayanan, "Enhanced resolution in sar/isar imaging using iterative sidelobe apodization," IEEE Transactions on image processing, vol. 14, no. 4, pp. 537–547, 2005.

[31] H. Stankwitz and M. Kosek, "Sparse aperture fill for sar using super-sva," in Proceedings of the 1996 IEEE National Radar Conference, IEEE, 1996, pp. 70–75.

[32] T. T. Peterson, "Three quarter spatially variant apodization," 8 232 915, Jul. 2012.

[33] S. Hu, C. Shu, Y. Alfadhl, and X. Chen, "A thz imaging system using linear sparse periodic array," IEEE Sensors Journal, vol. 20, no. 6, pp. 3285–3292, 2020. DOI: 10.1109/JSEN.2019.2958744.

[34] G. R. Lockwood, P.-C. Li, M. O'Donnell, and F. S. Foster, "Optimizing the radiation pattern of sparse periodic linear arrays," IEEE Transactions on Ultrasonics, Ferroelectrics, and frequency control, vol. 43, no. 1, pp. 7–14, 1996.

[35] A. V. Oppenheim, A. S. Willsky, S. H. Nawab, G. M. Hernández, et al., Signals & systems. Pearson Educación, 1997.

[36] M. Soumekh, Synthetic aperture radar signal processing. New York: Wiley, 1999, vol. 7.